To the Graduate Council:

I am submitting herewith a thesis written by Claire Elyse Campbell entitled "The effects of nutrient limitation and cyanophage on heterotrophic microbial diversity." I have examined the final electronic copy of this thesis for form and content and recommend that it be accepted in partial fulfillment of the requirements for the degree of Master of Science, with a major in Microbiology.

_____
Steven Wilhelm, Major Professor

We have read this thesis
and recommend its acceptance:

_____
Alison Buchan

_____
Erik Zinser

Accepted for the Council:

_____
Carolyn R. Hodges
Vice Provost and Dean of the Graduate School

The effects of nutrient limitation and cyanophage on heterotrophic microbial diversity

A Thesis Presented for the
Master of Science Degree
The University of Tennessee, Knoxville

Claire Elyse Campbell
May 2012

ACKNOWLEDGEMENTS

None of this would have been possible without the assistance of a number of people during my time at the University of Tennessee. It is appropriate to extend my deepest gratitude to my advisor, Dr. Steven Wilhelm for his guidance and mentorship to me as a graduate student. Thank you for providing me with an enriching graduate school experience. I would also like to extend my thanks to our collaborators at Michigan State University, Dr. Jay Lennon and Megan Larsen and my committee members, Dr. Alison Buchan and Dr. Erik Zinser for their invaluable insight and suggestions over the last two years.

While I cannot acknowledge everyone on the 6th floor of SERF, I would like to specifically recognize several past and present members of the Wilhelm lab: Especially Dr. Gary LeCleir for his technical assistance in the laboratory, Star Loar, Dr. Audrey Matteson, Dr. Matthew Saxton, Morgan Steffen and all of the undergraduates that have passed through the lab. To everyone else on the 6th floor in the Buchan and Zinser labs, I cannot thank you enough for your support as colleagues and friends especially Ashley Frank and Jeremy Chandler. A special thank you to my friends in Knoxville outside of the lab and the university and to those who are afar that still have no idea what I have been doing the last two years of my life. Thanks for pretending to understand and saying all of the right things at the right time.

I could not have made it this far without the love and encouragement from my parents, Bill and Rhonda, my brother, Austin, and my extended family. Dad, I hope this shows you that there is a little more to science than bar graphs and pie charts. And last but not least, I would not be where I am today without the love and patience of my best friend, Kyle. Thanks for teaching me not to take life too seriously and providing me with the confidence I needed to finish this degree. Without you, I would not be the same person I am today.

ABSTRACT

Marine viruses are critically important in the regulation of biogeochemical cycles and host microbial communities. In this study, we tested whether the indirect effects of virus predation on a phototroph (*i.e., Synechococcus*) affected the composition of co-occurring heterotrophic bacteria under nitrogen and phosphorus limitation in long-term chemostat experiments. Using 454 Titanium barcoded pyrosequencing of the 16S rRNA gene, microbial diversity and technical (*i.e.,* sequencing) reproducibility were assessed for nine individual chemostats across five different time points. A total of 325,142 reads were obtained; 194,778 high-quality, non-cyanobacterial sequences were assigned to 110 OTUs. Our results show high reproducibility with most communities clustering closest with their technical replicate, and a similar distribution of taxonomic assignments across replicates. The most abundant phylum was *Proteobacteria*, with *Cyanobacteria* representing only 20% of the sequences. OTU-based analyses revealed similar trends across chemostats; *Sulfitobacter* was the dominant genus while *Pseudomonas* was unique to the phosphorus-limited chemostats. A statistical examination of biological replicates revealed significant differences between the nitrogen- and phosphorus-limited treatments ($p = 0.0001$) and time ($p = 0.0001$), as well as a significant interaction between nutrient limitation and time ($p = 0.0091$). These results demonstrate the relative importance of nutrient-limitation as a potential primary driver of non-target heterotrophic community change as opposed to the indirect effects of viruses on a marine food web.

TABLE OF CONTENTS

Chapter Page

INTRODUCTION 1
Importance of microbes in marine systems 1
Interplay of cyanobacteria and heterotrophic bacteria 1
Marine Viruses 3
Cyanophages 4
Biogeochemical cycling 5
Carbon 5
Nitrogen and Phosphorus 6
Viral activity fuels nutrient cycling 7
Viruses shape community structure 8
Evidence for virus resistance 9
Chemostat studies reveal rapid evolution of virus resistance 9
Resistance in cyanobacteria 12
Next-generation sequencing 13
Bias in pyrosequencing studies 14
RESEARCH OBJECTIVES 17
METHODS 18
Chemostat setup and sample collection 18
Flow cytometry methods and acridine orange slide preparation 19
Community DNA extraction 21
PCR amplification 22
Barcoded amplicon library construction and 454 Titanium pyrosequencing 23
Sequence data processing 24
Pooling samples 26
Statistical analyses 26
RESULTS 28
Nitrogen-limited chemostat dynamics 28
Phosphorus-limited chemostat dynamics 33
Comparison of bacterial counts 39
Heterotrophic bacteria : *Synechococcus* ratios 40
454 Titanium pyrosequencing 42
Sequence analysis 42
Comparing technical sequencing reproducibility 44
Community Trends 47
RDP Assignments 47
OTU Assignments 48
Cluster analyses and non-metric multidimensional dimensional scaling analyses 60
Statistical analyses 64
DISCUSSION 67
Technical sequencing reproducibility 69
MDS and cluster analyses show differences in communities 70

Limitations and future directions 71
Conclusions 73
REFERENCES 75
VITA 89

LIST OF TABLES

Table Page

Table 1. PERMANOVA of chemostat bacterial community for the 10 most abundant OTUs showing the main tests for the factors of nitrogen or phosphorus treatment, no virus or virus addition, time and their interactions. *P<0.05. 65

Table 2. Pairwise comparisons of Treatment x Day (significant interaction identified by PERMANOVA main tests) for pairs of levels of Treatment for the 10 most abundant OTUs. *P<0.05. 65

Table 3. Pairwise comparisons of Treatment x Day (significant interaction identified by PERMANOVA main tests) for pairs of levels of Day for the 10 most abundant OTUs. *P<0.05. 66

Table 4: Universal primers, fusion primers and barcoded primers used to barcode chemostat libraries (Wang and Qian 2009). 88

LIST OF FIGURES

Figure Page

Figure 1: Microscope and flow cytometry counts of *Synechococcus* and heterotrophic bacteria from the nitrogen-limited control chemostat. 29

Figure 2: Microscope and flow cytometry counts of *Synechococcus,* heterotrophic bacteria and cyanophage from a nitrogen-limited, phage-amended chemostat (biological replicate 1)... 30

Figure 3: Microscope and flow cytometry counts of *Synechococcus,* heterotrophic bacteria and cyanophage from a nitrogen-limited, phage-amended chemostat (biological replicate 2)... 31

Figure 4: Microscope and flow cytometry counts of *Synechococcus*, heterotrophic bacteria and cyanophage from a nitrogen-limited, phage-amended chemostat (biological replicate 3)... 32

Figure 5: Microscope and flow cytometry counts of *Synechococcus* and heterotrophic bacteria from a phosphorus-limited control chemostat (biological replicate 1)..... 34

Figure 6: Microscope and flow cytometry counts of *Synechococcus* and heterotrophic bacteria from a phosphorus-limited control chemostat (biological replicate 2)..... 35

Figure 7: Microscope and flow cytometry counts of *Synechococcus*, heterotrophic bacteria and cyanophage from a phosphorus-limited, phage-amended chemostat (biological replicate 1) 36

Figure 8: Microscope and flow cytometry counts of *Synechococcus*, heterotrophic bacteria and cyanophage from a phosphorus-limited, phage-amended chemostat (biological replicate 2). 37

Figure 9: Microscope and flow cytometry counts of *Synechococcus*, heterotrophic bacteria and cyanophage from a phosphorus-limited, phage-amended chemostat (biological replicate 3). 38

Figure 10: Scatter plot with linear regression of flow cytometry counts versus epifluorescence counts of heterotrophic bacteria (n=15)..... 39

Figure 11: Ratios of heterotrophic bacteria to *Synechococcus*. Standard error bars represent mean ± SEM. 41

Figure 12: Relative abundances of RDP taxonomic assignments for two technical replicates at a 95% confidence threshold..... 43

Figure 13: Linear regression of relative abundances of OTUs for both technical replicates. 45

Figure 14: Dendrogram of relatedness of all technical and biological replicate (R) libraries..... 46

Figure 15: Dynamics of abundant (A) and rare (B) OTUs in a N-limited control chemostat. 50

Figure 16: Dynamics of abundant (A) and rare (B) OTUs in a N-limited, phage-amended chemostat (biological replicate 1). 51

Figure 17: Dynamics of abundant (A) and rare (B) OTUs in a N-limited, phage-amended chemostat (biological replicate 2). 52

Figure 18: Dynamics of abundant (A) and rare (B) OTUs in a N-limited, phage-amended chemostat (biological replicate 3). 53

Figure 19: Dynamics of abundant (A) and rare (B) OTUs in a P-limited control chemostat (biological replicate 1). 55

Figure 20: Dynamics of abundant (A) and rare (B) OTUs in a P-limited control chemostat (biological replicate 2).. 56

Figure 21: Dynamics of abundant (A) and rare (B) OTUs in a P-limited, phage-amended chemostat (biological replicate 1). 57

Figure 22: Dynamics of abundant (A) and rare (B) OTUs in a P-limited, phage-amended chemostat (biological replicate 2). 58

Figure 23: Dynamics of abundant (A) and rare (B) OTUs in a P-limited, phage-amended chemostat (biological replicate 3). 59

Figure 24: Average cluster analysis (A) and MDS ordination plot (B) of 110 non-cyanobacterial OTUs based on the zero-adjusted Bray-Curtis similarity index. 61

Figure 25: Average cluster analysis (A) and MDS ordination plot (B) of the 10 most abundant non-cyanobacterial OTUs based on the zero-adjusted Bray-Curtis similarity index. 63

Figure 26: Flow chart of experimental setup and methods (flow cytometry, pyrosequencing and sequence processing). 83

Figure 27. Sample dot plot (A) and histogram (B) of total bacterial counts. 84

Figure 28. Sample dot plot (A) and histogram (B) of autotrophic cell counts.. 85

Figure 29. Scatter plot with linear regression of flow cytometry counts versus epifluorescence counts of *Synechococcus* (n=90). 86

Figure 30: Example rarefaction curves generated using 1,000 randomizations in MOTHUR of 3 biological replicate libraries from day 73 of a phosphorus-limited, phage-amended chemostat. 87

LIST OF ABBREVIATIONS

- bp, basepairs
- C, carbon
- COR, cost of resistance
- CRISPR, clustered regularly interspaced short palindromic repeats
- DNA, deoxyribonucleic acid
- DOC, dissolved organic carbon
- DOM, dissolved organic matter
- EM, epifluorescence microscopy
- FC, flow cytometry
- MDS, non-metric multidimensional scaling
- N, nitrogen
- OTU, operational taxonomic unit(s)
- P, phosphorus
- PCR, polymerase chain reaction
- PERMANOVA, permutation-based analysis of variance
- POC, particulate organic carbon
- POM, particulate organic matter
- qPCR, quantitative polymerase chain reaction
- rDNA, ribosomal deoxyribonucleic acid
- RDP, Ribosomal Database Project
- rRNA, ribosomal ribonucleic acid
- SNPs, single nucleotide polymorphisms
- TEM, transmission electron microscopy

INTRODUCTION

Importance of microbes in marine systems

The importance of microbial processes in aquatic ecosystems has been increasingly recognized since the advent of Azam's "microbial loop" (Azam et al. 1983). This concept spurred interest in how microorganisms influence biogeochemical cycles and ecological processes. In that model, phytoplankton provide carbon (C) as dissolved organic matter (DOM) to heterotrophic bacteria as an energy source as well as materials ultimately converted into particulate organic matter (POM). Then, protozoans graze on these bacteria, providing a source of nutrients for microzooplankton at higher trophic levels. Since then, the concept has been revisited and the role of viruses has been integrated into the model (Fuhrman 1999; Wilhelm and Suttle 1999). Viruses are extremely abundant in marine systems and play an important but previously overlooked role in short circuiting up to one-quarter of organic carbon into DOM pools available to heterotrophic bacteria (Wilhelm and Suttle 1999). At a larger scale, this shunt controls the efficiency of the biological pump which alters the amount of carbon sequestered in the deep oceans (Suttle 2005).

Interplay of cyanobacteria and heterotrophic bacteria

Cyanobacteria (also referred to as blue-green algae) are considered the most diverse and widespread group of photoautotrophic prokaryotes in the marine environment (Stanier and Cohen-Bazire 1977). The world's oceans are dominated by two major genera of ecologically critical picophytoplankton: *Synechococcus* (Waterbury et al. 1979) and *Prochlorococcus* (Chisholm et al. 1988). Both genera are abundant in the marine environment, with higher *Synechococcus* abundances in nutrient-rich (near coastal) waters and *Prochlorococcus*

populations dominating oligotrophic waters (Partensky et al. 1999). Although they differ in their light-harvesting complexes, distribution and abundance, together these organisms contribute up to 50% of primary productivity in the world's oceans (Li 1995; Liu et al. 1997). Autotrophic picoplankton occurring at the ocean's surface serve as a high quality C source for heterotrophic bacteria in the form of DOM (Azam et al. 1983). Given their distribution and contribution to primary productivity, cyanobacteria are critical components of the marine environment.

Heterotrophic bacteria are also important to marine microbial food webs (Sherr and Sherr 1988). While cyanobacteria occur at high abundances in the marine environment, heterotrophic bacteria actually are the majority of microorganisms in marine systems. Since the early papers of Pomeroy and Azam (Pomeroy 1974; Azam et al. 1983), the role of heterotrophic bacteria in the environment has been of particular interest. Estimates suggest that heterotrophs make up 40-70% of the stored organic carbon in the euphotic zone of oligotrophic, open-ocean environments (Fuhrman et al. 1989; Cho and Azam 1990). Heterotrophic bacteria utilize DOM released by living or dead phytoplankton as a primary food source (Ducklow and Carlson 1992). In turn, heterotrophs at the base of the food web transfer energy to higher trophic levels (*i.e.*, larger zooplankton) through grazing. Therefore, heterotrophic bacteria are fundamental to microbial food webs as agents of organic matter decomposition and as a food source to higher organisms.

The complex interactions between cyanobacteria and heterotrophic bacteria in the oceans have been considered one of the most important factors regulating primary productivity (Fuhrman et al. 1989). Previous studies have shown that viral lysis of heterotrophic bacteria releases both DOM and POM (Riemann and Middelboe 2002). While cyanobacteria are capable of taking up DOM, heterotrophic bacteria break down POM and assimilate the carbon from it (Noble and Furhrman 1999; Poorvin et al. 2004). In the presence of viruses, lysate products

from phytoplankton release nutrients that are rapidly assimilated by heterotrophic bacteria (Gobler et al. 1997). Conversely, Weinbauer et al. (2011) suggested that the regeneration of nutrients released from the lysis of co-occurring heterotrophic bacteria in the environment may actually stimulate the growth of the ecologically critical cyanobacterium, *Synechococcus.* These findings provide evidence that heterotrophic bacterial lysis potentially regulates the growth of phytoplankton, which may have major implications on primary production. Elucidating the importance and influence of cyanobacteria and heterotrophic bacteria is essential to our current understanding of marine food webs.

Marine Viruses

Viruses are highly abundant, biologically active components of aquatic ecosystems. The first estimates of viral abundance via transmission electron microscopy (TEM) reported concentrations greater than 10^8 viruses per mL^{-1} in aquatic environments, stimulating new interest in their ecological contribution to aquatic food webs (Torrella and Morita 1979). While TEM still remains a standard method for visualizing viral morphology and estimating burst size, original abundance estimates based on this technique were largely underestimated (Bergh et al. 1989; Proctor and Fuhrman 1990; Hennes and Suttle 1995). In the early-1990s, direct counts via epifluorescence microcopy emerged as a more practical technique for enumerating viruses (Suttle et al. 1990; Hara et al. 1991; Proctor and Fuhrman 1992; Hennes and Suttle 1995). Since then, a number of fluorescent dyes (DAPI, Yo-Pro-1, SYBR Green and SYBR Gold) have been used for direct counts and flow cytometry for rapid enumeration of viruses (Suttle et al. 1990; Hennes and Suttle 1995; Noble and Fuhrman 1998; Chen et al. 2001). Although virus abundance varies widely across ecosystems, estimates in aquatic systems typically differ by at least two orders of magnitude (~10^6 to 10^8 viruses mL^{-1}) with recent estimates suggesting the

oceans contain upwards of ~10^{30} viruses (Wommack and Colwell 2000; Suttle 2005). Viral abundance depends on a number of environmental factors including productivity levels, bacteria and chlorophyll concentrations, and tends to decrease by one order of magnitude as nutrient conditions transition from nutrient-rich coastal waters to oligotrophic, open ocean waters (Hennes et al. 1995; Fuhrman 1999).

Cyanophages

Cyanophages (*i.e.*, viruses that specifically infect cyanobacteria) have been extensively studied since the first isolation reported in the early 1960s (Safferman and Morris 1963). Cyanophages that have been studied to date all belong to one of three morphologically distinct families of double-stranded DNA viruses: *Myoviridae* (T4-like phage), *Siphoviridae* (λ-like phage) and *Podoviridae* (T7-like phage) (Mann 2003). Although cyanophages were originally isolated from a freshwater system, they are widespread in the marine environment and ubiquitous across aquatic systems (Moisa et al. 1981; Suttle and Chan 1993; Waterbury and Valois 1993; Suttle and Chan 1994). Their ability to lyse host cells of numerically dominant cyanobacteria species plays a significant and potentially underestimated role in biogeochemical cycling (Fuhrman 1999; Wilhelm and Suttle 1999). Since viral infection is a selective process (Stoddard et al. 2007), it is not surprising that their presence can influence microbial communities. While previous studies have identified cyanophages as significant agents of mortality, others suggest that their role has been largely overestimated (Waterbury and Valois 1993). In these communities, a dominating resistant (*i.e.*, to co-occurring phage) population was thought to enable *Synechococcus* to maintain stable cell densities, resulting in different clonal populations

of *Synechococcus*. Therefore, the rapid evolution of cyanophage resistance alters and influences the dynamics and diversity of the host and infecting phage.

Biogeochemical cycling

Marine viruses are critically important in the regulation and transformation of both carbon and nutrients in biogeochemical cycles (Fuhrman 1999; Suttle 2005; Suttle 2007; Rohwer and Thurber 2009). Although the role of viruses was not originally included in early models of the marine food web or microbial loop, their significance in marine systems has been recognized by ecologists over the last two decades (Bergh et al. 1989; Proctor and Fuhrman 1990). Reports that viruses were potentially significant agents of microbial mortality increased interest in their effects on nutrient cycling. In the late 1990s, the viral shunt was introduced as a modification to the original microbial loop incorporating the lysis of phytoplankton and production of heterotrophic bacteria (Wilhelm and Suttle 1999). The revised model suggests that between 6-26% of organic carbon released from lysed host cells is transferred through the viral shunt to the DOM pool, resulting in higher respiration rates and reducing the transfer efficiency of energy to higher trophic levels. In addition to carbon, viral-mediated processes release other elements such as nitrogen (N) and phosphorus (P). Together carbon, nitrogen and phosphorus play an important role in nutrient cycling and regulating primary production.

Carbon

In marine systems, carbon is divided into two separate pools of particulate organic carbon (POC) and dissolved organic carbon (DOC). While POC is typically transferred to higher trophic levels in the marine food web, DOC is recycled through the microbial loop (Azam et al. 1983; Wilhelm and Suttle 1999). Viral lysis mediates the flux of the global carbon pool by

shifting carbon from POC to DOC (Suttle 2005). This transformation of carbon alters the efficiency of the biological pump (Longhurst and Glen Harrison 1989). Viral lysis reduces the rate that carbon sinks to the bottom of the ocean. As a result, a higher proportion of carbon is retained at the ocean's surface, resulting in higher respiration rates (Suttle 2005). Observations from laboratory studies have shown viral lysis of a phytoplankton bloom can stimulate the growth of heterotrophic bacteria (Gobler et al. 1997; Wilhelm and Suttle 1999). Results from the work of Gobler et al. (1997) predict that cell lysis in the field can potentially generate up to 40 μM of DOC for bacterial uptake. Additionally, experimental evidence suggests that carbon released from control cells is assimilated more readily than carbon released from virally-infected cells which may be larger and less labile (Gobler et al. 1997). Thus, viral lysis affects global carbon cycling and has implications on the amount of carbon sequestered to deep ocean waters.

Nitrogen and Phosphorus

Nitrogen and phosphorus are both important macronutrients in the marine environment. These elements, which can limit primary productivity and mediate the efficiency of the biological pump, exist in either a particulate or dissolved phase (organic or inorganic) (Smith 1984; Downing 1997; Zehr and Ward 2002; Suttle 2007). Despite the longstanding disagreement over which of the two nutrients are truly limiting in the marine environment, it is well understood that both elements play important roles in biogeochemistry (Smith 1984; Downing 1997; Arrigo 2005). More importantly, phytoplankton are capable of readily assimilating labile forms of N and P in the environment, which are recycled in the oceans through processes such as grazing or cell lysis (Tyrrell 1999). The liberated nitrogen and

phosphorus-based compounds from lysed phytoplankton cells are readily available for subsequent uptake by heterotrophic bacteria as a nutrient source.

Viral activity fuels nutrient cycling

Viral activity contributes to the elemental cycling of nitrogen and phosphorus by diverting organic matter away from the classical grazing model and promoting heterotrophic bacterial growth (Proctor and Fuhrman 1990; Haaber and Middelboe 2009). Cell lysis releases phage and cellular debris in the form of DOM (Fuhrman 1999; Middelboe and Jorgensen 2006). A number of studies have shown that viral lysis catalyzes the transfer of energy through the food web (Gobler et al. 1997; Bratbak et al. 1998; Haaber and Middelboe 2009). The results from a study investigating the effects of viral lysis of *Aureococcus anophagefferens* on elemental cycling suggest that bacteria rapidly consume nutrients following lysis. The demise of the bloom was correlated to increases in organic N and bacterial abundance (Gobler et al. 1997). The bacteria were able to re-assimilate more phosphorus in its inorganic form compared to phosphorus released from the lysed phytoplankton. Additionally, it has been shown experimentally that there are differences in the mineralization efficiency of viral-induced substrates (Gobler et al. 1997; Haaber and Middelboe 2009). Both authors found that the lysate-derived P was recycled less efficiently than N. Examples of specific lysate products sustaining heterotrophic growth include both dissolved DNA (D-DNA) (Brum 2005; Holmfeldt et al. 2010) and cell wall compounds (Middelboe and Jorgensen 2006) which provide important sources of amino acids and nucleic acids. The literature collectively suggests that viral activity is of critical importance to the rapid recycling of nitrogen and phosphorus in the oceans.

Viruses shape community structure

In addition to altering the biogeochemistry of marine systems, viruses can impact the genetic diversity and structure of microbial communities. At any given time, approximately 20% of marine heterotrophs are thought to be infected by viruses (Suttle 1994). Furthermore, estimates suggest that viruses may be responsible for removing 20-40% of the prokaryotic standing stock per day, which likely equals or exceeds mortality rates due to grazing (Suttle 1994; Suttle 2007). The influence of viral lysis on prokaryotic diversity has previously been described in the literature through the "killing the winner" hypothesis (Thingstad and Lignell 1997). The "killing the winner" theory explains that once a competitive specialist becomes dominant in a system, its contact rates with viruses should increase, leading to a decline in the dominant species (Thingstad and Lignell 1997; Winter et al. 2010). This theory enables the survival of less abundant members as well as virus-resistant populations in a bacterial community. The selection of virus-resistant populations has been examined in depth through a number of bacterial community studies (Waterbury and Valois 1993; Middelboe 2000; Fuhrman and Schwalbach 2003; Bouvier and del Giorgio 2007).

In other cases, specific populations may benefit from the release of different cell lysis products (*i.e.,* organic matter) allowing resource specialists to become dominant (Riemann et al. 2000; Weinbauer 2004). For example in a chemostat study investigating the dynamics between a single marine phage and its host (*Pseudoalteromonas*), the phage-resistant population replaced the sensitive population (Middelboe 2000). The lysis products released from the infected host stimulated the growth of the resistant population, enabling the non-infected population to dominate. Another study using multiple host-phage systems confirmed these results and concluded that the change in clonal composition was likely due to viral lysis over a long time

scale (Middelboe et al. 2001). Based on these results, specific lysate products stimulate the growth of nutrient specialists and the overall growth of the surviving bacterial community.

In contrast to focusing on the direct effects of viruses, others have studied the indirect effects of viral lysis on non-target bacteria. Middelboe et al. (1996) investigated the growth rates of non-infected bacteria in a natural bacterioplankton community and found that lysis products may serve as an important nutrient source for the non-infected bacterial community. Lennon and Martiny (2008) conducted a chemostat experiment examining the direct effects of a cyanophage on *Synechococcus* population dynamics, nutrient availability and microbial stoichiometry in a P-limited system. This study also provided insight into the indirect effects of a cyanophage on heterotrophic bacterial community structure. Findings from this study suggested that the presence of viruses did not significantly impact the abundance or composition of the heterotrophic bacterial community based on T-RFLP (terminal restriction fragment length polymorphism) profiles. Additionally, viruses may also indirectly influence community composition via viral-mediated grazer lysis (reducing bacterial predation) or through species-specific growth responses to organic substrates recycled in the system (Weinbauer and Rassoulzadegan 2004; Suttle 2007). To date, the indirect effects of viruses on the non-target bacterial community are unclear and have yet to be further investigated in detail.

Evidence for virus resistance

Chemostat studies reveal rapid evolution of virus resistance

Chemostats (also referred to as continuous cultures) have been used for years as model systems to link simple laboratory communities to large-scale, complex ecological dynamics and community-level evolutionary theory (Droop 1974; Lenski and Levin 1985; Bohannan and

Lenski 1997; Bohannan et al. 1999; Bohannan and Lenski 2000; Middelboe 2000; Lennon et al. 2007; Middelboe et al. 2009). The earliest models of virus-host systems within chemostats examined the co-evolution of *Escherichia coli* (*E. coli*) B and its lytic T-series bacteriophages (Lenski and Levin 1985; Lenski 1988). In this set of experiments, phage-resistant and resource-limited *E. coli* populations readily evolved in the closed system (Lenski and Levin 1985). Although no phage mutants co-evolved in the experiment, the wildtype phage was able to persist due to a small population of susceptible bacteria that were able to outcompete the resource-limited resistant *E. coli*. Other studies have investigated the effects of nutrient enrichment on bacteria-bacteriophage dynamics (Bohannan and Lenski 1997). Increases in the equilibrium density of both *E. coli* B and bacteriophage T4 were observed in response to glucose enrichment. The enrichment reduced the amount of time it took for phage-resistant mutants to emerge and increased the rate at which they appeared. Collectively, these small-scale evolutionary processes frequently observed in chemostats imply that resistant populations are selected for in response to bacteriophage, enabling the coexistence of competitors (sensitive and resistant phenotypes) and altering the dynamics and structure of the bacterial community.

For *E. coli*, populations resistant to all of the T-series phages have been reported (Lenski 1988). When a specific mutation occurs that confers resistance to a lytic phage, the density of bacteria can dramatically increase, sometimes by orders of magnitude until the population becomes resource-limited in a chemostat (Chao et al. 1977). After resistant populations evolve and dominate the system, the virulent phage is sustained by a minority population of sensitive bacteria that are successful resource competitors (Lenski and Levin 1985). Furthermore, a tradeoff between resistance and competitive ability is typically associated with the evolution of viral resistance (Bohannan and Lenski 2000). This tradeoff is often referred to as a cost of

resistance (COR). Examples of fitness reductions in bacteria include lower rates of resource uptake, reduced growth rates or increased susceptibility to other phages (Bohannan and Lenski 1997; Bohannan et al. 1999). Thus, phage-resistant strains have a competitive disadvantage to their co-occurring wildtype strains. The magnitude of the COR can vary depending on a number of factors including the specific mutation, resource availability and the identity of other phages in the system (Bohannan et al. 1999; Bohannan et al. 2002; Lennon et al. 2007).

While a number of chemostat studies have focused on clinically relevant bacteria (Chao et al. 1977; Lenski and Levin 1985), population dynamics have also been explored in marine systems. Evolution of virus resistance in these systems has become increasingly recognized, but still remains highly understudied (Suttle and Chan 1994; Lennon et al. 2007; Stoddard et al. 2007). These studies have investigated the effects of phage on ecologically relevant marine bacteria and cyanobacteria (Bratbak and Thingstad 1985; Bratbak et al. 1998; Middelboe 2000; Middelboe et al. 2001; Lennon et al. 2007). In the mid-1980s, Bratbak and Thingstad (1985) sought to understand how a mixed algal-bacterial system would respond to P-limited conditions in a continuous culture. Their conclusions suggest that increasing the degree of nutrient limitation resulted in higher abundances of bacteria and lower abundances of algae. Middelboe et al. (2001) found that bacterial diversity was driven by interspecies competition following the initial lytic event. Although the overall bacterial density was not affected by phage, the clonal composition was significantly influenced, resulting in a complete shift of sensitive to resistant cells within a time span of 5 to 10 generations (Middelboe et al. 2001). This example of clonal composition change in a biological system supports the production of high phage titers in the presence of sensitive and resistant populations which refutes previous assumptions rejecting the importance of resistant strains in marine communities (Fuhrman 1999).

Resistance in cyanobacteria

Despite previous literature on host-phage interactions, a general mechanism of loss of infectivity in cyanobacterial host systems has yet to be investigated in detail. Hypothesized resistance mechanisms in cyanobacteria include variability in phage receptors, lipopolysaccharide modifications, restriction-endonuclease systems, lysogeny as a form of immunity and the novel CRISPR (Clustered Regularly Interspaced Short Palindromic Repeats) defense system (Wilson et al. 1993; Xu et al. 1997; Mann 2003; Barrangou et al. 2007). The discovery that marine cyanophages were capable of infecting both *Prochlorococcus marinus* and a *Synechococcus* strain, suggests conservation of phage receptor expression among cyanobacteria (Sullivan et al. 2003). The identity and diversity of receptors and other receptor-like structures likely contribute to the attachment specificity of cyanophages in the environment, leading to evolved resistance in some cyanobacterial populations (Stoddard et al. 2007).

Avrani et al. (2011) unveiled genome-level evidence of viral resistance among mutant strains of *Prochlorococcus*. In the study, a virus-resistant population of *Prochlorococcus* emerged following a lytic podocyanophage infection. The resulting phage-resistant population was characterized by gene mutations involved in the biosynthesis of putative viral receptors on the host cell surface with the majority of mutant genes confined to a specific region of the genome. In addition to impaired phage attachment to the cell surface, the mutations also imposed a COR on the mutant genotypes resulting in a reduced growth rate and increased susceptibility to other viruses similar to previous studies (Bohannan and Lenski 2000; Lennon et al. 2007). These findings suggest that gene mutations are capable of shaping host subpopulations of both sensitive and resistant genotypes and support the stable existence of co-occurring cyanophages in the environment (Avrani et al. 2011).

Next-generation sequencing

Accurately estimating the diversity of a microbial community remains a challenge in the field of microbial ecology. Prior to its development, automated Sanger sequencing dominated the DNA sequencing industry (Sanger et al. 1977). However, a number of limitations and challenges associated with Sanger-based sequencing gave rise to next-generation sequencing technologies (Metzker 2010). These new sequencing methods have enabled deeper community analyses by generating orders of magnitude more sequence data and revealing a remarkable degree of prokaryotic diversity in the environment (Tringe and Hugenholtz 2008). Next-generation sequencing platforms (e.g. Roche's 454 Genome Sequencers, Illumina's Solexa/Genome Analyzer and Applied Biosystem's SOLiD) can be coupled with a culture-independent 16S ribosomal ribonucleic acid (rRNA) gene analysis. The 16S rDNA technique is widely used to identify and understand the diversity of bacteria, and the universality of the gene makes it ideal for comparison to current databases (Woese 1987; Wang et al. 2007).

These methods are more robust and increasingly cost-effective compared to traditional Sanger sequencing. Although next-generation sequencing platforms can rapidly generate enormous amounts of data in a short amount of time (Mardis 2008), the technologies are still limited by shorter read lengths and less accurate base-calls (Shendure and Ji 2008). The development of 454 Titanium-based pyrosequencing (454 GS FLX Titanium) increased the average read length to 400-500 base pairs (bp) (Sogin et al. 2006), compared to 250 bp generated by 454 GS FLX chemistry. While the Illumina and SOLiD systems provide more sequence data, they both produce much shorter reads making the 454/Roche system a cost-effective option for relatively longer sequence lengths. The pyrosequencing process also offers the capability to multiplex through the use of unique DNA sequence tags referred to as barcodes that can be

incorporated via primers (Parameswaran et al. 2007). Using barcoding technology, multiple samples can be pooled in one run for high-throughput sequencing. Pyrosequencing data can then be used to classify sequences taxonomically to reference databases and standard indices (*i.e.,* species richness, species evenness, and diversity) can be calculated to assess the dynamics and microbial composition of bacterial communities.

Bias in pyrosequencing studies

Despite the powerful nature of the approach, pyrosequencing suffers from a set of challenges and drawbacks. Sampling size is considered one of the biggest challenges in microbial diversity studies (Lemos et al. 2011). Two factors that must be considered in microbial community studies are i) how many sequences must be acquired from each sample to adequately characterize diversity (*i.e.,* sequencing depth) and ii) how unequal sample sizes affect overall conclusions. A number of studies have concluded that diversity indices are directly tied to sampling effort and must be normalized to make reasonable comparisons across studies (Hughes et al. 2001; Youssef et al. 2009; Gihring et al. 2011; Lemos et al. 2011). A recent study conducted by Gihring et al. (2011) emphasized the importance of randomly subsampling pyrosequenced libraries to overcome the variation often reported across samples. Remarkably, only one quarter of the studies they reviewed normalized their dataset by subsampling. The authors suggest that future studies should subsample to eliminate this type of bias.

Other factors reported to bias pyrosequencing data include PCR conditions (Martin 2002), primer choice (Engelbrektson et al. 2010), amplicon length (Huber et al. 2009), operational taxonomic unit (OTU) clustering (Hughes et al. 2001; Huse et al. 2010) and fragment choice (Wang and Qian 2009; Youssef et al. 2009). OTUs are frequently described at different levels in the literature making diversity comparisons across studies very challenging (Martin

2002). This source of bias could be overcome by keeping OTU cutoffs defined and consistent across studies (Hughes et al. 2001). For amplicon length, shorter amplicons (less than 400 bp) have resulted in higher richness estimates than longer ones (Huber et al. 2009). Furthermore, fragment choice can underestimate or overestimate the number of OTUs defined at different cutoffs (Youssef et al. 2009). Thus, region choice of the 16S rRNA gene must be selected with great caution depending on the desired fragment length to make appropriate conclusions using taxonomic assignments and standard indices (Wang and Qian 2009). Another source of error in pyrosequencing of the 16S rRNA gene is the formation of chimeras (Haas et al. 2011; Quince et al. 2011). Chimeras are generated during the PCR step when an aborted extension product serves as a primer in the next PCR cycle, resulting in a sequence derived from two separate parents (Meyerhans et al. 1990). In order to reduce sequencing error, a number of programs have been developed such as Bellerophon, ChimeraSlayer and UCHIME to detect chimeras (Huber et al. 2004; Edgar et al. 2011; Haas et al. 2011). Previous pyrosequencing studies of the 16S rRNA gene have also included sequencing a mock community sample as a control (Huse et al. 2010). By including a defined community of 16S rRNA gene sequences with each run, pyrosequencing error and processing drift can be accurately assessed.

To date, the reproducibility of amplicon-based sequencing has not been addressed extensively in the literature. A recent study by Zhou et al. (2011) reported low reproducibility with regards to OTU overlap among technical replicates due to random sampling processes (e.g. selective PCR amplification, bead deposition). However, when singletons or less representative sequences of OTUs were removed from the dataset, the OTU overlap increased significantly. Conversely, other studies using the GS FLX and Illumina platforms have demonstrated much higher levels of sequencing reproducibility (Bartram et al. 2011; Kauserud et al. 2011). Others

have developed methods to improve pyrosequencing reproducibility such as using a two-step barcoding approach that reveals more sequence diversity than the standard one-step method (Berry et al. 2011). The bias resulting from their barcoded primers is unclear, but the authors suggest it may be a result of unknown interactions between the DNA template and barcode. With the limited number of publications in the literature, more comparisons will be necessary to validate the technical sequencing reproducibility of next-generation sequencing platforms.

RESEARCH OBJECTIVES

While the direct effect(s) of viruses on marine microbial communities have been well documented in the literature, less emphasis has been placed on understanding the indirect effects of viruses on the non-target microbial community. The overall goal of this study was to determine if the indirect effects of a cyanophage (*Cyanomyoviridae*) or nutrient limitation (nitrogen or phosphorus deplete conditions) affected the structure of the co-occurring heterotrophic bacteria in a long-term chemostat experiment. In our approach, we used 454 Titanium barcoded pyrosequencing of the 16S rRNA gene to characterize the structure and microbial diversity of nine individual nutrient-limited chemostats with or without cyanophage over time. We also assessed the technical reproducibility of sequencing on the 454 Titanium platform. In this thesis, we address our questions with the following specific hypotheses:

> H_1: The heterotrophic bacterial community structure in a chemostat is different under nitrogen-limited conditions than phosphorus-limited conditions.
>
> H_2: The presence of cyanophage results in a different heterotrophic community structure in a chemostat.

METHODS

Chemostat setup and sample collection

The experimental setup was based on a set of established techniques from a previous chemostat experiment (Lennon et al. 2007). Briefly, chemostats were set up based on a 2 x 2 factorial design altering N : P ratios and exposure to the phage (Larsen and Lennon, unpublished). Stoichiometric nutrient ratios of N ($NaNO_3$, sodium nitrate) : P (K_2HPO_4, dipotassium phosphate) were adjusted to 10 : 1 and 40 : 1, respectively to simulate N-limiting and P-limiting growth conditions. The host, *Synechococcus* strain (WH7803) was derived from a single colony isolate and was added to ten chemostats (five per nutrient supply ratio, each consisting of three phage additions and two controls). Each chemostat was maintained at 40 mL volumes of a modified version of 'AN' artificial seawater (Waterbury and Willey 1988) at a dilution rate of 1 d^{-1} and stirred continuously with a star stir bar. All chemostats were incubated in a growth chamber at 25°C on a 14 : 10 light : dark cycle at 15-17 μmol photons $m^{-2}s^{-1}$. Prior to phage addition (day -62), one of the N-limited controls was lost due to fungal contamination. Beginning on day -63, the 'AN' media was further amended with cyclohexamide to control fungal growth. Nitrogen and phosphorus concentrations were adjusted as necessary to achieve equal steady state densities, but ratios remained constant. The cyanomyovirus, S-RIM8 (Marston and Sallee 2003) was added to the phage-amended chemostats (2.5 mL of 7.65 x 10^6 phage mL^{-1}) 126 days after bacterial equilibrium was achieved. Bacterial equilibrium was defined based on predictions by previous chemostat models.

Cyanobacteria and cyanophage were quantified 3 times per week via epifluorescence microscopy (Larsen and Lennon, unpublished). One hundred to 500 μL of each chemostat

sample was filtered onto black polycarbonate filters and visualized under a CY3 filter set. For viral counts, samples were pre-filtered through a 0.2-µm syringe filter and filtered onto a 0.02 micron Anodisc™ filter (Whatman®). Filters were stained with SYBR Green® (Invitrogen) and incubated for 10 min in the dark (Noble and Fuhrman 1998). After drying, filters were fixed with an anti-fade solution, 4 : 1 Citifluor : Vectashield, and counted under a FITC filter set. A counting program was used to enumerate total cyanomyophages from ten images per sample with the assumption that all phages in the chemostat samples were cyanophages.

Whole, unfiltered aliquots were sampled from each chemostat every other day and cryopreserved with a final concentration of 2.5% glutaraldehyde for flow cytometry. Additionally, whole samples were frozen without a cryoprotectant for downstream qPCR analysis. All frozen samples were stored at -80°C until further analysis. A flow chart of methods is available in the appendix (Figure 26).

Note: Chemostat setup, microscope counts and cryopreservation steps were completed by Megan Larsen at Michigan State University. All subsequent steps were performed as a part of this study at the University of Tennessee – Knoxville.

Flow cytometry methods and acridine orange slide preparation

Although the *Synechococcus* was originally derived from a single colony isolate, contaminating heterotrophic bacteria were present in the chemostats based on preliminary microscopic observations. These heterotrophs were likely introduced to the chemostats from the picked colony or may have entered the system over the course of the experiment during sampling. In order to gate and confirm heterotrophic bacterial populations on the flow cytometer, bacteria were enumerated on an epifluorescence microscope using a published acridine orange protocol. Acridine orange (Invitrogen) counts were used as a reference for

gating total bacteria on the Guava EasyCyte 6HT 2L (Millipore) flow cytometer. Three replicate samples were thawed, diluted and filtered onto slides stained with acridine orange using a slightly modified published protocol (Sherr et al. 1993). Diluted, 2-mL samples were collected on a 25 mm 0.45-μm HAWP backing filter (Millipore) and a 0.2-μm GTBP Isopore™ membrane filter (Millipore). Ten μL of 1% w/v 0.22 μm-filtered acridine orange stain was mixed into the sample. After staining for 3 minutes under reduced light, the filter was rinsed and mounted onto a slide with immersion oil. Autotrophic (*Synechococcus*) cells were enumerated via epifluorescence microscopy using a Leica DMRXA under a Texas Red filter set (λ_{Ex}, 595 nm; λ_{Em}, 610 to 615 nm) while total bacteria were counted under a blue light filter (λ_{Ex}, 450 to 490 nm; λ_{Em}, 510 nm). Total counts were recorded for a minimum of 10 fields or 200 total cells. The number of heterotrophic bacteria was calculated as the difference between *Synechococcus* counts and total bacterial counts. The average number of heterotrophic bacteria from the replicate filters was used to gate total bacterial populations on the flow cytometer.

A modification of an established protocol by Tripp (2008) was used to count heterotrophic bacterial cells and *Synechococcus* cells. Frozen 1-mL samples preserved in 2.5% glutaraldehyde were thawed on ice and prepared using a 10-fold dilution series in 0.22 μm filtered 'AN' media. Diluted samples were transferred to two 96-well clear, flat bottom, polystyrene plates (BD-Falcon™) for flow cytometry. In addition to chemostat samples, media blanks were also prepared in triplicate. To enumerate total bacteria, a working stock of SYBR Green (Molecular Probes) was added to each well of one plate at a final dilution of 1 : 3000. The stained plate was incubated in the dark at room temperature for one hour. No SYBR Green was added to the second plate in order to enumerate *Synechococcus* via autofluorescence.

Both 96-well plates were counted using a Guava 6HT 2L (Millipore) flow cytometer. A combination of autotrophic cell counts, acridine orange microscope counts and histogram gating was used to differentiate and rapidly enumerate heterotrophic bacterial cells and *Synechococcus* cells using plots of log green and log red fluorescence versus forward scatter (Figure 27 and Figure 28 in Appendix). Flow cytometer counts were subtracted from blanks and compared to direct microscope counts of *Synechococcus* cells. To assess technical reproducibility of our counts, some samples were run in triplicate as analytical replicates for 6 of the time points for the N-limited control and one of the P-limited controls to calculate the coefficient of variance. The average overall coefficient of variance for *Synechococcus* counts was 26% while the average coefficient of variance for heterotrophic bacteria counts was 19%.

Community DNA extraction

For community DNA analysis, cryopreserved chemostat samples were thawed and maintained on ice for all subsequent steps. Each tube was vortexed for 5 seconds prior to being aliquoted into a 1.5-mL microcentrifuge tube. A 500 µL sample was brought to 1000 µL with autoclaved, 0.22-µm PVDF filter-sterilized (Millipore) Milli-Q water. Cells were pelleted by centrifugation at 21,000 g for 20 minutes at 4°C (Thermo IEC MicroMax RF centrifuge). The supernatant was removed using a P1000 pipettor followed by a P40 pipettor.

Cells were lysed and DNA was extracted using a modification of a direct PCR protocol (Long and Azam 2001). Pellets were resuspended in 10 µL of Lyse-N-Go™ (Thermo Scientific) and transferred to a 200-µL autoclaved, UV-sterilized PCR tube. The tubes were heated briefly in a thermal cycler (Bio-Rad PTC-200 DNA Engine® Peltier Thermal Cycler) to enhance DNA release. Cycling conditions for cell lysis of the Lyse-N-Go™ treated cells were set as indicated by the manufacturer's protocol: 65°C for 30 seconds, 8°C for 30 seconds, 65°C for 1.5 minutes,

97°C for 3 minutes, 8°C for 1 minute, 65°C for 3 minutes, 97°C for 1 minute, 65°C for 1 minute, and held at 80°C until PCR reagents were added.

PCR amplification

Genomic DNA from each sample was amplified using 16S rRNA gene bacterial primers 338F (5'-ACTCCTACGGGAGGCAGCAG-3') and 926R (5'-CCGTCAATTCMTTTRAGT-3') spanning the V3 to V4 hypervariable regions (Huse et al. 2008) (Table 4 in Appendix). A primer matrix was performed to optimize primer concentrations for 16S rRNA gene amplification. Pairwise combinations of four different primer concentrations (0.1 µm, 0.2 µm, 0.4 µm, and 0.8 µm) were tested to identify the optimal primer concentrations for the samples.

PCR reactions were performed in 25 µL volumes consisting of 1 µL of template DNA, 5X High Fidelity PCR Buffer (Invitrogen), 0.4 mM DNTPs (Invitrogen), 0.7 mM $MgCl_2$ (Promega), 0.2 µm of primer 338F (Operon), 0.8 µm of primer 926R (Operon) and 1 U of Platinum® TaqDNA Polymerase High Fidelity (Invitrogen). Thermal cycling conditions consisted of an initial denaturation of 95°C for 5 minutes, followed by 30 cycles of denaturation at 95°C for 30 seconds, annealing at 56°C for 30 seconds, extension at 72°C for 1.5 minutes, and a final extension at 72°C for 10 minutes in a Bio-Rad PTC-200 DNA Engine® Peltier Thermal Cycler. The products were run on a 1% agarose gel at 120 volts for 40 minutes and stained with ethidium bromide for 20 minutes. PCR products were purified using the QIAquick PCR purification kit (Qiagen), eluting with 30 µL Tris-HCl, according to the manufacturer's specifications. The DNA concentration and quality ($A_{260/280}$) were quantified on a NanoDrop® ND-1000 Spectrophotometer (Thermo Scientific) and final products were stored at -20°C.

Barcoded amplicon library construction and 454 Titanium pyrosequencing

Oligonucleotides were designed to include GS FLX Titanium sequence adapters (A and B) fused to the 5' end of 338F (A adapter: 5'-CCATCTCATCCCTGCGTGTCTCCGAC-3') and 926R (B adapter: 5' CCTATCCCCTGTGTGCCTTGGCAGTC-3') (Operon), a key sequence (TCAG) for quality control, and a unique 8 nucleotide (nt) error-correcting barcode for each sample (Hamady et al. 2008). Twenty-two individual barcodes were used twice to barcode a total of 44 samples (Table 4 in Appendix). Samples were divided into 5 groups to achieve an equimolar concentration (1 ng/µL) of template DNA based on direct quantification from spectroscopy. PCR reactions were performed in 25 µL volumes consisting of 1 to 3 µL of template DNA, 5X High Fidelity PCR Buffer (Invitrogen), 0.4 mM DNTPs (Invitrogen), 0.7 mM $MgCl_2$ (Promega), 0.2 µm of primer 338F with adapter A (Operon), 0.8 µm of primer 926R with adapter B, (Operon) and 1 U of Platinum® TaqDNA Polymerase High Fidelity (Invitrogen). One or two duplicates of each template DNA volume were prepared to run on the agarose gel to verify attachment of the barcode.

Barcoding PCR parameters consisted of an initial denaturation of 95°C for 5 minutes, then 6 cycles of denaturation at 95°C for 30 seconds, annealing at 55°C for 30 seconds, and extension at 72°C for 30 seconds, followed by a final extension at 72°C for 10 minutes on a thermal cycler. The barcoded products were run on a 1% agarose gel at 120 volts for 40 minutes and stained with ethidium bromide to visualize bands. At least two unbarcoded duplicate samples from the first PCR amplification were run on the gel adjacent to barcoded samples to confirm the 50 bp product shift expected with barcode attachment.

The 44 barcoded products were purified using QIAquick PCR purification columns (Qiagen) and pooled as two separate sets (22 samples each) with one modification to the

manufacturer's protocol; PCR water was used to elute 40 uL of pooled DNA from each column. Each set of pooled amplicons was quantified on a NanoDrop® ND-1000 Spectrophotometer (Thermo Scientific) and stored at -20°C. Pooled amplicons were submitted to the UT/ORNL *Joint Institute of Biological Sciences* for unidirectional pyrosequencing using GS FLX Titanium chemistry (LIB-L kit) on a Roche 454 GS FLX Instrument (454 Life Sciences). The LIB-L kit has been recommended over other kits given its low cost and high number of reads (Tamaki et al. 2011). To compare technical sequencing reproducibility, both sets of barcoded samples were sequenced in duplicate across four regions of a PicoTiter Plate (454 Life Sciences).

Sequence data processing

Initial sequence pre-processing was completed using the program MOTHUR v.1.20.0 (Schloss et al. 2009) following the Costello stool analysis tutorial (http://www.mothur.org/wiki/Costello_stool_analysis). In order to compare technical sequencing reproducibility, both technical replicates were analyzed separately. Sequences were trimmed in MOTHUR to remove the following: sequences with 2 mismatches to their respective primers, sequences with 1 mismatch to their respective barcode, sequences with an average quality score lower than 35 over an average window size of 50 bases, sequences with more than 8 homopolymers, and sequences with ambiguous bases. After screening and sorting, good quality sequences were submitted to the Ribosomal Database Project (RDP, http://rdp.cme.msu.edu) Classifier (Cole et al. 2009) to compare taxonomic classifications across technical replicates. Each region was submitted individually and classified using the RDP Naïve Bayesian rRNA Classifier Version 2.2 (March 2010) to examine and compare the technical sequencing reproducibility of 454 Titanium pyrosequencing at the phylum level.

To simplify the dataset, a set of non-redundant sequences was obtained. Good quality sequences were aligned with the MOTHUR-formatted SILVA-compatible database (http://www.arb-silva.de/) (Pruesse et al. 2007). Newly produced replicates from the sequence dataset were removed and screened in MOTHUR to achieve the greatest region of overlap for sequence analysis. The following parameters were set to maximize sequence overlap: the start and end positions were set to 6428 and 15500, respectively and the minimum base length setting was optimized to retain 85% of the sequences. The resulting filtered alignment was 442 positions long with a range of 185 to 215 bases. To reduce pyrosequencing noise, the single-linkage preclustering method was used to "pre-cluster" sequences to reduce spurious clustering (Huse et al. 2010). The algorithm is designed to identify rarer sequences with one mismatch and merge them with more abundant sequences.

Chimera-like sequences were identified using the chimera.uchime algorithm in MOTHUR based on the original UCHIME program (Edgar et al. 2011) using the SILVA-database as a reference to detect chimeric sequences. After removing potentially chimeric sequences, the dataset was classified using the MOTHUR-formatted RDP training set. Sequences were assigned using the Bayesian method with a kmer value of 8 and 100 iterations. In order to analyze the heterotrophic bacterial community, all sequences classified as cyanobacteria were removed from the dataset for the remainder of the analysis.

In MOTHUR, a distance matrix was generated, clustered using the average-neighbor algorithm (Huse et al. 2010) and assigned to OTUs using 97% similarity. To compare the similarity of communities across technical replicates, a dendrogram was generated in MOTHUR using the Yue and Clayton measure of dissimilarity. The sequences were clustered again using

the average neighbor algorithm and assigned to OTUs using 97% similarity in order to analyze the heterotrophic community by itself.

Pooling samples

In order to increase the number of sequences used in the analysis, sequences for both technical replicates from each library were pooled after sorting, removing barcodes and primers and setting quality parameters enabling analysis of sequences of the same filtered length. All subsequent steps in the pooled analysis of technical replicates were repeated as previously mentioned for the non-pooled sequence steps including removal of cyanobacterial sequences and OTU-based analyses using 97% similarity.

Statistical analyses

Differences in community structure among time points and between nutrient-limited and cyanophage treatments were analyzed in PRIMER 6.0 (Anderson et al. 2006). Data was standardized to relative abundances and fourth-root transformed to downweight the importance of the most abundant OTUs. Samples were compared based on OTU abundances using the zero-adjusted Bray-Curtis measure of similarity (Clarke et al. 2006). The Bray-Curtis measure is a popular index used widely in ecological studies involving species abundance data. Results from the resemblance matrix were visualized using hierarchical cluster analysis (average cluster linkage) and non-metric multidimensional scaling (MDS) (Field et al. 1982) with Kruskal's stress formula set to a minimum stress of 0.01 using 25 iterations. To determine the effect of singletons, doubletons and less abundant sequences, an additional resemblance matrix was generated from the 10 most abundant OTUs from our dataset. This subset of data was clustered using the average cluster linkage method and visualized on a MDS plot for comparison.

PERMANOVA+ (permutational-based analysis of variance) for PRIMER 6 was used to perform multivariate data analyses to test for significant differences in community structure between nitrogen and phosphorus-limited libraries ("Nutrient") as well as control and cyanophage-amended libraries ("Virus"). PERMANOVA+ was also used to detect community change over the course of the experiment ("Day"). A PERMANOVA was performed with 9,999 iterations and the Type III sums of squares to compare the following factors: "Nutrient" versus "Virus," "Nutrient" versus "Day" and "Virus" versus "Day." If there were significant differences between any of the main factors with more than two levels (*i.e.*, day), further pairwise comparisons were tested separately for each factor to identify within-group differences. For statistically significant interactions, further pairwise tests were performed among pairs of levels of the factor of interest.

RESULTS

Nitrogen-limited chemostat dynamics

In the N-limited control chemostat without cyanophage (Figure 1), *Synechococcus* populations maintained an equilibrium density of $1.2 \times 10^7 \pm 3.5 \times 10^6$ cells mL^{-1} for the subset of ten time points selected for flow cytometry (FC). Epifluorescence counts (EM) of autotrophic cells for time points after steady state was achieved ($1.4 \times 10^7 \pm 1.5 \times 10^6$ cells mL^{-1}) were statistically similar to FC counts (Figure 29 in Appendix, $r^2 = 0.4258$, n=90, $p < 0.0001$). Heterotrophic bacterial populations fluctuated, increasing to 1.3×10^8 and decreasing to 2.9×10^7 cells mL^{-1} at the final FC time point (day 132).

Conversely, in the N-limited, phage-amended chemostats (Figure 2, Figure 3, Figure 4), *Synechococcus* densities declined rapidly in all 3 replicate chemostats, reaching very low densities (FC: 1.7×10^5 cells mL^{-1}; EM: 9.3×10^4 cells mL^{-1}) within the first 50 days of phage addition (day 0). Cyanomyophage reached abundances as high as 1.0×10^9 virus-like particles mL^{-1} during the period of decline. However around day 50, the *Synechococcus* population recovered in all 3 replicate chemostats, as indicated by an exponential increase in cell abundance. By day 100, *Synechococcus* abundances declined again (FC: 2.7×10^7 cells mL^{-1}; EM: 3.5×10^6 cells mL^{-1}) in phase with high phage counts reaching upwards of 5.8×10^8 virus-like particles mL^{-1}. In 1 out of 3 chemostats, *Synechococcus* populations recovered again around day 150. Heterotrophic bacterial counts via flow cytometry were consistently higher than *Synechococcus* counts with the exception of one time point in each of the phage-amended chemostats. Heterotrophs reached their maximum abundances during the initial crash at times when *Synechococcus* counts were lowest in 2 of 3 replicate chemostats.

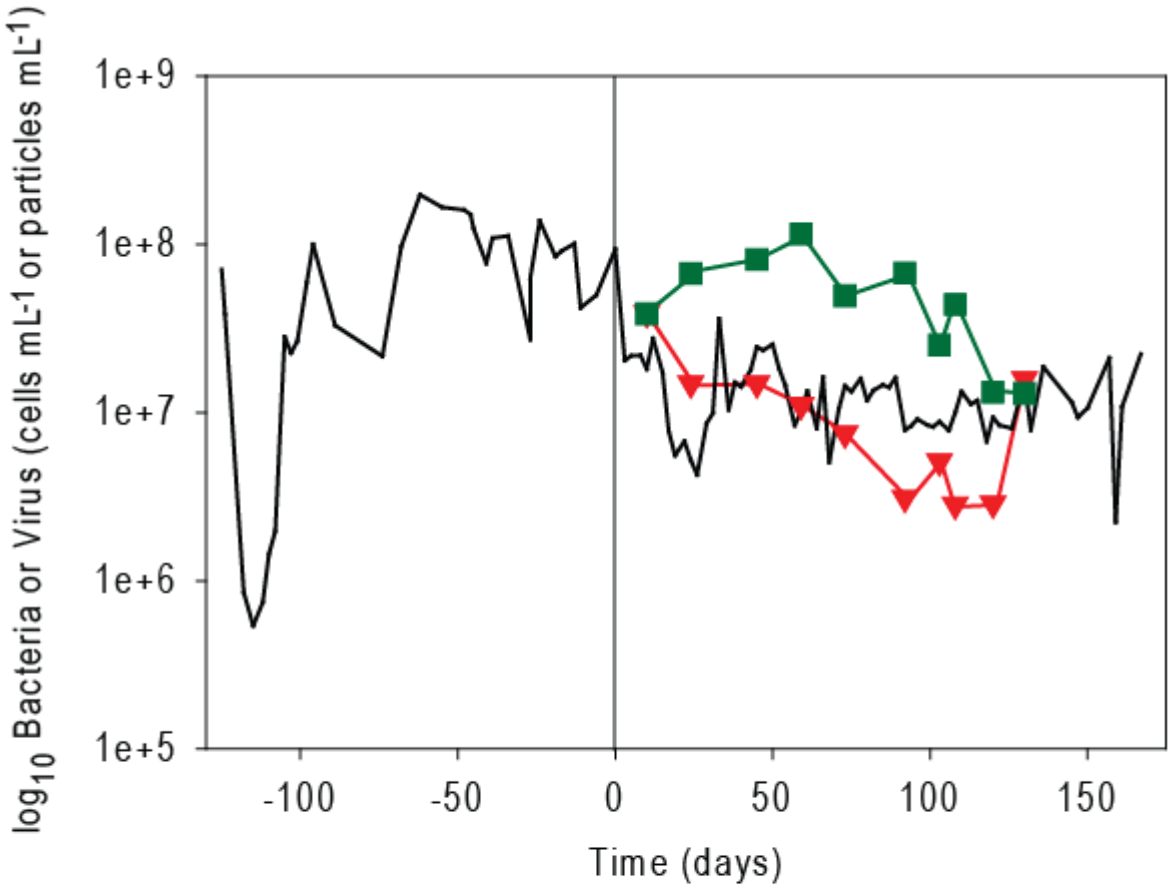

Figure 1: Microscope and flow cytometry counts of *Synechococcus* and heterotrophic bacteria from the nitrogen-limited control chemostat. *Synechococcus* microscope counts (black lines), *Synechococcus* flow cytometry counts (red triangles) and heterotrophic bacteria flow cytometry counts (green squares) are shown for one individual chemostat (n=1). The vertical line at day 0 denotes the day after steady state was achieved. Epifluorescence microscope counts were provided by Megan Larsen (Michigan State University).

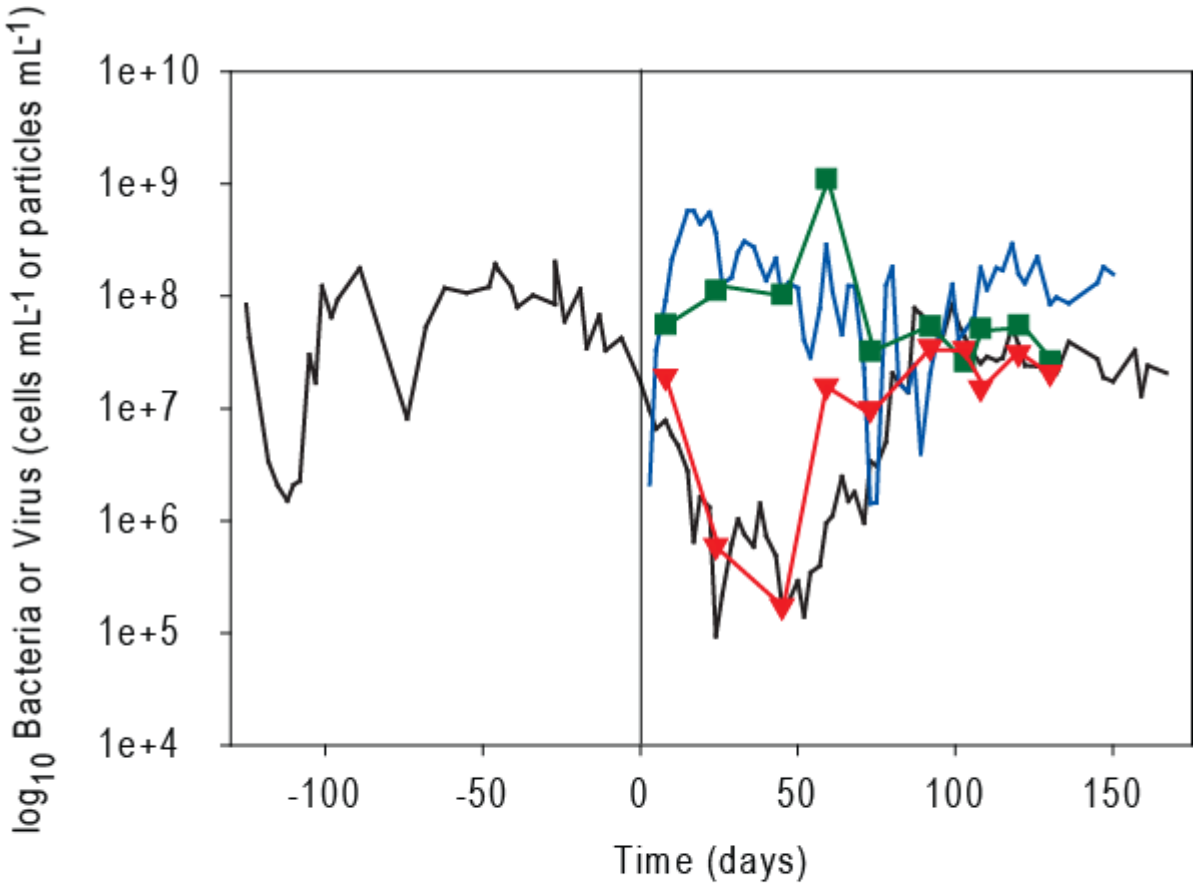

Figure 2: Microscope and flow cytometry counts of *Synechococcus,* heterotrophic bacteria and cyanophage from a nitrogen-limited, phage-amended chemostat (biological replicate 1). *Synechococcus* microscope counts (black lines), *Synechococcus* flow cytometry counts (red triangles), heterotrophic bacteria flow cytometry counts (green squares) and phage microscope counts (blue lines) are shown for one chemostat (n=3). The vertical line at day 0 denotes the day phage was added. Epifluorescence microscope counts were provided by Megan Larsen (Michigan State University).

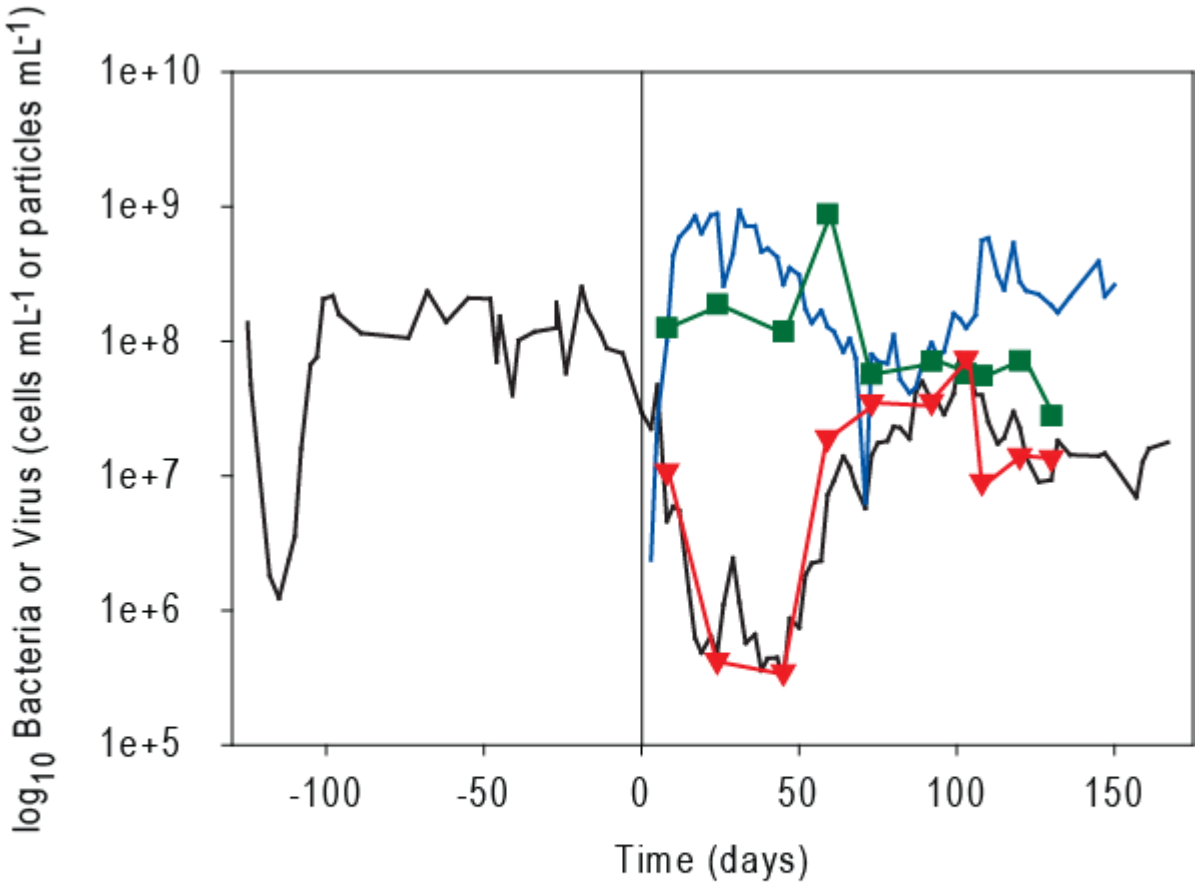

Figure 3: Microscope and flow cytometry counts of *Synechococcus,* heterotrophic bacteria and cyanophage from a nitrogen-limited, phage-amended chemostat (biological replicate 2). *Synechococcus* microscope counts (black lines), *Synechococcus f*low cytometry counts (red triangles), heterotrophic bacteria flow cytometry counts (green squares) and phage microscope counts (blue lines) are shown for one chemostat (n=3). The vertical line at day 0 denotes the day phage was added. Epifluorescence microscope counts were provided by Megan Larsen (Michigan State University).

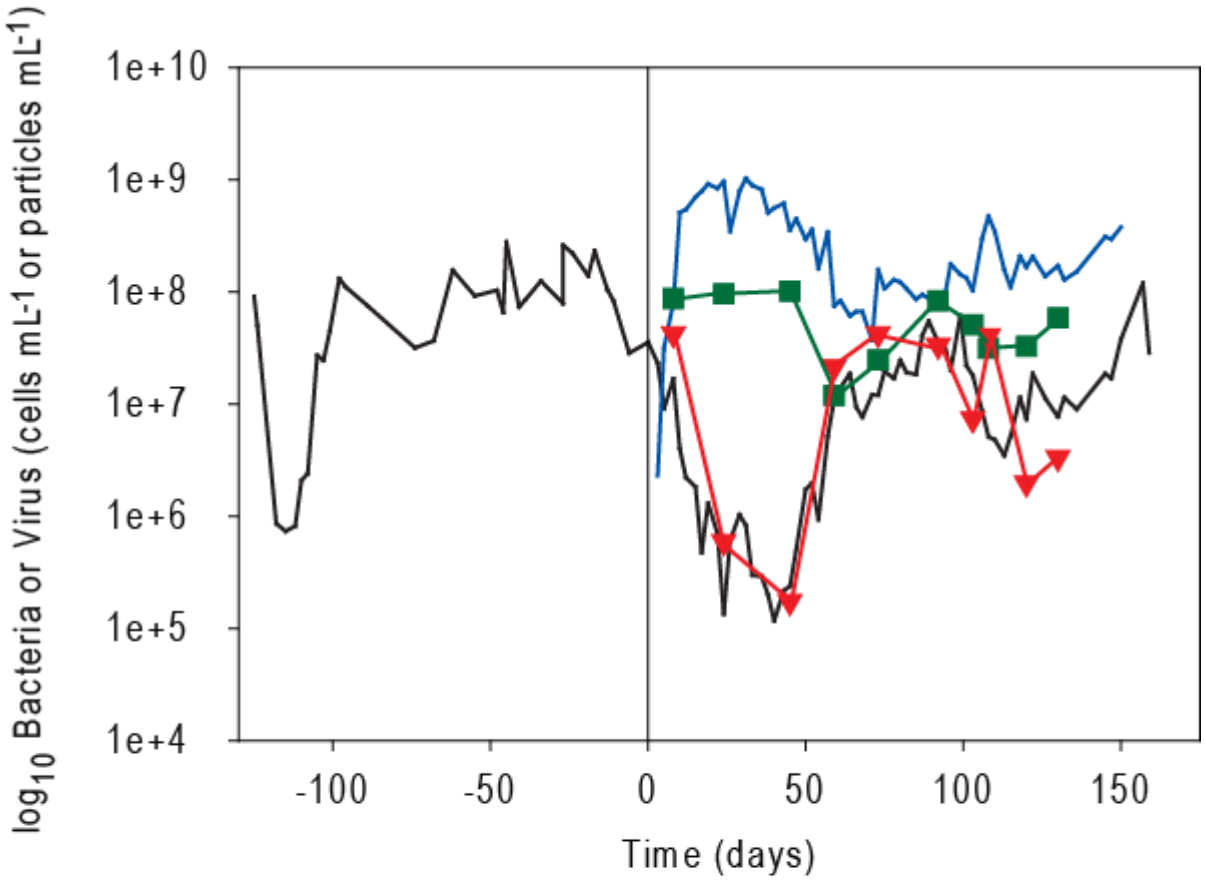

Figure 4: Microscope and flow cytometry counts of *Synechococcus*, heterotrophic bacteria and cyanophage from a nitrogen-limited, phage-amended chemostat (biological replicate 3). *Synechococcus* microscope counts (black lines), *Synechococcus* flow cytometry counts (red triangles), heterotrophic bacteria flow cytometry counts (green squares) and phage microscope counts (blue lines) are shown for one chemostat (n=3). The vertical line at day 0 denotes the day phage was added. Epifluorescence microscope counts were provided by Megan Larsen (Michigan State University).

Phosphorus-limited chemostat dynamics

Similar to the N-limited control chemostat, *Synechococcus* populations maintained an equilibrium density in the P-limited replicate control chemostats (EM: $2.6 \times 10^7 \pm 3.6 \times 10^6$ cells mL^{-1} and $9.9 \times 10^6 \pm 6.9 \times 10^6$ cells mL^{-1} for replicate 1 and replicate 2, respectively) (Figure 5 and Figure 6). Flow cytometry counts of autotrophic cells for the subset of time points ($2.6 \times 10^7 \pm 8.6 \times 10^6$ cells mL^{-1}) were statistically similar to epifluorescence counts ($1.4 \times 10^7 \pm 4.0 \times 10^6$ cells mL^{-1}) (Figure 29 in Appendix, $r^2 = 0.4258$, n=90, $p < 0.0001$). Heterotrophic bacterial abundances in the P-limited controls reached densities as high as 5.3×10^8 cells mL^{-1} in one of the replicates on day 45 (Figure 6). In both biological replicates, heterotrophic bacteria varied slightly with a noticeable increase within the first 50 days following phage addition. By day 130, heterotrophic bacterial counts had decreased again to their initial abundances (Figure 5).

In the P-limited, phage-amended chemostats, *Synechococcus* populations declined in all 3 biological replicates (Figure 7, Figure 8, Figure 9). However, the decrease in *Synechococcus* (EM: 2.3×10^5 cells mL^{-1}; FC: 5.1×10^5 cells mL^{-1}) was not as low as the N-limited chemostats with phage (Figure 8). In phase with the crash, cyanomyophage reached abundances as high as 8.6×10^8 virus-like particles mL^{-1} (Figure 9). Around day 75, *Synechococcus* populations recovered again similar to the exponential increase at day 50 in the N-limited replicates. Unlike the second crash at day 100 observed in the N-limited treatment, the host continued to grow exponentially in 2 of the 3 P-limited replicates (Figure 7, Figure 9) while abundances leveled off in the other biological replicate (Figure 8). Heterotrophic bacterial populations maintained higher abundances than *Synechococcus* at all time points except 2 with heterotrophs peaking at 4.8×10^8 cells mL^{-1} (Figure 8) during a period of host decline.

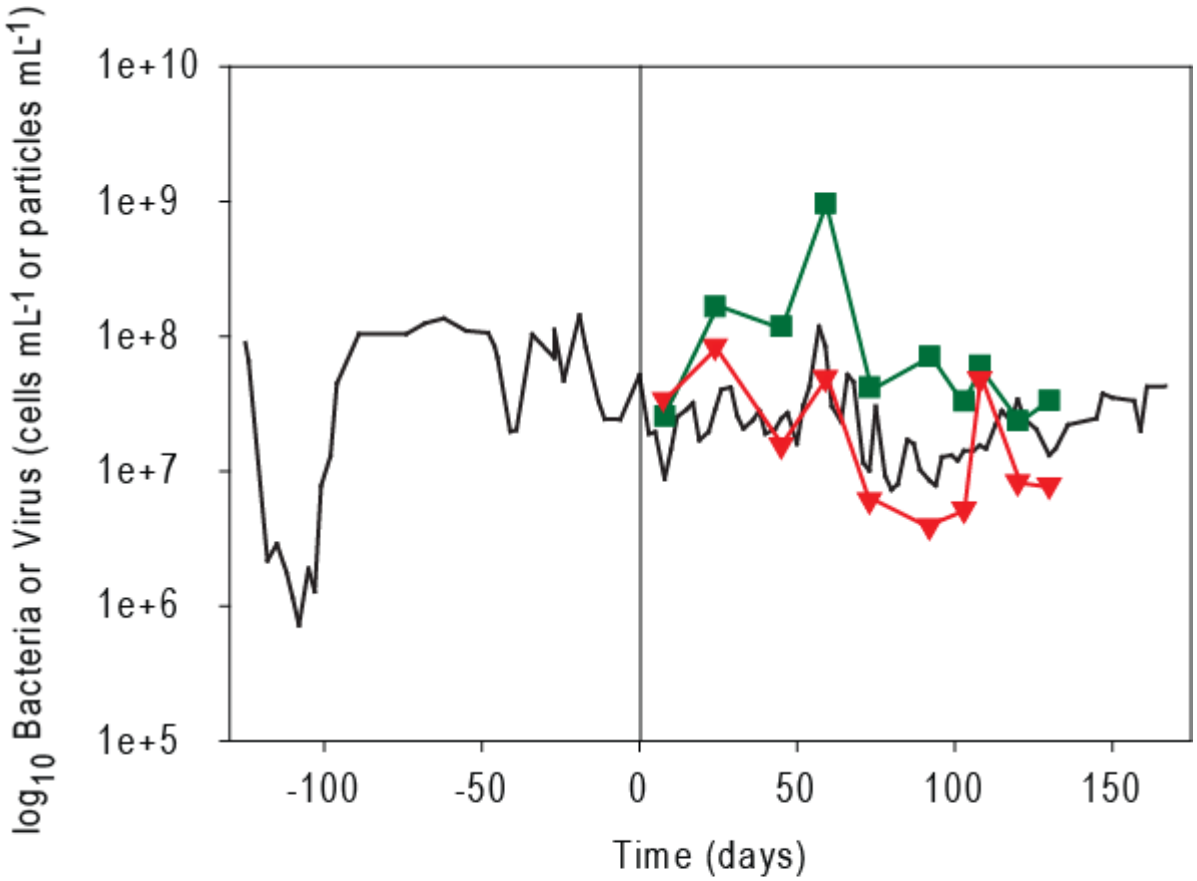

Figure 5: Microscope and flow cytometry counts of *Synechococcus* and heterotrophic bacteria from a phosphorus-limited control chemostat (biological replicate 1). *Synechococcus* microscope counts (black lines), *Synechococcus* flow cytometry counts (red triangles) and heterotrophic bacteria flow cytometry counts (green squares) are shown for one chemostat (n=2). The vertical line at day 0 denotes the day after steady state was achieved. Epifluorescence microscope counts were provided by Megan Larsen (Michigan State University).

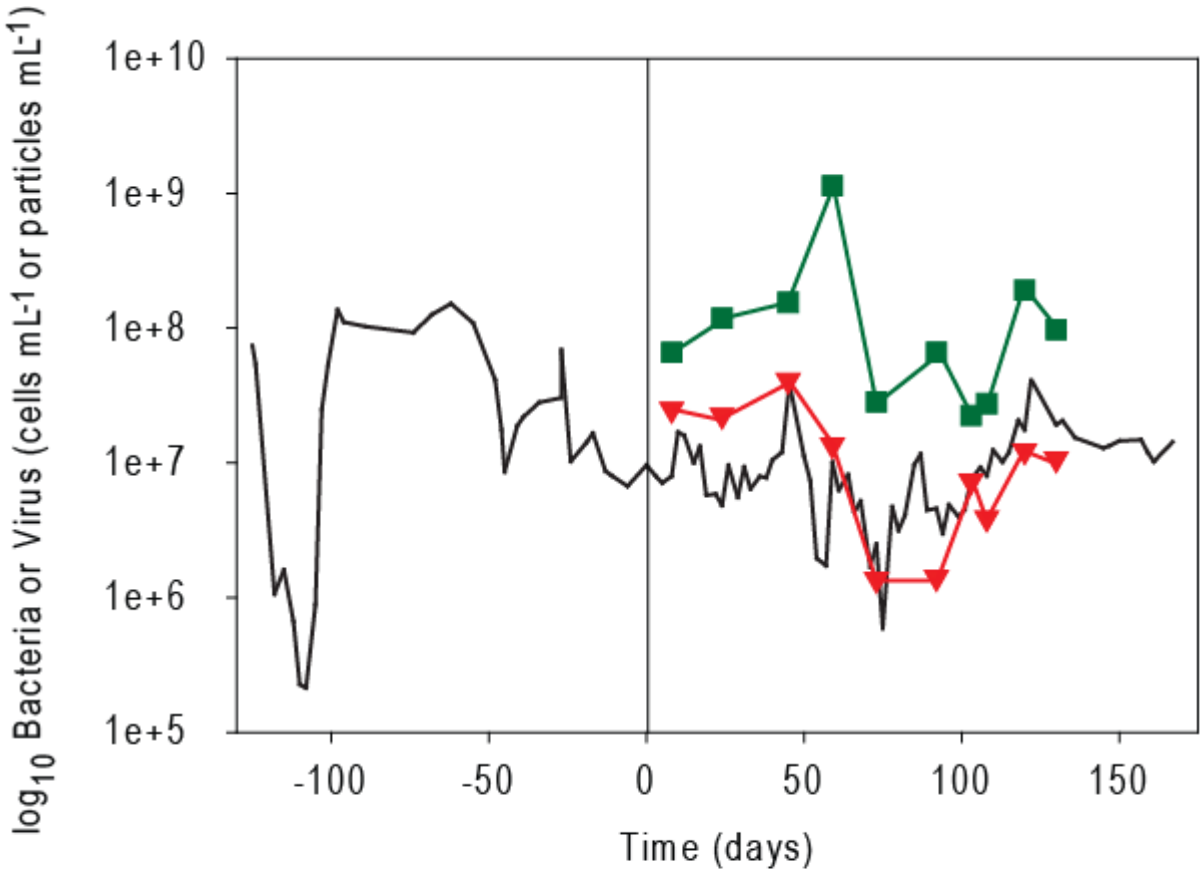

Figure 6: Microscope and flow cytometry counts of *Synechococcus* and heterotrophic bacteria from a phosphorus-limited control chemostat (biological replicate 2). *Synechococcus* microscope counts (black lines), *Synechococcus* flow cytometry counts (red triangles) and heterotrophic bacteria flow cytometry counts (green squares) are shown for one chemostat (n=2). The vertical line at day 0 denotes the day after steady state was achieved. Epifluorescence microscope counts were provided by Megan Larsen (Michigan State University).

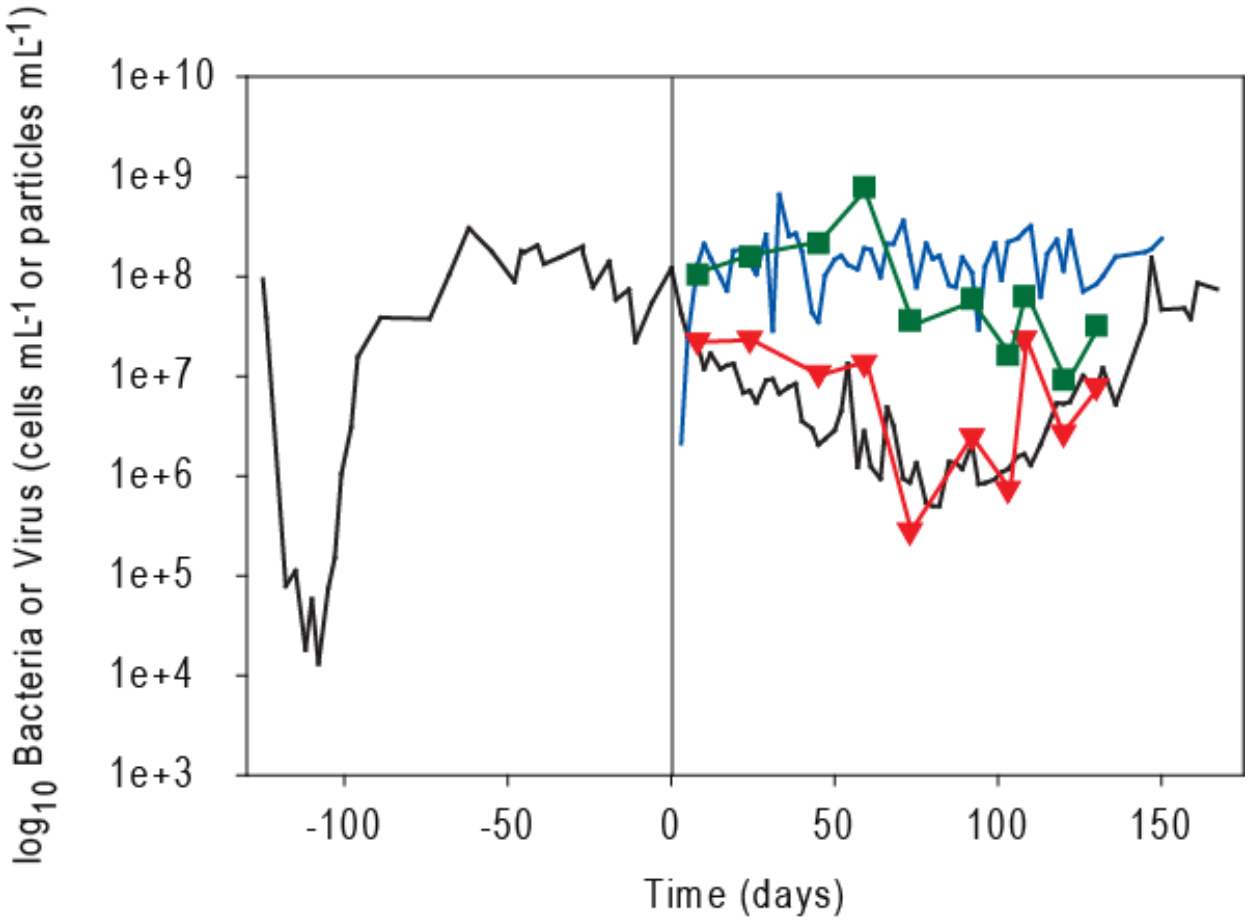

Figure 7: Microscope and flow cytometry counts of *Synechococcus*, heterotrophic bacteria and cyanophage from a phosphorus-limited, phage-amended chemostat (biological replicate 1). *Synechococcus* microscope counts (black lines), *Synechococcus* flow cytometry counts (red triangles), heterotrophic bacteria flow cytometry counts (green squares) and phage microscope counts (blue lines) are shown for one chemostat (n=3). The vertical line at day 0 denotes the day phage was added. Epifluorescence microscope counts were provided by (Michigan State University).

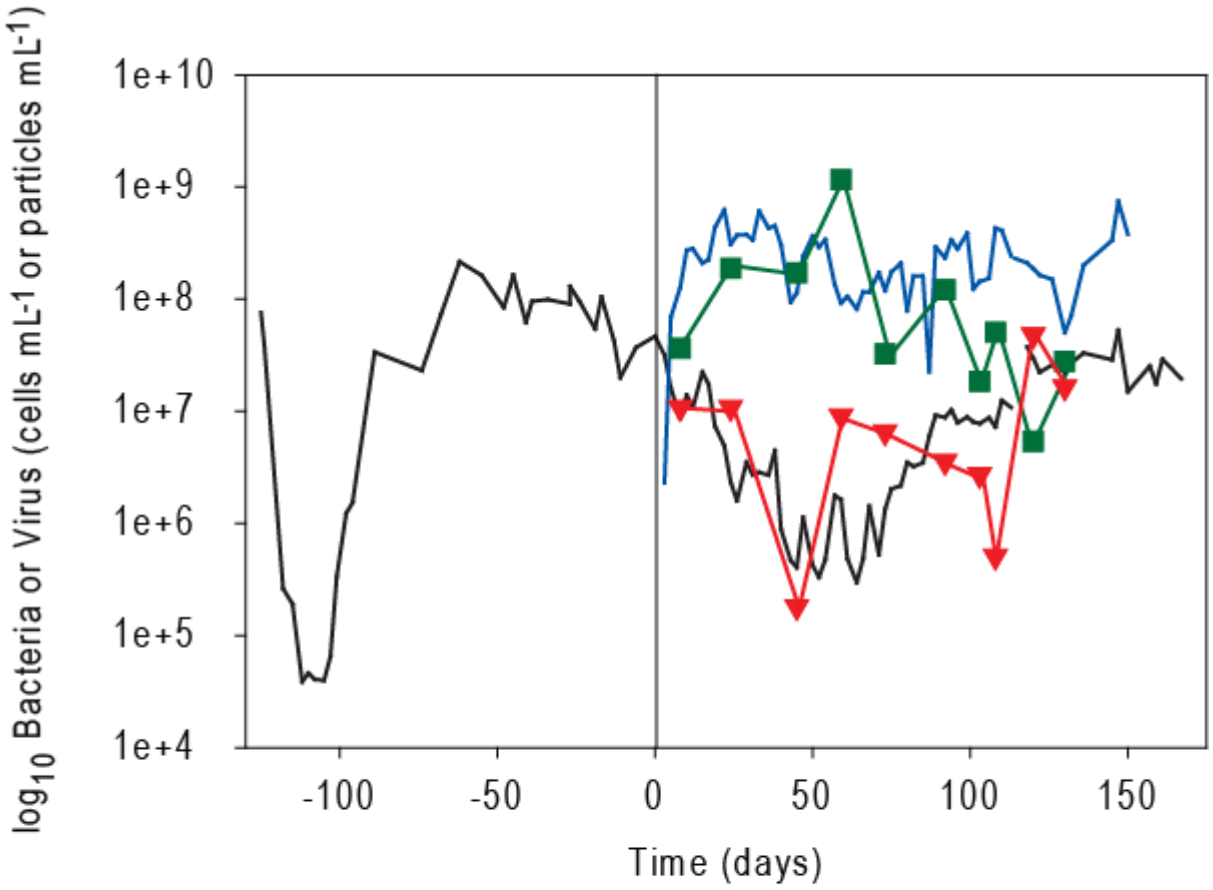

Figure 8: Microscope and flow cytometry counts of *Synechococcus*, heterotrophic bacteria and cyanophage from a phosphorus-limited, phage-amended chemostat (biological replicate 2). *Synechococcus* microscope counts (black lines), *Synechococcus* flow cytometry counts (red triangles), heterotrophic bacteria flow cytometry counts (green squares) and phage microscope counts (blue lines) are shown for one chemostat (n=3). The vertical line at day 0 denotes the day phage was added. Epifluorescence microscope counts were provided by Megan Larsen (Michigan State University).

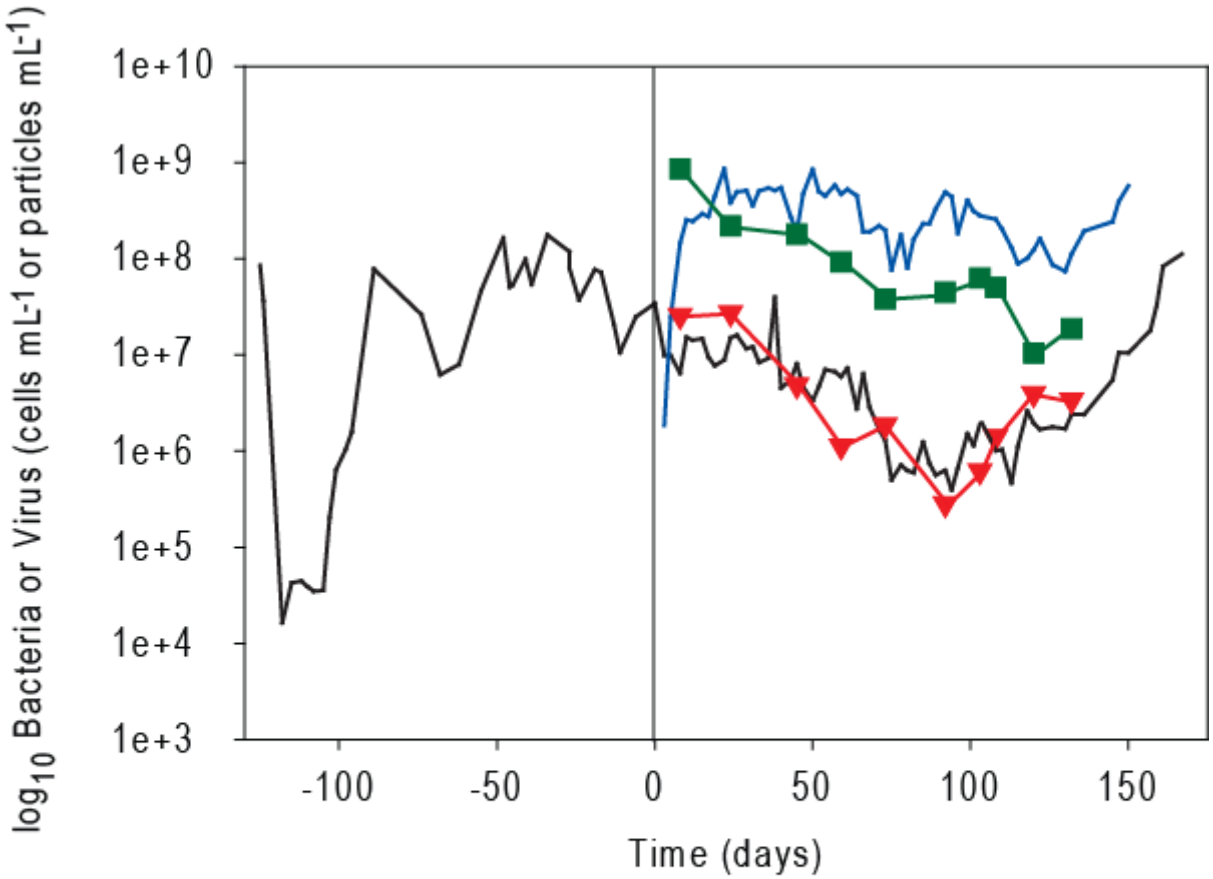

Figure 9: Microscope and flow cytometry counts of *Synechococcus*, heterotrophic bacteria and cyanophage from a phosphorus-limited, phage-amended chemostat (biological replicate 3). *Synechococcus* microscope counts (black lines), *Synechococcus* flow cytometry counts (red triangles), heterotrophic bacteria flow cytometry counts (green squares) and phage microscope counts (blue lines) are shown for one chemostat (n=3). The vertical line at day 0 denotes the day phage was added. Epifluorescence microscope counts were provided by Megan Larsen (Michigan State University).

Comparison of bacterial counts

To validate flow cytometry counts for bacteria, direct counts were completed on representative samples using epifluorescence microscopy. A simple linear regression was performed on a scatter plot of flow cytometry versus epifluorescence counts (Figure 10). The slope resulting from the regression (1.004) was very close to 1 indicating a strong linear relationship between flow cytometry and epifluorescence microscopy counts. Flow cytometry counts of SYBR Green-stained bacterial cells were highly correlated with epifluorescence counts of acridine orange stained cells ($r^2 = 0.9972$). The variation between the two methods was within the range reported by others (Lebaron et al. 1998; Hall et al. 2006).

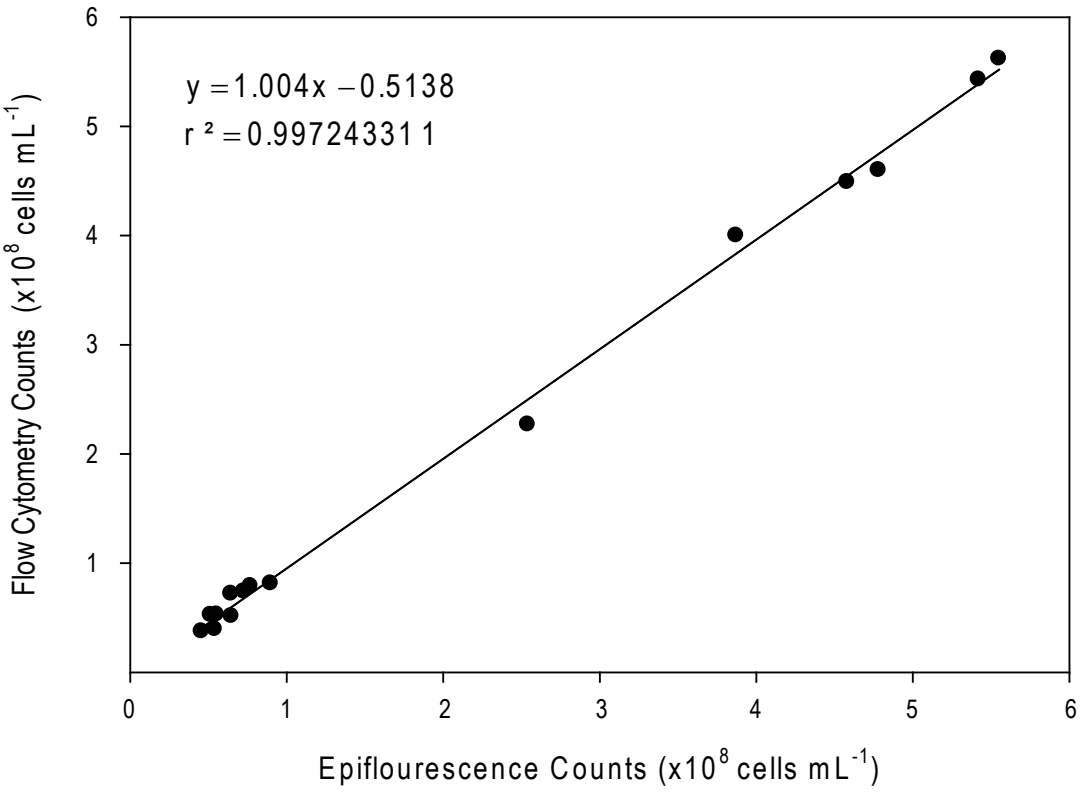

Figure 10: Scatter plot with linear regression of flow cytometry counts versus epifluorescence counts of heterotrophic bacteria (n=15).

Heterotrophic bacteria : *Synechococcus* ratios

Using the flow cytometry counts, the ratio of heterotrophic bacteria to *Synechococcus* was determined for each time point. For the N-limited control chemostat (n=1), the ratio ranged from 0.8 (day 130) to 21.7 (day 92) heterotrophs per *Synechococcus*. In contrast, the N-limited, phage-amended chemostats (n=3) supported a higher number of heterotrophic bacteria ranging from 1.83 ± 0.8 (day 73) to 507.3 ± 83.7 (day 45) (mean ± SEM). Ratios for all four N-limited chemostats were averaged for both treatments and graphed over time (Figure 11A). The ratio of heterotrophic bacteria to *Synechococcus* increased to its highest average value at day 45 (381.8 ± 138.7) and declined at day 59 (11.8 ± 1.1). Time points following day 59 maintained a ratio of 5.3 ± 1.4 (n=7) heterotrophs to *Synechococcus* for the remainder of the experiment.

Ratios of heterotrophic bacteria to *Synechococcus* were also calculated from flow cytometry counts for the P-limited control and phage-amended treatments. For the P-limited controls (n=2), ratios ranged from 1.7 ± 0.9 (day 10) to 32.7 ± 14.5 (day 92). The averaged controls maintained a relatively steady ratio (9.8 ± 2.8) over the course of the experiment. Conversely, in the P-limited, phage-amended chemostats (n=3), values were much higher reaching a ratio of 1005.5 ± 307.1 heterotrophs per *Synechococcus* (day 45). Ratios for all five P-limited chemostats were also averaged for both control and phage treatments and graphed over time (Figure 11B). The initial increase was similar to the trend in the N-limited graph (Figure 11A). However, after day 45 the P-limited ratios increased slightly until day 92 (216.0 ± 43.1) and gradually decreased, maintaining a slightly higher ratio of heterotrophs : *Synechococcus* for the remainder of the experiment (34.7 ± 8.6).

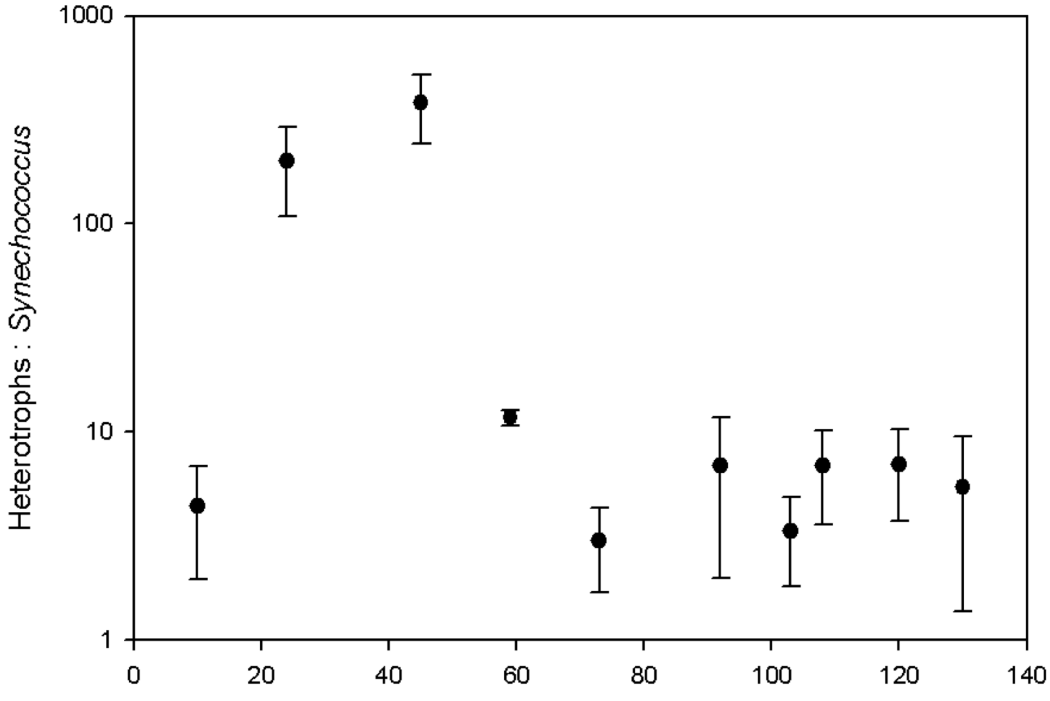

(**A**)

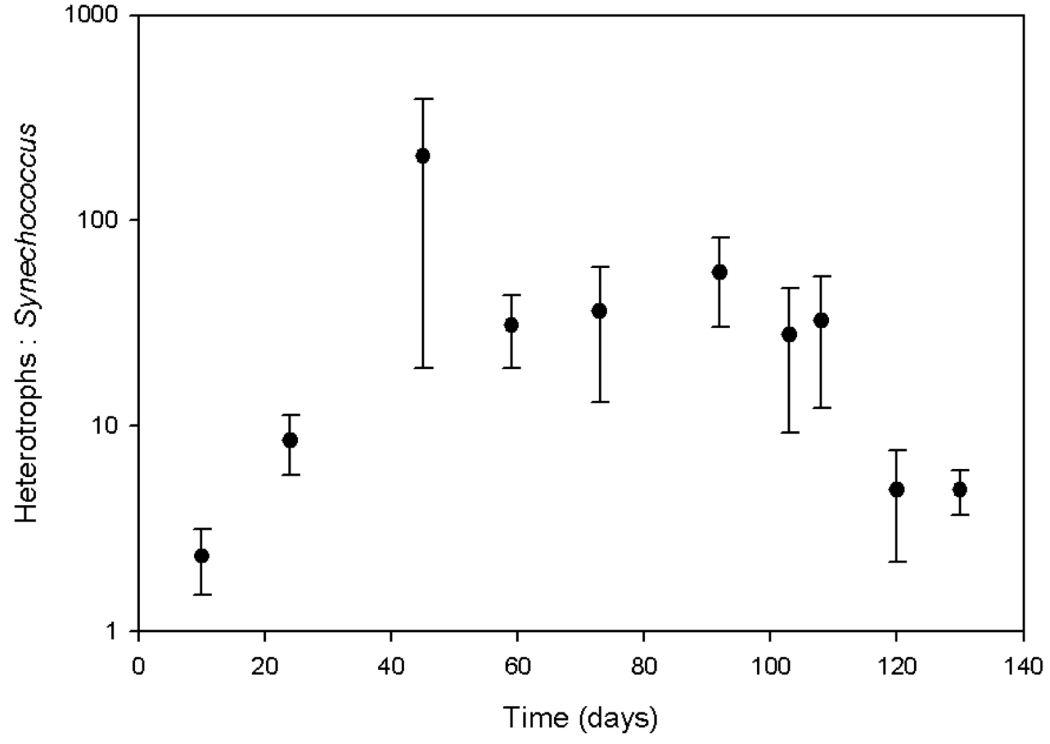

(**B**)

Figure 11: Ratios of heterotrophic bacteria to *Synechococcus*. Standard error bars represent mean ± SEM. Each time point represents the mean and standard error of 4 replicate nitrogen-limited chemostats (**A**) and 5 replicate phosphorus-limited chemostats (**B**).

454 Titanium pyrosequencing

Sequence analysis

The 454 Titanium pyrosequencing platform produced a total of 325,142 raw reads from 43 individual libraries sequenced in duplicate (86 total). One of the samples was lost in sample collection and another (P-limited phage, biological replicate 3, day 24) was not included in the analysis due to unsuccessful barcoding. An average of 81,286 reads were acquired from each region with an average length of 541 bp. The number of reads acquired from each library varied for each region with a range of 2,828 to 4,775 sequences, resulting in an average of 3,525 reads. The dataset was reduced to 314,068 sequences after the initial trim step in MOTHUR (See Materials and Methods) resulting in a 3.4% reduction. After removing low quality reads, sequences were assigned to taxonomic groups.

In order to generate taxonomic profiles of each technical replicate, 314,068 high-quality sequences were assigned to taxonomic groups using the RDP Naïve Bayesian rRNA Classifier Version ver. 2.2 (Wang et al. 2007). Taxonomic assignments of all reads were standardized to relative abundances for both technical replicates (R1, R2). At the phylum-level, the distribution of taxonomic assignments was highly similar across technical replicates (Figure 12). Based on a 95% confidence interval, the majority of sequences (~70%) were assigned to the phylum, *Proteobacteria*. The next largest proportion of sequences was assigned to *Cyanobacteria* (21% and 24% for R1 and R2, respectively). The remaining sequences were classified as *Acidobacteria*, *Bacteroidetes*, *Actinobacteria* and *Firmicutes* (less than 7% for each), and approximately 1% of the sequences were unclassifiable. One obvious difference between the two sets was the difference in the proportion of sequences assigned to *Actinobacteria*. For half

of the libraries (set 1), *Actinobacteria* represented an average of 1.3% of the sequences across both technical replicates. However in set 2, *Actinobacteria* was more abundant (9.0%).

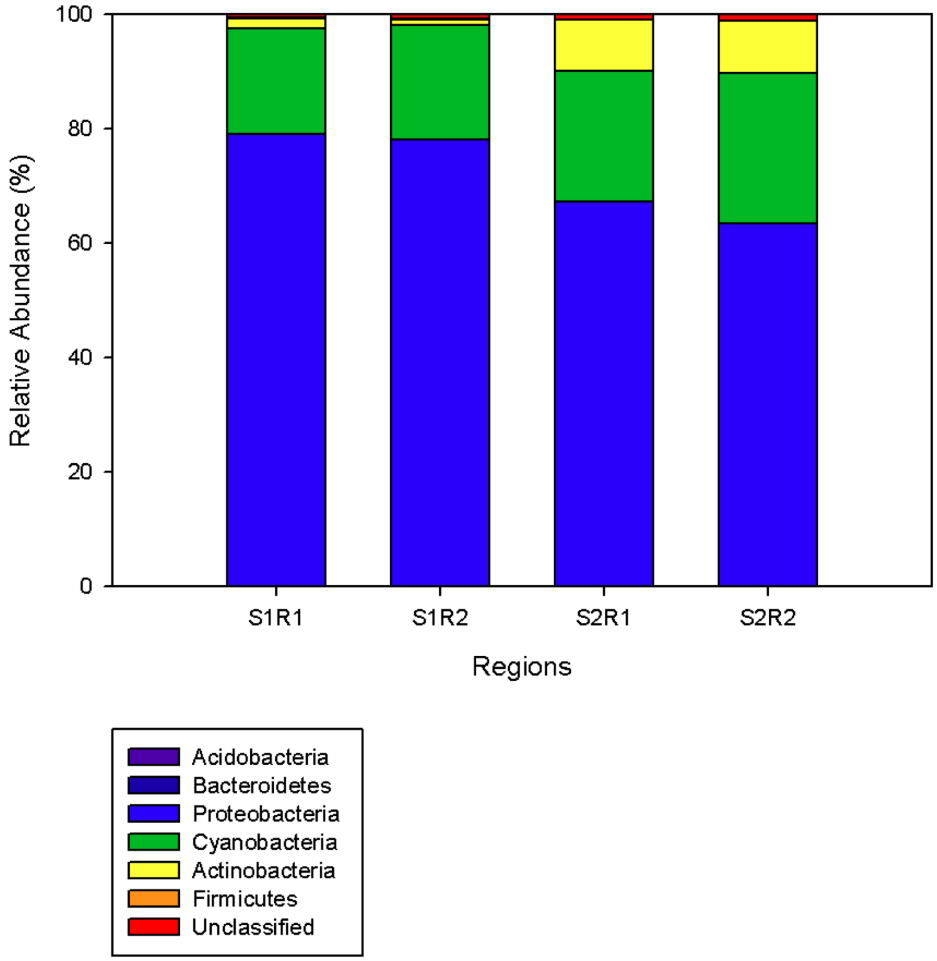

Figure 12: Relative abundances of RDP taxonomic assignments for two technical replicates at a 95% confidence threshold. Individual sets of barcodes are denoted by an S and technical replicates are denoted by R. Submitted sequences were trimmed in MOTHUR prior to submission to the RDP Classifier ver. 2.2 as previously described.

Approximately 81% of the original sequences were retained (263,606) after further sequence processing in MOTHUR. The resulting filtered alignment was 442 positions long and 190 to 215 bases were used for sequence analyses. The libraries were dominated by non-cyanobacterial sequences (194,778), while the remaining 68,828 sequences were classified as cyanobacterial sequences.

Comparing technical sequencing reproducibility

Sequence analyses of libraries were performed two separate ways. Initially, all of the technical replicates were analyzed together. In order to examine the heterotrophic bacterial community, all cyanobacterial sequences were removed from the dataset. A column-formatted distance matrix of uncorrected pairwise distances between sequences was generated using 194,778 heterotrophic bacterial sequences and clustered into OTUs using the average neighbor algorithm in MOTHUR (method between the nearest and furthest neighbor) at a 0.03 cutoff level. The sequences clustered into 110 OTUs, of which 40 represented singletons (36.4%) and 14 represented doubletons (12.7%). A large proportion (67.5%) of the singleton sequences were identified in replicate 1, while a lower percentage (33.5%) was unique to replicate 2.

To compare OTU recovery across technical replicates, read counts were standardized to relative abundances. Relative abundances for each library and its technical replicate were highly correlated ($r^2 = 0.9864$) (Figure 13). There was a strong linear relationship between technical replicates as indicated by the slope of 0.9844. While the majority of data points were tightly associated with the regression line, one point clustered away. The outlier was from a N-limited, phage-amended replicate representing the *Sulfitobacter* overlap (78.26% versus 42.1%) at Day 108. When this outlier was removed from the scatter plot the r^2 value increased to 0.9936.

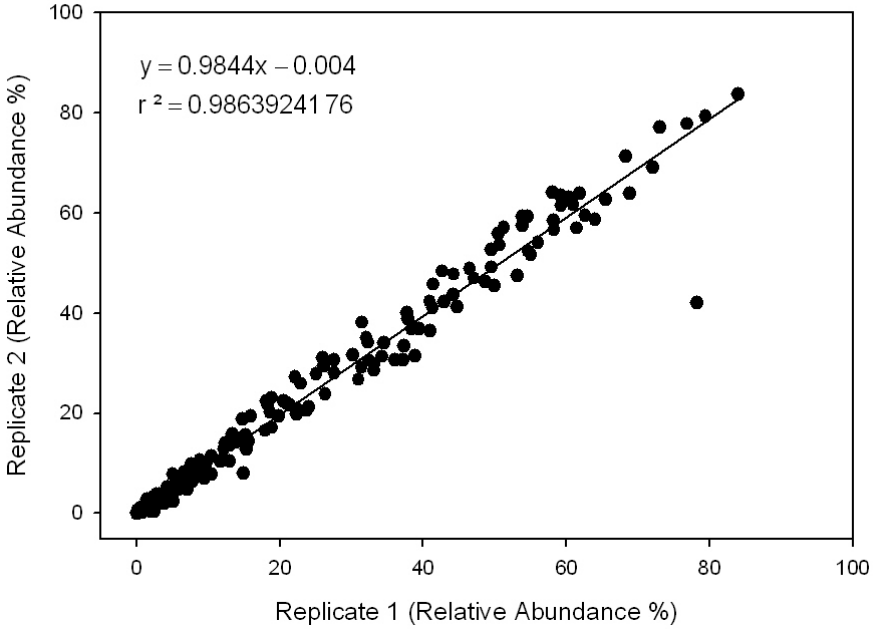

Figure 13: Linear regression of relative abundances of OTUs for both technical replicates.

A dendrogram was generated in MOTHUR to compare the reproducibility of community structure among technical replicates (Figure 14). The Yue and Clayton measure of dissimilarity (Θ_{YC}) was used to construct the dendrogram of all 86 groups (Yue and Clayton 2005). Although treatments and specific time points did not consistently cluster together, 40 of the 43 libraries clustered most closely with its technical replicate. For the 3 technical replicate libraries that did not cluster together, the distance was very short (Day 132, P-limited, phage-amended biological replicate 2: 0.0391; Day 132, P-limited, control, biological replicate 1: 0.0783; Day 233, N-limited, control, biological replicate 1: 0.047).

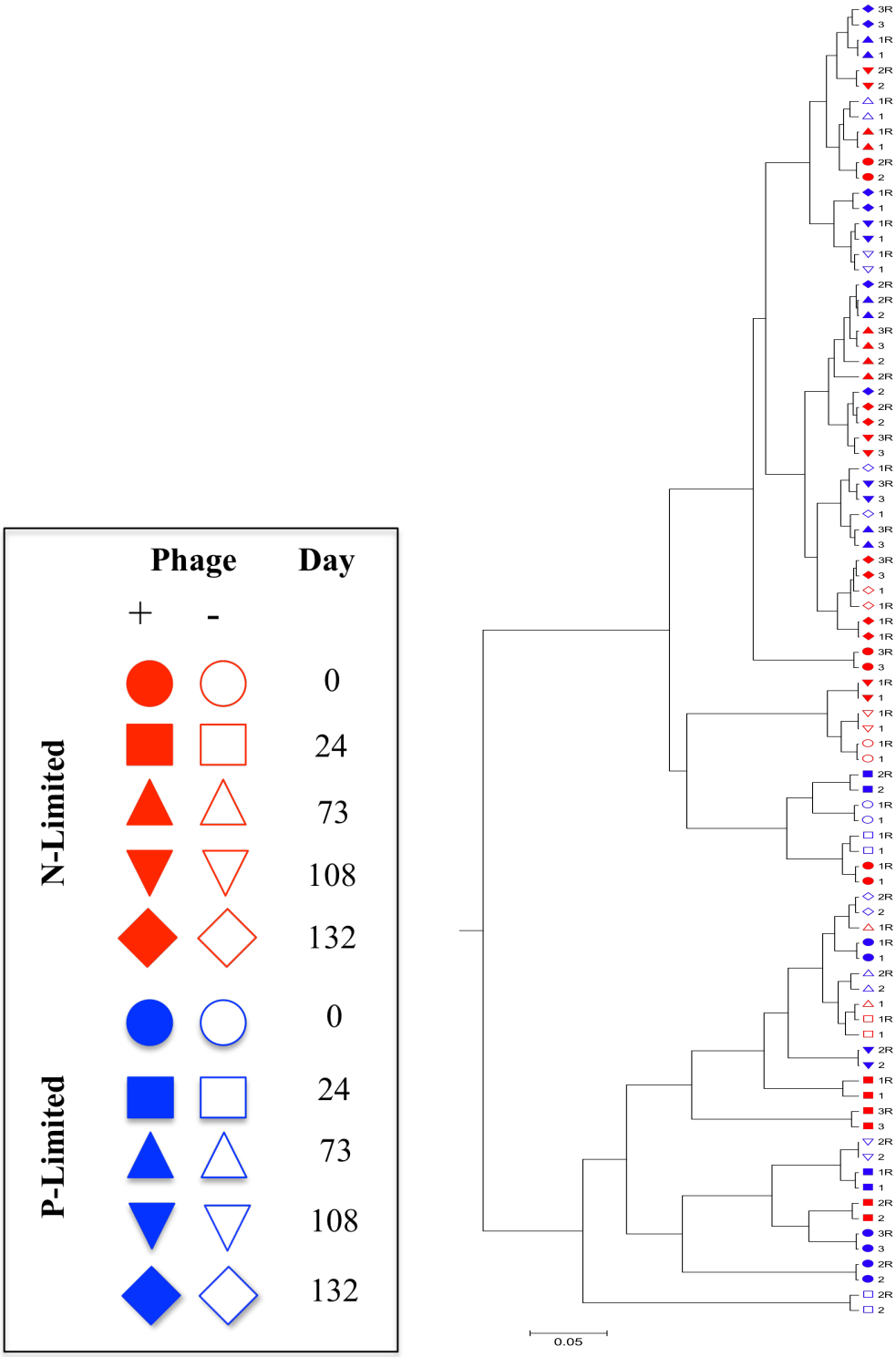

Figure 14: Dendrogram of relatedness of all technical and biological replicate (R) libraries generated by MOTHUR using the Yue and Clayton measure of dissimilarity (Θ_{YC}).

After observing similar phylum-level distributions among technical replicates (Figure 12), highly similar relative abundances of OTUs (Figure 13) and reproducible community clustering (Figure 14), technical replicate libraries were pooled in MOTHUR to increase read numbers. All subsequent analyses were based on the pooled sequence dataset. Each pooled library had an average of 4529.72 ± 247.16 reads (mean ± SEM).

Community Trends

RDP Assignments

All pooled sequences were classified to RDP by comparing sequences to the MOTHUR-formatted RDP reference files using a bootstrapping algorithm to classify sequences to a 60% or greater confidence limit. A total of 194,778 reads represented 5,201 unique sequences. Out of the 5,201 unique sequences, 5,120 sequences had 5 or less reads (6,446 reads comprising 3.32% of all reads) while the 81 remaining sequences had 6 or more reads (188,312 reads comprising 96.7% of all reads). Of the 81 unique sequences with 6 or more reads, 77.3% (51 reads) could be classified with a 60% bootstrap value to the genus level. The remaining 30 sequences could not be classified at the genus level. Of these, sequences were assigned to 3 different classes including *Alphaproteobacteria* (28), *Actinobacteria* (1) and *Betaproteobacteria* (1). Within the *Alphaproteobacteria* class, sequences were further classified to the families of *Sphingomonadaceae* (13) and *Erythrobacteraceae* (2). The remaining 13 sequences could not be classified at the family level. A large proportion of reads from the dataset were assigned to one of the *Sphingomonadaceae* sequences (28,245) and one of the *Rhizobiales* sequences (15,700). The reads from this *Sphingomonadaceae* sequence were abundant among the P-limited

chemostats. However reads from the abundant *Rhizobiales* sequence were distributed more evenly across both nutrient-limited chemostats.

OTU Assignments

Since less than half of the sequences were unsuccessfully assigned to the genus level using RDP at a 60% bootstrap value, community structure was analyzed using an OTU-based approach at a 0.03 cutoff. A high percentage of sequences (95.5%) were successfully assigned to the genus level. While there was typically one OTU for each genus, more than half of the genus-level classifications were assigned to more than one OTU. For example, there were 13 *Sulfitobacter* OTUs, 8 *Arthrobacter* OTUs, 6 *Pseudomonas* OTUs and 5 *Alcanivorax and Erythrobacter* OTUs. Individual OTUs from each genus were pooled and represented as a single OTU. In our analyses, 99.5% of our sequences were assigned to the first 6 OTUs (*Sulfitobacter*, *Sphingomonas*, *Rhizobium, Arthrobacter*, *Pseudomonas* and *Alcanivorax*). Out of these 6 OTUs, over 80% of the sequences were assigned to *Sulfitobacter* or *Sphingomonas*, which are referred to as "abundants" in subsequent graphs. These OTUs were the most abundant across all of the chemostats regardless of treatment. The next 4 OTUs (*Rhizobium*, *Arthrobacter*, *Pseudomonas* and *Alcanivorax*) made up approximately 17% of all the sequences in the dataset and are referred to as "rares." The top 6 OTUs each had a significant number of reads (more than 20 across at least 2 separate libraries), therefore we are confident in the calls and consider them real. The reads from the remaining 104 OTUs only contributed to 0.5% of all the sequences in the dataset.

For the N-limited chemostats with or without phage, the *Sulfitobacter* population inversely oscillated in abundance with *Sphingomonas* (Figure 15A, Figure 16A, Figure 17A, Figure 18A). Across all N-limited chemostats, there was a higher relative abundance of *Sulfitobacter* OTU at day 0 relative to *Sphingomonas.* Trends for both abundant OTUs are

highly similar across all N-limited chemostats characterized by an initial decrease in *Sulfitobacter,* decreasing to half of its relative abundance and increasing again at day 73 along with opposite *Sphingomonas* trends.

In the case of the rares, some patterns in OTU abundance were highly predictable while others were far less predictable (Figure 15B, Figure 16B, Figure 17B, Figure 18B). For example, a similar decline in *Rhizobium* was observed across all N-limited chemostats regardless of phage addition. *Pseudomonas* populations were consistently negligible across all 4 chemostats (3 *Pseudomonas* reads across 2 different libraries). For *Alcanivorax*, a decline was observed in two of the chemostats (Figure 15B and Figure 18B) but in the other two phage-amended chemostats, *Alcanivorax* consistently made up less than 5% of all reads (Figure 16B and Figure 17B). The relative abundance of *Arthrobacter* was less predictable. In one phage-amended chemostat, *Arthrobacter* peaked at day 24 and declined at day 73 (Figure 18B). In the remaining chemostats (1 control and 2 phage-amended), there was a consistent peak to 5 or 15% of the sequences in the *Arthrobacter* populations at later time points (Figure 15B, Figure 16B, Figure 17B, Figure 19B).

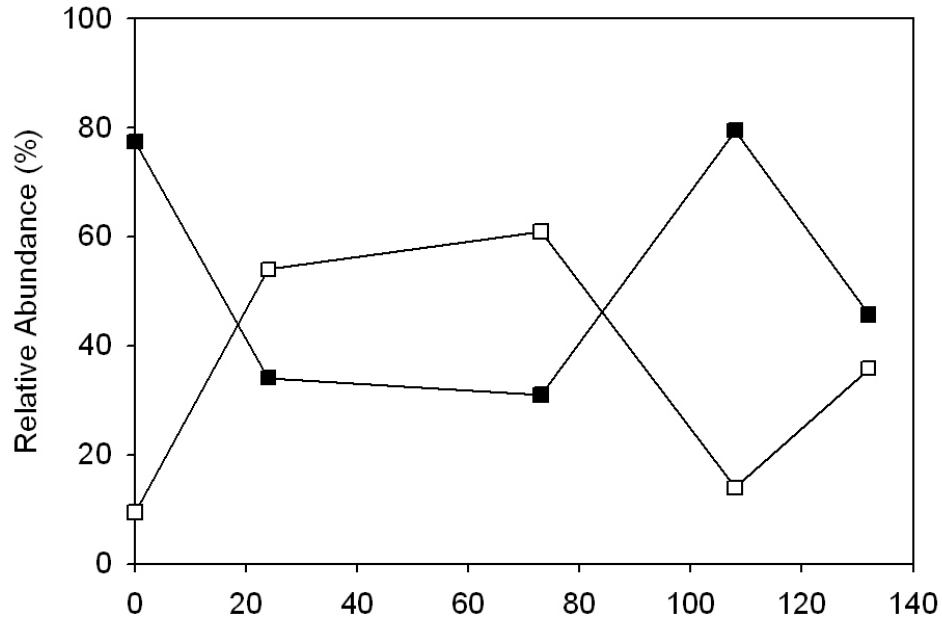

(**A**)

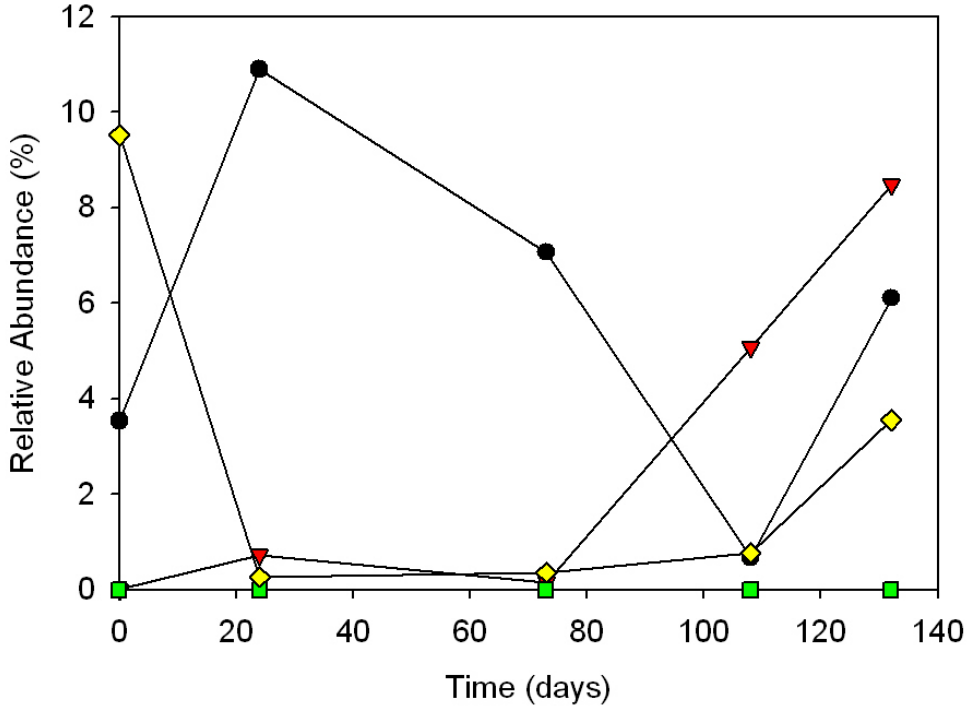

(**B**)

Figure 15: Dynamics of abundant (**A)** and rare (**B)** OTUs in a N-limited control chemostat. Abundant OTUs include: *Sulfitobacter* (black squares) and *Sphingomonas* (white squares). Rare OTUs include: *Rhizobium* (black circles), *Arthrobacter* (red triangles), *Alcanivorax* (yellow diamonds) and *Pseudomonas* (green squares).

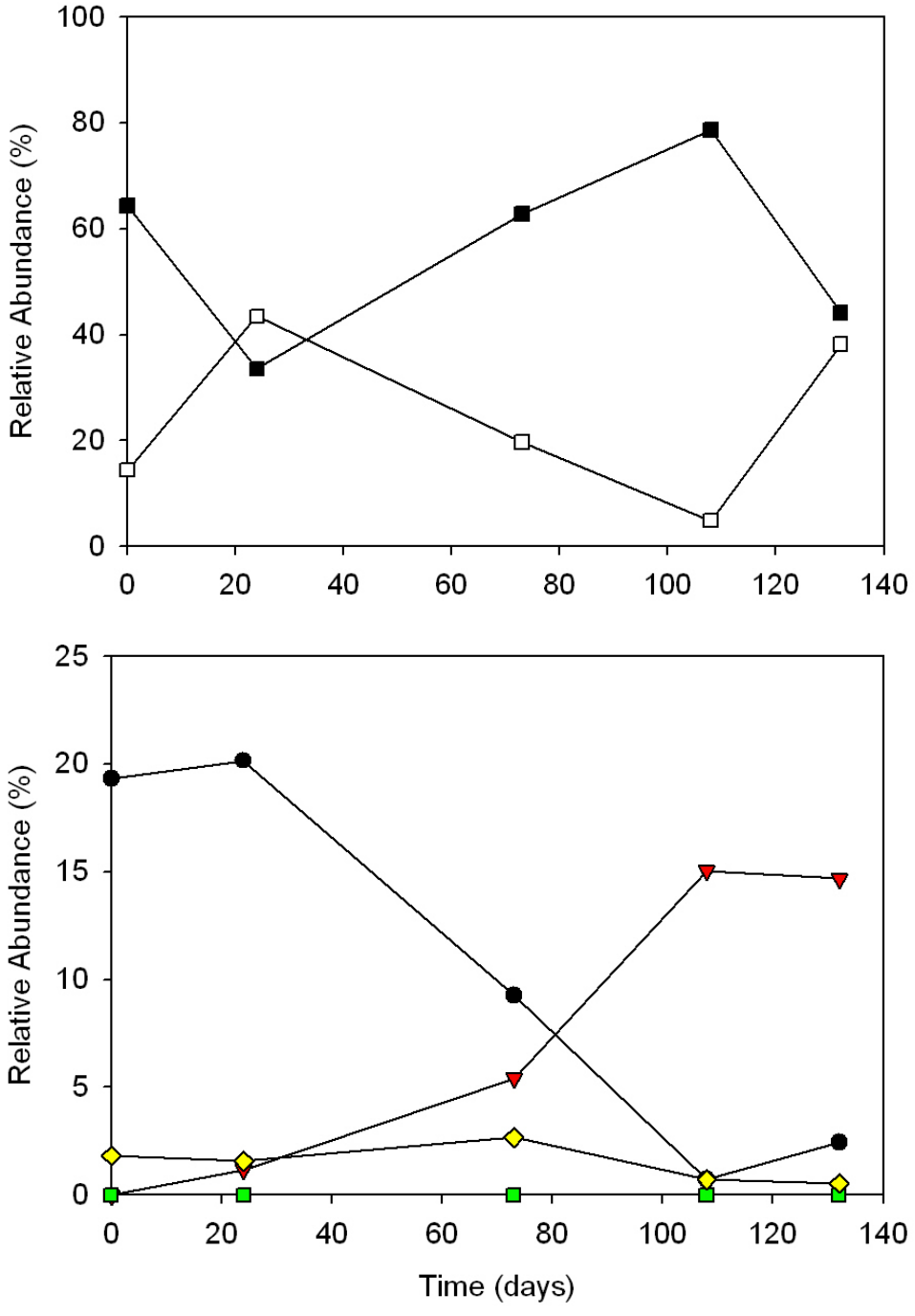

Figure 16: Dynamics of abundant (**A**) and rare (**B**) OTUs in a N-limited, phage-amended chemostat (biological replicate 1). Abundant OTUs include: *Sulfitobacter* (black squares) and *Sphingomonas* (white squares). Rare OTUs include: *Rhizobium* (black circles), *Arthrobacter* (red triangles), *Alcanivorax* (yellow diamonds) and *Pseudomonas* (green squares).

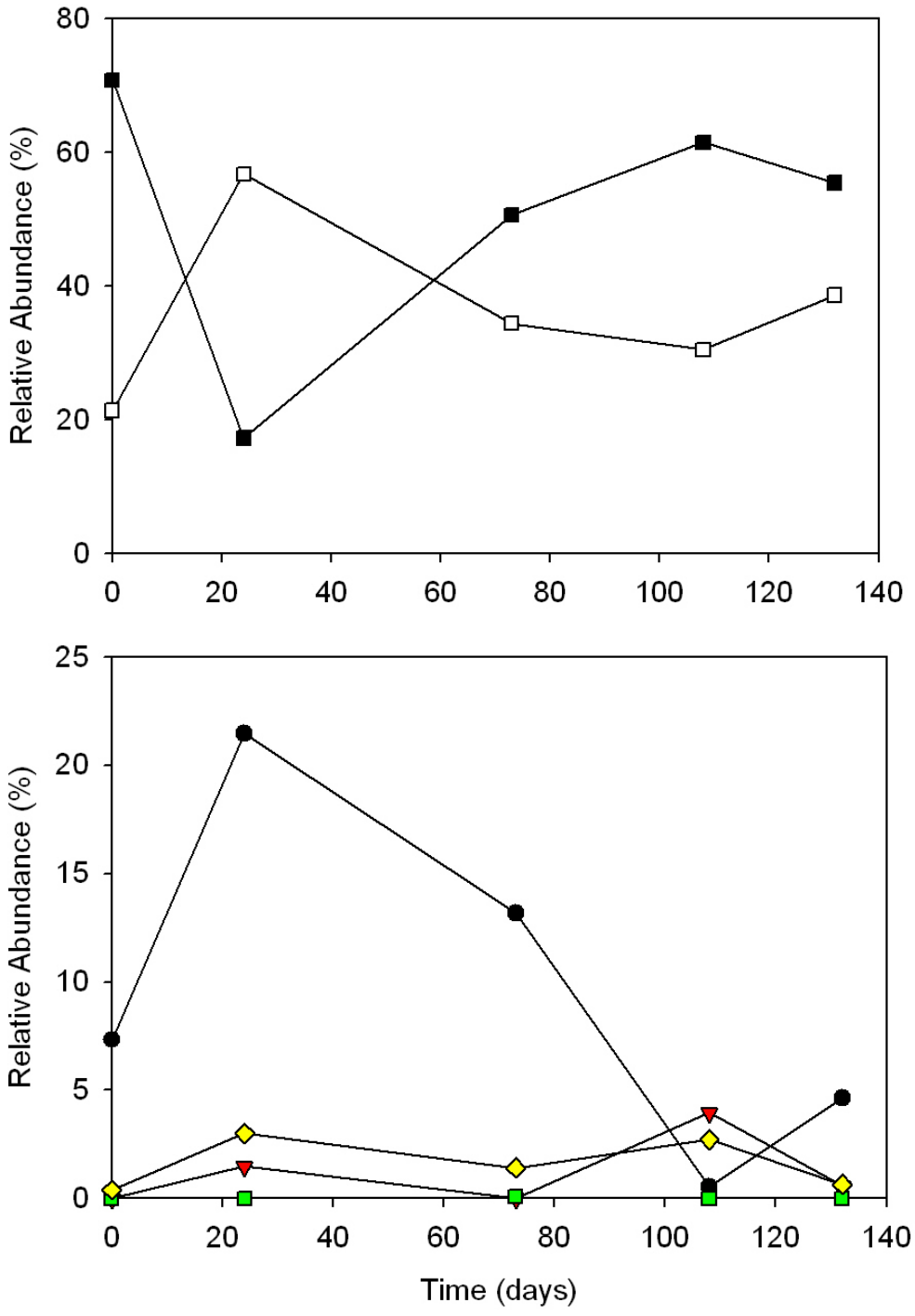

Figure 17: Dynamics of abundant (**A)** and rare (**B)** OTUs in a N-limited, phage-amended chemostat (biological replicate 2). Abundant OTUs include: *Sulfitobacter* (black squares) and *Sphingomonas* (white squares). Rare OTUs include: *Rhizobium* (black circles), *Arthrobacter* (red triangles), *Alcanivorax* (yellow diamonds) and *Pseudomonas* (green squares).

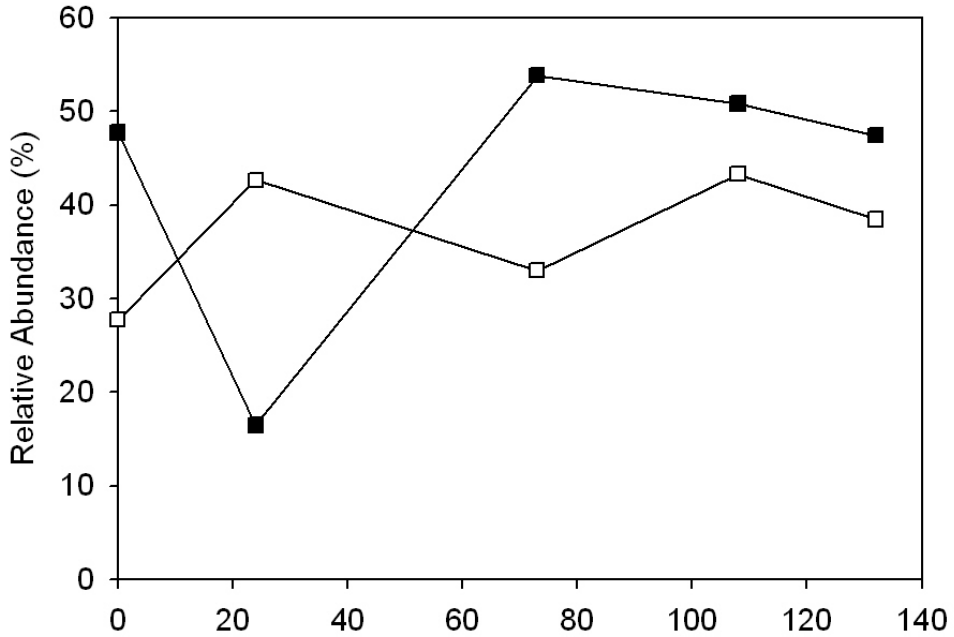

(**A**)

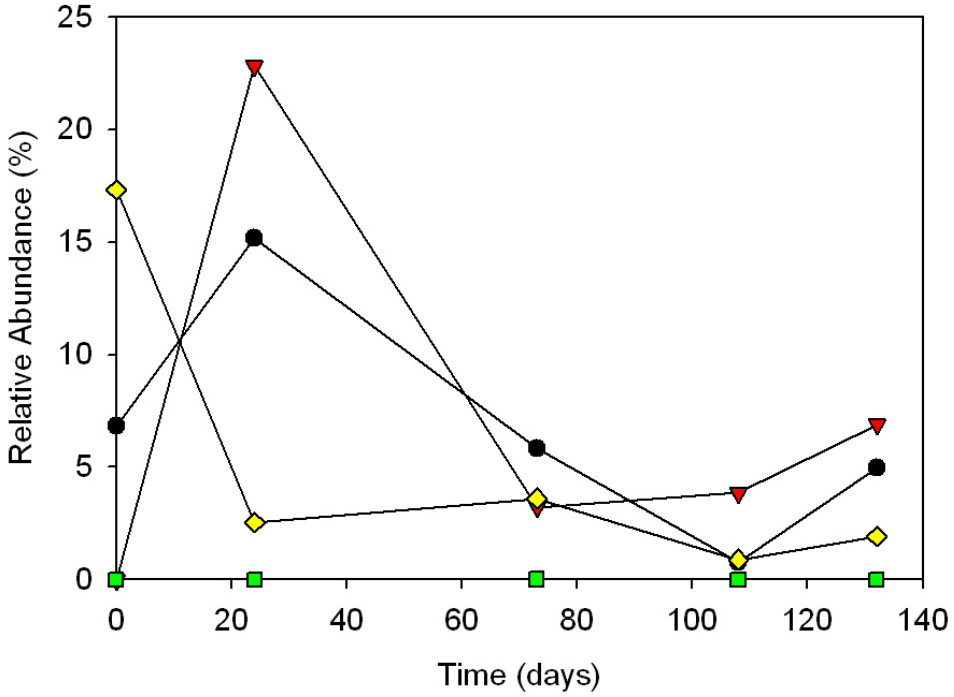

(**B**)

Figure 18: Dynamics of abundant (**A**) and rare (**B**) OTUs in a N-limited, phage-amended chemostat (biological replicate 3). Abundant OTUs include: *Sulfitobacter* (black squares) and *Sphingomonas* (white squares). Rare OTUs include: *Rhizobium* (black circles), *Arthrobacter* (red triangles), *Alcanivorax* (yellow diamonds) and *Pseudomonas* (green squares).

Overall in the P-limited chemostats, trends in OTUs were far less consistent than the N-limited chemostats. Similar to the N-limited chemostats, the *Sulfitobacter* and *Sphingomonas* genera were the two most abundant OTUs. In contrast to results from the N-limited libraries, *Sphingomonas* was more abundant than *Sulfitobacter* at day 0 in 3 out of the 5 libraries (Figure 20A, Figure 22A, Figure 23A). For the remaining libaries, *Sulfitobacter* was more abundant (Figure 19A) and relative abundances were unknown at day 0 due to a missing sample (Figure 21A). Although similar fluctuations in *Sulfitobacter* and *Sphingomonas* populations were characteristic of all the N-limited chemostats, patterns in the P-limited chemostats were more variable. For example in 3 of the 5 chemostats (Figure 20A, Figure 22A, Figure 23A), *Sulfitobacter* gradually increased but decreased in the other 2 chemostats (Figure 19A, Figure 21A). No obvious patterns specific to the phage-amended or control treatments were observed.

Similar to the N-limited chemostats, there was a rapid decline in *Rhizobium* in the rare populations of all the P-limited chemostats. One major difference between both nutrient treatments was the presence of *Pseudomonas* in the P-limited chemostats. In both P-limited controls, the *Pseudomonas* OTU increased to similar relative abundances (15-20% of all reads) (Figure 19B and Figure 20B). The *Alcanivorax* population was less abundant in the P-limited chemostats compared to the N-limited chemostats making up less than 5% of sequences across all of the chemostats. There was also a similar trend in *Arthrobacter* populations as noted for the N-limited treatments with peaks in abundance occuring at later time points between day 73 and day 132. However, there was no obvious trend in *Arthrobacter* consistently unique to control or phage-amended chemostats.

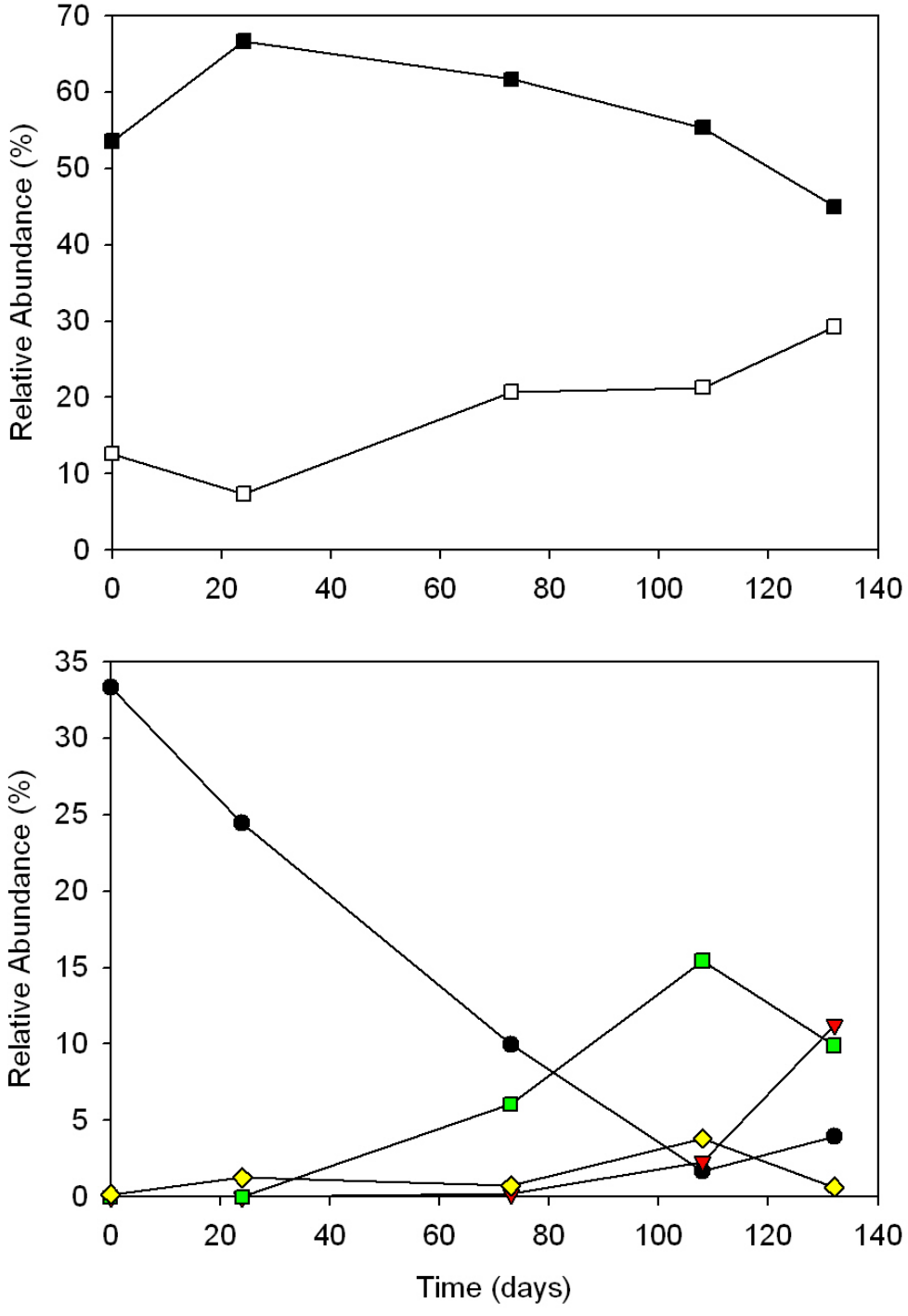

Figure 19: Dynamics of abundant (**A**) and rare (**B**) OTUs in a P-limited control chemostat (biological replicate 1). Abundant OTUs include: *Sulfitobacter* (black squares) and *Sphingomonas* (white squares). Rare OTUs include: *Rhizobium* (black circles), *Arthrobacter* (red triangles), *Alcanivorax* (yellow diamonds) and *Pseudomonas* (green squares).

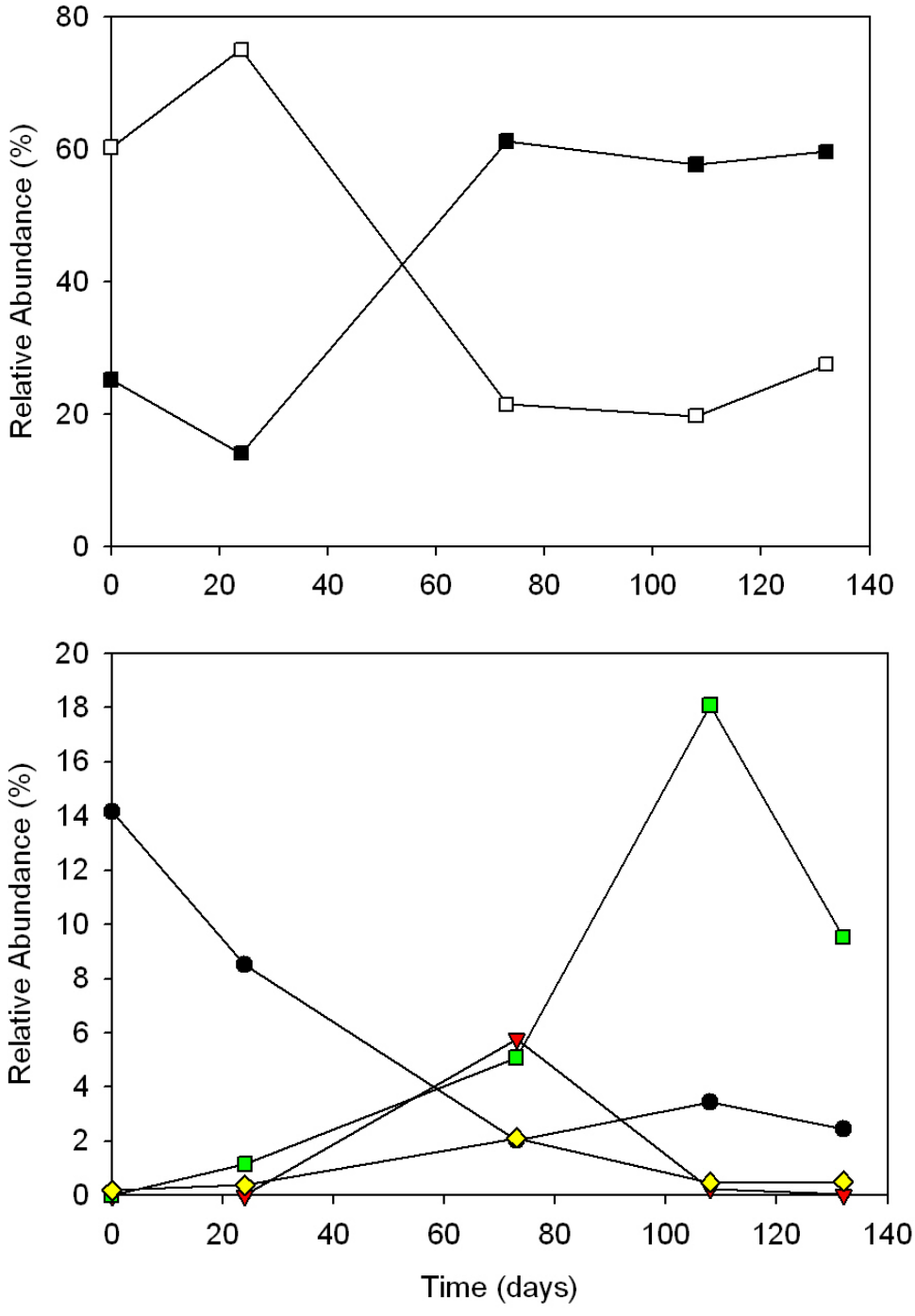

Figure 20: Dynamics of abundant (**A**) and rare (**B**) OTUs in a P-limited control chemostat (biological replicate 2). Abundant OTUs include: *Sulfitobacter* (black squares) and *Sphingomonas* (white squares). Rare OTUs include: *Rhizobium* (black circles), *Arthrobacter* (red triangles), *Alcanivorax* (yellow diamonds) and *Pseudomonas* (green squares).

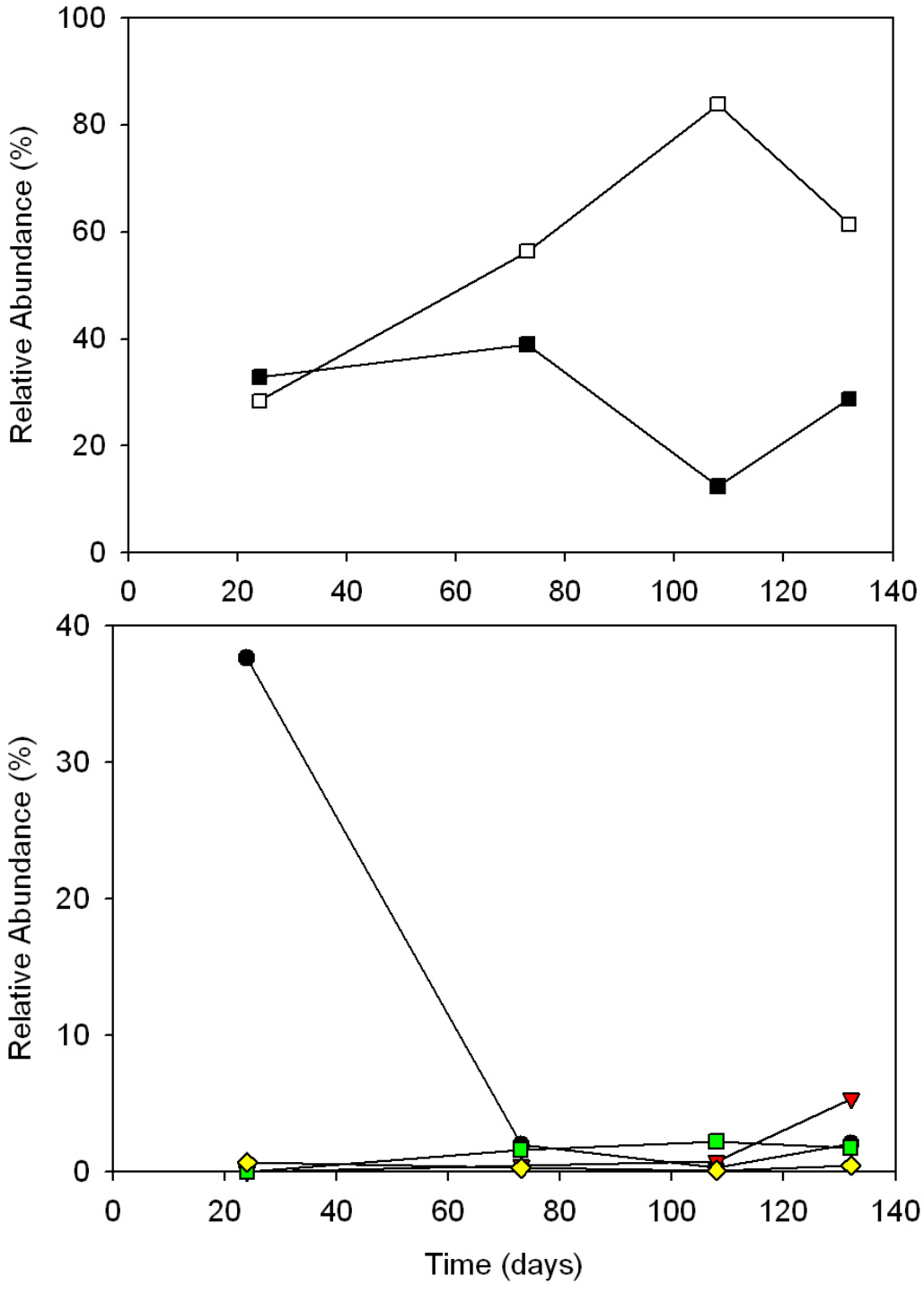

Figure 21: Dynamics of abundant (**A)** and rare (**B)** OTUs in a P-limited, phage-amended chemostat (biological replicate 1). Abundant OTUs include: *Sulfitobacter* (black squares) and *Sphingomonas* (white squares). Rare OTUs include: *Rhizobium* (black circles), *Arthrobacter* (red triangles), *Alcanivorax* (yellow diamonds) and *Pseudomonas* (green squares). Sample for the first time point was lost.

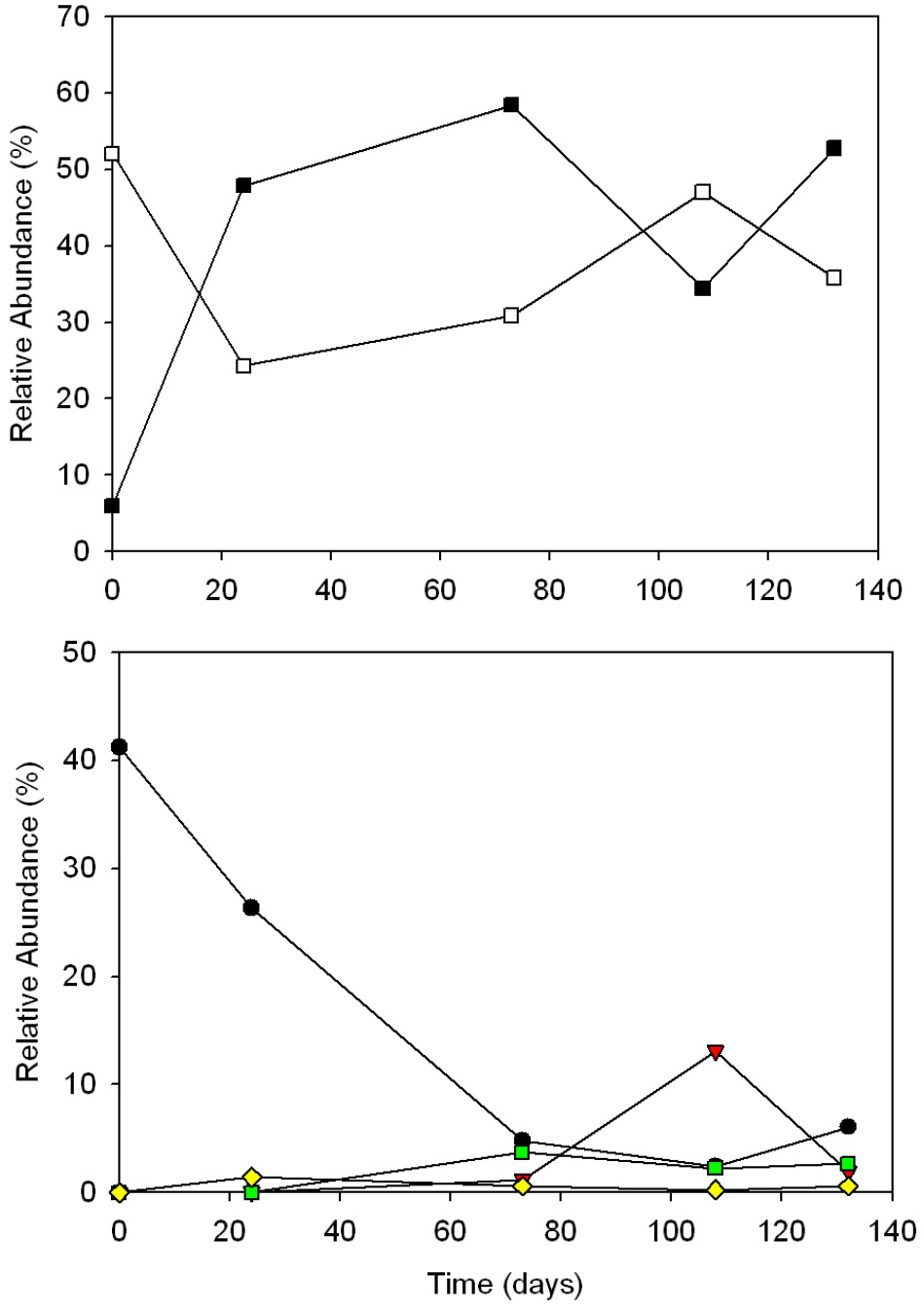

Figure 22: Dynamics of abundant (**A)** and rare (**B)** OTUs in a P-limited, phage-amended chemostat (biological replicate 2). Abundant OTUs include: *Sulfitobacter* (black squares) and *Sphingomonas* (white squares). Rare OTUs include: *Rhizobium* (black circles), *Arthrobacter* (red triangles), *Alcanivorax* (yellow diamonds) and *Pseudomonas* (green squares).

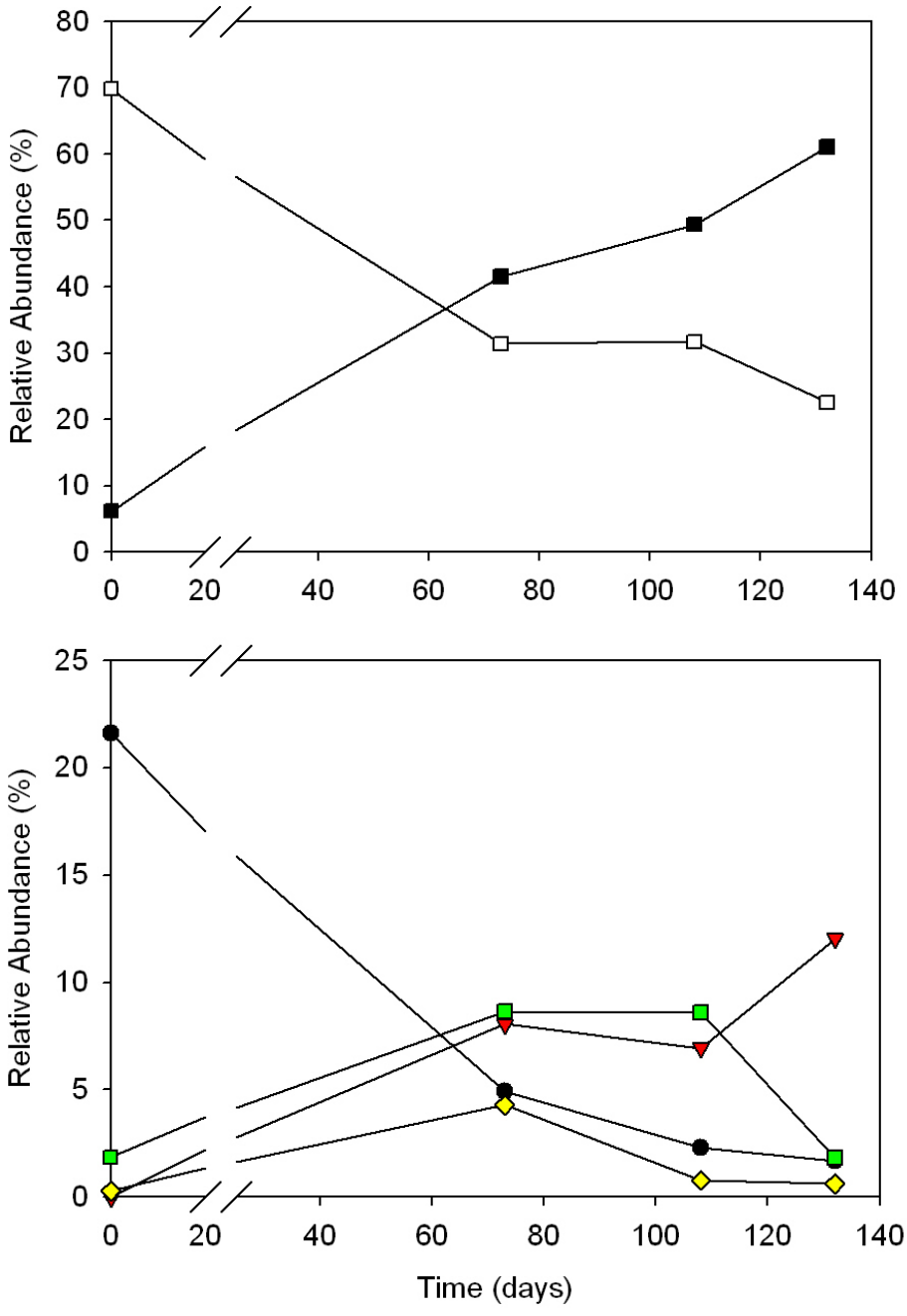

Figure 23: Dynamics of abundant (**A)** and rare (**B)** OTUs in a P-limited, phage-amended chemostat (biological replicate 3). Abundant OTUs include: *Sulfitobacter* (black squares) and *Sphingomonas* (white squares). Rare OTUs include: *Rhizobium* (black circles), *Arthrobacter* (red triangles), *Alcanivorax* (yellow diamonds) and *Pseudomonas* (green squares). Day 24 was not barcoded correctly.

Cluster analyses and non-metric multidimensional dimensional scaling analyses

OTU abundance for pooled libraries was standardized to relative abundances and fourth-root transformed. After a distance matrix was generated, OTUs were clustered in PRIMER using the average linkage method and visualized on a dendrogram (Figure 24A). Although clustering between technical replicates was common (Figure 14), clustering between biological replicate treatments was less frequent. Only 4 out of the 43 pooled samples clustered closest with one of its biological replicate chemostats. Three out of the four were N-limited phage treatments, while the other was a P-limited, phage-amended time point. Clustering of N-limited or P-limited samples (regardless of time or phage treatment) was more common.

The similarity matrix was visualized in PRIMER using a 2-dimensional MDS plot. The stress value of 0.19 (< 0.2) for the ordination plot (Figure 24B) was moderately high but the superimposed clustering further supported that the graph was an adequate representation of the relationships between libraries. Three separate groups formed at a 60% similarity level. Two of the three groups (both P-limited controls at day 0 and the P-limited phage-amended library at day 24) clustered away from the majority of the dataset. At a higher similarity level (70%), the rest of the libraries clustered into 6 separate groups. With the exception of four P-limited libraries, the P-limited treatments clustered into three separate groups away from the three N-limited groups. Additionally, libraries from earlier time points were less similar than those from later time points for both nutrient-limited chemostats. For example, earlier time points from N-limited samples were more similar to earlier time points from P-limited samples than later time points for the same nutrient treatment. Therefore, there was an obvious trajectory of early to late time points across the MDS plot. No distinct clustering of phage-amended groups from control groups was observed for either nutrient-limited treatment.

(**A**)

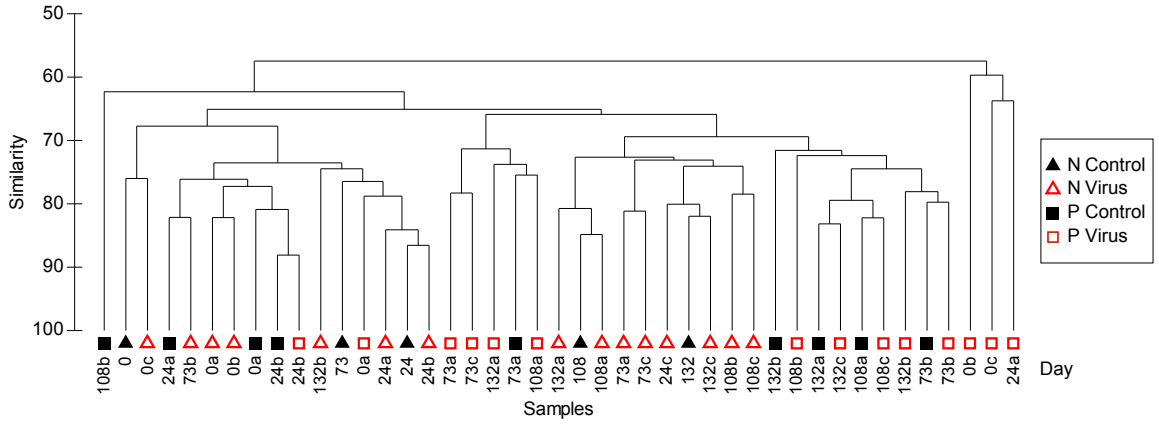

(**B**)

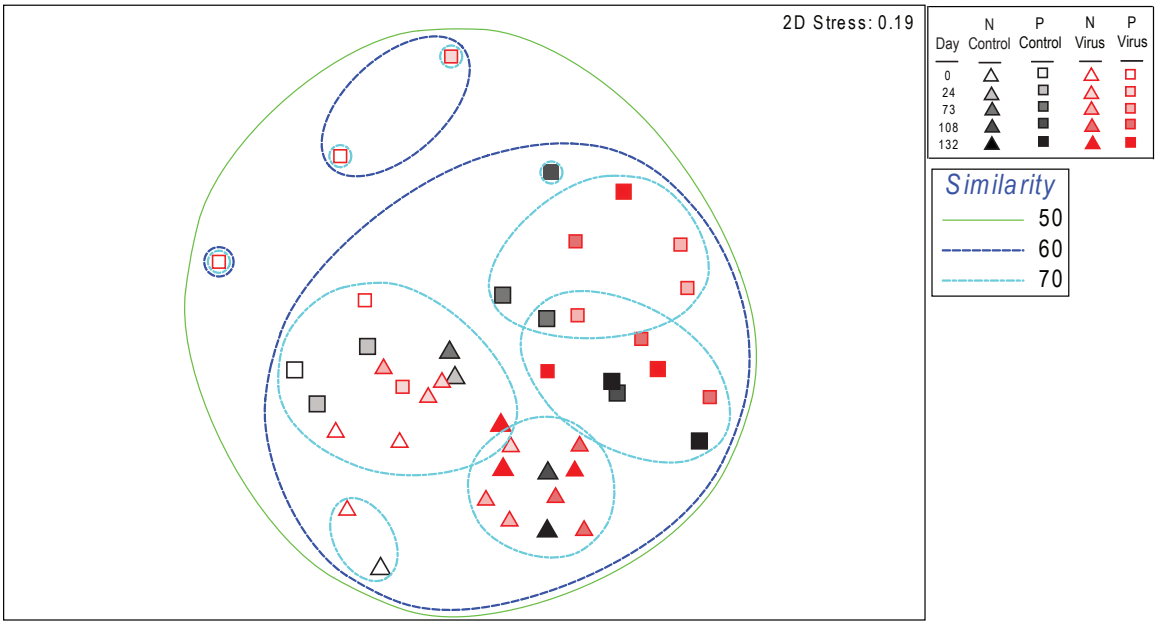

Figure 24: Average cluster analysis (**A**) and MDS ordination plot (**B**) of 110 non-cyanobacterial OTUs based on the zero-adjusted Bray-Curtis similarity index. Biological replicates (**A**) are denoted by a, b and c.

To determine if the less abundant OTUs had an effect on the cluster analysis or ordination plot, the sequence data for the 10 most abundant non-cyanobacterial OTUs were analyzed separately. The 10 most abundant OTUs made up 99.7% of all sequences in the dataset while the remaining sequences (0.03%) were assigned to 100 additional OTUs. Abundance data was standardized to relative abundances and fourth-root transformed. The distance matrix was clustered using the average-linkage method as previously mentioned (Figure 25A). Samples from the N-limited treatments clustered away from the P-limited treatments more distinctly than in the cluster analysis of all the OTUs (Figure 24A). Lastly, clustering of biological replicates was more common than in the dendrogram representing all of the OTUs.

An additional MDS plot was generated from the distance matrix of the 10 most abundant OTUs in the dataset (Figure 24A). The stress value (0.18) was slightly lower and well within the range of the previous MDS plot (< 0.2). Although the stress value was still at the upper end of the range (0.1 to 0.2), the superimposed clustering at 40, 60 and 80% confirmed that the graph was an adequate representation of the data. The slightly lower stress value provided an improved representation of the relationships between samples than the previous graph (Figure 23B). All libraries were within the same group at a 60% similarity level. Four separate groups formed at an 80% similarity level. Two of the clusters consisted of all three P-limited phage-amended biological replicates at day 0 and one P-limited, phage-amended replicate at day 24. The 2 remaining groups consisted largely of all N-limited or P-limited libraries with the exception of 4 P-limited libraries (early time points) within the N-limited cluster. Earlier time points appeared to be more similar to each other than later time points regardless of treatments with a noticeable trajectory in time across the plot. As noted in the previous cluster analyses, no distinct grouping of phage-amended or control treatments was observed for N- or P-limited libraries.

(**A**)

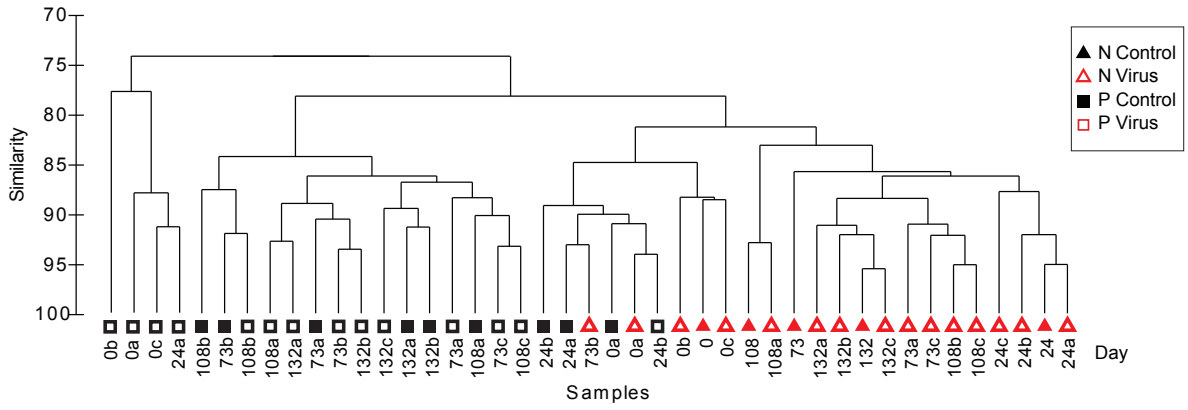

(**B**)

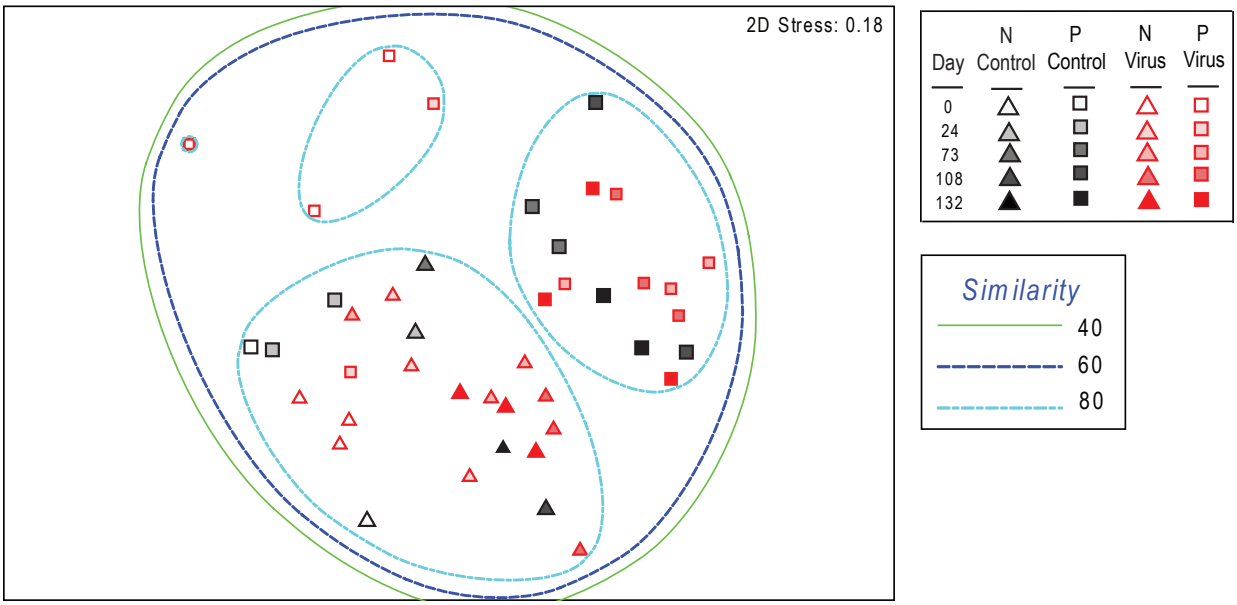

Figure 25: Average cluster analysis (**A**) and MDS ordination plot (**B**) of the 10 most abundant non-cyanobacterial OTUs based on the zero-adjusted Bray-Curtis similarity index. Biological replicates (**A**) are denoted by a, b and c.

Statistical analyses

While the cluster analyses and ordination plots both showed differences in the grouping of N-limited libraries and P-limited libraries, statistical analyses were run in PERMANOVA+ to test for significant differences in community structure among treatments. "Nutrient" (N- or P-limitation), "Virus" (virus-amended or control) and "Day" (0, 24, 73, 108, 132) were established as the main factors. *P*-values were obtained under a reduced model and Type III partial sums of squares. After comparing all combinations of main factors, statistically significant *P*-values ($\alpha < 0.05$) were detected (Table 1). Significant differences were identified between nutrient treatments (*P*=0.0001) and day sampled (*P*=0.0001) and a significant interaction was identified between "Treatment" and "Day" (*P*=0.0091). No significant interactions were identified between the other main factors: "Treatment" vs. "Virus" (*P*=0.643), "Virus" vs. "Day" (*P*=0.2871) or "Treatment" vs. "Virus" vs. "Day" (*P*=0.9231).

Further pairwise comparisons were tested separately for the statistically significant interactions to detect differences within the groups (Table 2). *P*-values of less than 0.05 were identified between N- and P-limited treatments on day 0 (*P*=0.007) and day 73 (*P*=0.012). No statistically significant interactions were detected for the three other time points (24, 108, 132). For statistically significant interactions within groups, additional pairwise tests were performed among pairs of levels of the factor of interest (Table 3). Within the N-limited groups, there were significant differences between all pairwise comparisons of time points. Five out of the eight combinations had *P*-values of less than 0.005. In the P-limited groups, significant differences were detected between all groups except three (0, 24: *P*=0.6435; 73, 108: *P*=0.7129; 108, 132: *P*=0.193). These *P*-values provided statistically significant evidence for differences in our libraries visualized through cluster analyses and MDS plots.

Table 1. PERMANOVA of chemostat bacterial community for the 10 most abundant OTUs showing the main tests for the factors of nitrogen or phosphorus treatment, no virus or virus addition, time and their interactions. *P<0.05.

Source of Variation	**d.f.**	**SS**	***pseudo-F***	**P**
Treatment = Tr	1	1187.1	12.676	0.0001*
Virus = V	1	208.73	2.2288	0.0832
Day = Da	4	2704.8	7.2203	0.0001*
Tr x V	1	57.761	0.61676	0.643
Tr x Da	4	978.24	2.4512	0.0091*
V x Da	4	463.82	1.2382	0.2871
Tr x V x Da	4	159.33	39.833	0.9231
Residuals	23	2154	93.652	
Total	42	9054.2		

P-values were obtained using 9999 permutations of residuals under a reduced model using Type III (partial) sums of squares.

Table 2. Pairwise comparisons of Treatment x Day (significant interaction identified by PERMANOVA main tests) for pairs of levels of Treatment for the 10 most abundant OTUs. *P<0.05.

	Treatment (N vs. P)	
Day	**t**	**P**
0	2.0902	0.007*
24	1.5128	0.1234
73	2.1319	0.012*
108	2.3385	0.006
132	2.6008	0.0048

Table 3. Pairwise comparisons of Treatment x Day (significant interaction identified by PERMANOVA main tests) for pairs of levels of Day for the 10 most abundant OTUs. *P<0.05.

Within N (Nitrogen-Limited)			**Within P (Phosphorus-Limited)**		
Groups	**t**	**P**	**Groups**	**t**	**P**
0, 24	2.8561	0.0018*	0, 24	0.84779	0.6435
0, 73	2.3539	0.0023*	0, 73	2.9003	0.0028*
0, 108	2.5369	0.0012*	0, 108	2.7043	0.0023*
0, 132	2.4327	0.0047*	0, 132	3.2127	0.0029*
24, 73	1.7322	0.0292*	24, 73	2.4921	0.0121*
24, 108	2.6089	0.0039*	24, 108	2.6184	0.0111*
24, 132	1.8162	0.0416*	24, 132	2.7575	0.0083*
73, 108	2.4505	0.0213*	73, 108	0.75186	0.7129
73, 132	2.039	0.0157*	73, 132	1.8123	0.0186*
108, 132	1.7554	0.0682	108, 132	1.3138	0.193

P-values were obtained using 9999 permutations of residuals under a reduced model using Type III (partial) sums of squares.

DISCUSSION

Since our *Synechococcus* inoculum was initially derived from a single colony isolate at the beginning of the experiment, the high number of heterotrophs in our chemostats was particularly surprising. This observation, however, highlights the inherent difficulties in maintaining an axenic strain of cyanobacteria in the laboratory and particularly in a chemostat system. While previous experiments have reported the successful maintenance of axenic cyanobacteria in continuous culture (Groeneweg and Soeder 1978; Bruyant et al. 2001; Fu et al. 2006), others have used non-axenic strains of cyanobacteria (De Nobel et al. 1997; Lennon and Martiny 2008). Our results suggest that each individual chemostat supported approximately 10^8 heterotrophic bacterial cells mL^{-1}, and these cells were consistently more abundant than the autotrophic host with the exception of a few time points (Figure 1, Figure 3, Figure 4, Figure 8).

Although heterotrophic bacteria peaked during the *Synechococcus* crash in a few of the chemostats, there were no consistent trends in heterotrophic bacterial abundance across biological replicate chemostats. Virus-mediated lysis of the host cyanobacterium has been shown to liberate both carbon and nutrients that can be rapidly assimilated and mineralized by the co-occurring heterotrophic bacterial community (Noble and Furhrman 1999; Weinbauer et al. 2011). Heterotrophic bacterial growth in our chemostats was ultimately limited by the quantity and quality of these substrates, which likely regulated the consistent density of heterotrophs (Middelboe et al. 1996; Gobler et al. 1997).

Overall the ratios of heterotrophic bacteria to *Synechococcus* in our study did not appear to be controlled by the abundance of *Synechococcus* at any given time point. When the cyanobacterial population crashed after phage infection, the heterotrophic bacteria density remained relatively similar, resulting in an increased heterotroph : *Synechococcus* ratio. We

would have expected that the indirect effects of cyanobacterial lysis would have resulted in an increase in nutrients (*i.e.,* lysate products) that would be rapidly assimilated by heterotrophic bacteria and lead to a marked increase in heterotrophic bacterial abundance (Gobler et al. 1997). However, this was not the case in our chemostats. Additionally, with regards to host-phage dynamics, differences in *Synechococcus* abundance were also observed between the initial N- and P-limited lytic events. In the N-limited chemostats, host lysis occurred immediately following phage addition (Figure 2, Figure 3, Figure 4). However, in the P-limited chemostats there was a delay in cell lysis of *Synechococcus* (Figure 7, Figure 8, Figure 9). This delay was similar to a report from a previous chemostat study by Wilson et al. (1996) investigating the effect of phosphate on cyanophage infection kinetics. Their work suggests that this delay may have been due to lysogeny, reducing cyanophage production under P-deplete conditions.

Heterotrophic bacteria : *Synechococcus* ratios in our chemostats were similar to those reported across natural marine environments (Li 1998). The results from our flow cytometry counts indicated averages (across all time points) of 7.6 ± 0.3 (mean ± SEM) and 9.8 ± 0.3 heterotrophic bacteria for every *Synechococcus* cell for the N- and P-limited controls, respectively. This average ratio was much higher for the phage-amended chemostats with ratios of 81.5 ± 1.3 and 185.4 ± 1.7 for the N-limited and P-limited chemostats. Furthermore, if the phage-amended and control averages were combined for either nutrient-limited treatment, they resulted in very similar ratios (63.1 ± 1.1 and 51.3 ± 0.9 for the N-limited and P-limited chemostats, respectively). Based on these results it appears that overall, the P-limited chemostats supported a higher ratio of heterotrophs to *Synechococcus* compared to the N-limited chemostats. In order for our system to support this number of heterotrophs, the organic carbon turnover rate of phytoplankton must have been faster than that of the heterotrophic bacteria (Fuhrman et al.

1989). Furthermore, the growth of phytoplankton and heterotrophic bacteria were likely limited by different resources (Daufresne et al. 2008). The coexistence of both competitors was facilitated by C-limitation of the heterotrophs and nutrient limitation of the phytoplankton.

Technical sequencing reproducibility

The results from this study provide strong evidence for the potential of the Roche 454 Titanium pyrosequencing platform. To our knowledge, technical sequencing reproducibility has not been compared using the 454 Titanium platform. Our sequence analysis revealed a high degree of reproducibility among technical replicates at both the phylum and OTU levels. Given the inherent technical issues with next-generation sequencing, pyrosequencing results from community DNA studies have been variable (Zhou et al. 2011). Results from the 454 GS FLX and Illumina platforms have been assessed but the quality of sequencing replication differs largely between the two methods (Bartram et al. 2011; Zhou et al. 2011).

Taxonomic distributions at the phylum-level were similar across technical replicates, which has been noted previously in the literature (Bartram et al. 2011). Using OTU analyses to compare our technical replicate libraries, we found that 40 of our 43 biological replicate libraries clustered most closely with its technical replicate, indicating a high degree of relatedness between technical replicates for individual libraries. Additionally, the 3 libraries that did not cluster most closely with each other were a short distance (*i.e.*, 1 to 2 steps away) from their technical replicates. The results from this dendrogram and our rarefaction curves suggested that we had sequenced deep enough (Figure 14, Figure 29 in Appendix) and gave us reason to pool our sequences to increase our sampling depth. We also evaluated OTU recovery across technical replicates by comparing the relative abundance of all OTUs. Again, the relative abundances between technical replicate libraries were remarkably similar and highly correlated indicating a

similar assignment of reads at a 97% similarity level. Together, these findings imply that sequencing was highly reproducible on our 454 Titanium run providing a baseline to compare 454 Titanium runs that include technical replication in future studies.

MDS and cluster analyses show differences in communities

Our OTU-based analyses showed similar trends across biologically replicated chemostats. Comparable OTU trends were evident among individual replicate chemostats with the same treatments (e.g. all 3 P-limited, phage-amended chemostats). The major difference between the N-limited and P-limited chemostats was the consistent presence of the *Pseudomonas* OTU in the P-limited chemostats regardless of phage addition. For the most part, the results from our OTU trends were very similar across all treatments and we observed no marked differences between the control and phage-amended chemostats. Even when the OTU abundance data was not pooled, there were no major clonal differences within multiple OTUs assigned to the same genus (e.g. within the 13 *Sulfitobacter* OTUs). However, the results from our OTU abundance trends were relatively unsatisfying in our attempt to address the aforementioned hypotheses.

Using MDS plots and overlaid cluster analyses of the 10 most abundant OTUs identified in our chemostats, we were able to address our hypotheses with higher confidence. Although no heterotrophic bacterial counts were completed prior to phage addition, we can make the following conclusions regarding differences in our chemostat communities: 1) N-limited libraries largely clustered away from the P-limited libraries. 2) Libraries from earlier time points clustered loosely together, while libraries from later time points clustered together away from the earlier time points. A trajectory is observed between early and late time points suggesting that our chemostats were not in steady state but evolving. 3) Control and phage-amended libraries

clustered together regardless of nutrient limitation. These differences (*i.e.*, in nutrients and day sampled) were further supported by statistically significant *P*-values.

Based on these results, we failed to reject our first null hypothesis (H_1: The heterotrophic bacterial community structure in a chemostat is different under nitrogen-limited conditions than phosphorus-limited conditions). Indeed, the heterotrophic bacterial community structure did appear to be different under N-limited conditions compared to P-limited conditions. Differences in nutrient availability between the N- and P-limited chemostats likely induced the selection of substrate specialists, resulting in a slightly different bacterial community structure for each treatment. Therefore, we propose that under different nutrient-limiting conditions, lysed phytoplankton released different organic substrates in our chemostats. Differences in our communities based on the Bray-Curtis similarity coefficient were likely due to the presence of *Pseudomonas* among the P-limited chemostats and minor differences in OTUs. However, we must reject our second null hypothesis. Similar to previous findings (Lennon and Martiny 2008), the presence of cyanophage in our chemostats did not strongly affect the structure and composition of non-target bacterial populations. Collectively, the results from our MDS plots and statistical analyses suggest that the direct effects of nutrient limitation drove non-target heterotrophic bacterial diversity instead of the indirect effects of a cyanophage.

Limitations and future directions

These results demonstrate the relative importance of nutrient-limiting conditions as a potential primary driver of non-target heterotrophic community change as opposed to the indirect effects of viruses on a marine food web. While we can make these conclusions for our chemostat study, there are four caveats in this experiment that must be addressed: 1) Our chemostat is a closed system. As a result, nothing new comes in and anything that is lost is

never returned. 2) Our chemostat represents a relatively simple model. Assumedly, we began the study with relatively low levels of diversity and no new bacteria could enter the system. 3) The richness in our chemostats does not mimic natural systems. We would expect different bacterial richness levels in a marine or coastal system based on variations in nutrient availability and substrate competition. 4) Lastly, the cyanobacteria in our chemostat evolved. We were able to isolate cyanophage-resistant *Synechococcus* cells during the chemostat experiment as well as isolate mutant cyanophage that are capable of lysing previously resistant cell lines.

Our hypotheses may be further tested using three additional approaches, which include quantifying cyanomyoviruses, determining the heterotrophic bacterial diversity prior to phage addition and detecting single nucleotide polymorphisms or SNPs in our *Synechococcus* sequences. Although we have assumed in our counts that all phage in the chemostats are indeed cyanophages, it is likely that other bacteriophages are also present given the number of heterotrophic bacteria in our system. Over the last two decades, the *g20* portal vortex gene has been used in studies as a proxy for cyanomyovirus diversity, richness and abundance (Fuller et al. 1998; Wilhelm et al. 2006; Matteson et al. 2011). By employing quantitative PCR, we can use the *g20* gene as a proxy for cyanomyovirus abundance to extract the number of heterotrophic bacteriophage relative to cyanophage from our total phage counts. With regards to our flow cytometry results, our initial heterotrophic bacterial counts began 9 days following phage addition. By enumerating the heterotrophs prior to phage addition, we can confidently estimate the number of heterotrophic bacteria in our chemostats at the beginning of the experiment. Additionally, it would be ideal to pyrosequence or generate a clone library of the basal heterotrophic bacterial community from our initial inoculum to compare to the bacterial community at the end of the chemostat experiment. Results from this 16S rRNA gene

community data should provide stronger evidence to support our initial conclusion that nutrient limitation appears to be a potential driver of heterotrophic bacterial diversity in our chemostats.

As previously mentioned, the cyanophage in our chemostat appeared to have co-evolved with its host over the course of the experiment resulting in a phage capable of lysing previously resistant *Synechococcus*. We plan to re-sequence this virulent mutant cyanophage and compare its genome to the wildtype cyanophage. Characterization of genome-level differences leading to infection of previously resistant cyanobacterial phenotypes has the potential to improve our understanding of the arms race between host and phage. Since these results are based on a subset of all the non-cyanobacterial sequences, we intend to analyze the remaining 16S *Synechococcus* sequences. In doing this, we hope to address differences in the abundance of specific clonal populations of the host cyanobacteria across treatments and over time. We also would like to identify SNPs within our cyanobacterial sequences. Previous literature suggests that SNPs may confer phage resistance phenotypes in bacteria (Barrangou et al. 2007). By comparing the host *Synechococcus* genome to the wildtype and mutant cyanophages, we may be able to identify a nucleic acid-level mechanism of cyanobacterial resistance in our host-phage system.

Conclusions

Several important conclusions can be made from this dataset. First, our flow cytometry counts of heterotrophic bacteria reveal an abundance of heterotrophic bacterial contaminants in our cyanobacterial chemostats. The heterotrophic bacterial counts provided motivation for us to pyrosequence our bacterial communities to determine if direct (nutrient limitation) or indirect effects (cyanomyovirus) were driving the non-target heterotrophic bacterial diversity in our chemostats. Results from our phylum-level assignments, cluster analysis of non-cyanobacterial libraries and OTU overlap among technical replicates suggest high levels of sequencing

reproducibility on the 454 Titanium platform. Next, we observed high reproducibility among our technical replicates and also highly similar patterns in our OTUs across biological replicate chemostats. Lastly, we were able to detect differences in our chemostat libraries with regards to nutrient limitation and time. Results from our cluster analyses, MDS plots and statistical tests indicated statistically significant differences between both nutrient-limited treatments and day sampled. We did not reject our first hypothesis (*i.e.,* in that we determined N-limited and P-limited communities are different) but rejected our second null hypothesis (*i.e.,* cyanophage addition did not result in a different heterotrophic community structure). Although there were caveats that must be acknowledged in our study, the results from this study collectively suggest that in our chemostats, the indirect effects of a cyanophage did not have a significant effect on the diversity of non-target hosts, but that the direct effects of nutrient limitation and time resulted in a different non-target heterotrophic community structure.

REFERENCES

Anderson, M. J., K. E. Ellingsen and B. H. McArdle. 2006. Multivariate dispersion as a measure of beta diversity. **Ecology Letters** 9(6): 683-693.

Arrigo, K. R. 2005. Marine microorganisms and global nutrient cycles. **Nature** 437(7057): 349-355.

Avrani, S., O. Wurtzel, I. Sharon, R. Sorek and D. Lindell. 2011. Genomic island variability facilitates *Prochlorococcus*-virus coexistence. **Nature** 474(7353): 604-608.

Azam, F., T. Fenchel, J. G. Field, J. S. Gray, L. A. Meyer and F. Thingstad. 1983. The ecological role of water column microbes in the sea. **Marine Ecology Progress Series** 10: 257-263.

Barrangou, R., C. Fremaux, H. Deveau, M. Richards, P. Boyaval, S. Moineau, D. A. Romero and P. Horvath. 2007. CRISPR provides acquired resistance against viruses in prokaryotes. **Science** 315(5819): 1709-1712.

Bartram, A. K., M. D. J. Lynch, J. C. Stearns, G. Moreno-Hagelsieb and J. D. Neufeld. 2011. Generation of multimillion-sequence 16S rRNA gene libraries from complex microbial communities by assembling paired-end Illumina reads. **Applied and Environmental Microbiology** 77(15): 5569-5569.

Bergh, O., K. Y. Borsheim, G. Bratbak and M. Heldal. 1989. High abundance of viruses found in aquatic environments. **Nature** 340(6233): 467-468.

Berry, D., K. Ben Mahfoudh, M. Wagner and A. Loy. 2011. Barcoded primers used in multiplex amplicon pyrosequencing bias amplification. **Applied and Environmental Microbiology.** 77(21): 7846-7849.

Bohannan, B., B. Kerr, C. Jessup, J. Hughes and G. Sandvik. 2002. Trade-offs and coexistence in microbial microcosms. **Antonie van Leeuwenhoek** 81(1): 107-115.

Bohannan, B. J. M. and R. E. Lenski. 1997. Effect of resource enrichment on a chemostat community of bacteria and bacteriophage. **Ecology** 78(8): 2303-2315.

Bohannan, B. J. M. and R. E. Lenski. 2000. Linking genetic change to community evolution: insights from studies of bacteria and bacteriophage. **Ecology Letters** 3(4): 362-377.

Bohannan, B. J. M., M. Travisano and R. E. Lenski. 1999. Epistatic interactions can lower the cost of resistance to multiple consumers. **Evolution** 53(1): 292-295.

Bouvier, T. and P. A. del Giorgio. 2007. Key role of selective viral-induced mortality in determining marine bacterial community composition. **Environmental Microbiology** 9(2): 287-297.

Bratbak, G., A. Jacobsen, M. Heldal, K. Nagasaki and F. Thingstad. 1998. Virus production in *Phaeocystis pouchetii* and its relation to host cell growth and nutrition. **Aquatic Microbial Ecology** 16(1): 1-9.

Bratbak, G. and T. F. Thingstad. 1985. Phytoplankton-bacteria interactions: an apparent paradox? Analysis of a model system with both competition and commensalism. **Marine Ecology - Progress Series** 25: 23-30.

Brum, J. R. 2005. Concentration, production and turnover of viruses and dissolved DNA pools at Stn ALOHA, North Pacific Subtropical Gyre. **Aquatic Microbial Ecology** 41(2): 103-113.

Bruyant, F., M. Babin, A. Sciandra, D. Marie, B. Genty, H. Claustre, J. Blanchot, A. Bricaud, R. Rippka, S. Boulben, F. Louis and F. Partensky. 2001. An axenic cyclostat of

Prochlorococcus PCC 9511 with a simulator of natural light regimes. **Journal of Applied Phycology** 13(2): 135-142.
Chao, L., B. R. Levin and F. M. Stewart. 1977. A complex community in a simple habitat: an experimental study with bacteria and phage. **Ecology** 58(2): 369-378.
Chen, F., J. R. Lu, B. J. Binder, Y. C. Liu and R. E. Hodson. 2001. Application of digital image analysis and flow cytometry to enumerate marine viruses stained with SYBR gold. **Applied and Environmental Microbiology** 67(2): 539-545.
Chisholm, S. W., R. J. Olson, E. R. Zettler, R. Goericke, J. B. Waterbury and N. A. Welschmeyer. 1988. A novel free-living prochlorophyte abundant in the oceanic euphotic zone. **Nature** 334(6180): 340-343.
Cho, B. C. and F. Azam. 1990. Biogeochemical significance of bacterial biomass in the ocean's euphotic zone. **Marine Ecology Progress Series** 63: 253-259.
Clarke, K. R., P. J. Somerfield and M. G. Chapman. 2006. On resemblance measures for ecological studies, including taxonomic dissimilarities and a zero-adjusted Bray-Curtis coefficient for denuded assemblages. **Journal of Experimental Marine Biology and Ecology** 330(1): 55-80.
Cole, J. R., Q. Wang, E. Cardenas, J. Fish, B. Chai, R. J. Farris, A. S. Kulam-Syed-Mohideen, D. M. McGarrell, T. Marsh, G. M. Garrity and J. M. Tiedje. 2009. The Ribosomal Database Project: improved alignments and new tools for rRNA analysis. **Nucleic Acids Research** 37: D141-D145.
Daufresne, T., G. Lacroix, D. Benhaim and M. Loreau. 2008. Coexistence of algae and bacteria: a test of the carbon hypothesis. **Aquatic Microbial Ecology** 53(3): 323-332.
De Nobel, W. T., J. Huisman, J. L. Snoep and L. R. Mur. 1997. Competition for phosphorus between the nitrogen-fixing cyanobacteria *Anabaena* and *Aphanizomenon*. **FEMS Microbiology Ecology** 24(3): 259-267.
Downing, J. A. 1997. Marine nitrogen: Phosphorus stoichiometry and the global N:P cycle. **Biogeochemistry** 37(3): 237-252.
Droop, M. R. 1974. The nutrient status of algal cells in continuous culture. **Journal of the Marine Biological Association of the United Kingdom** 54(04): 825-855.
Ducklow, H. W. and C. A. Carlson. 1992. Oceanic bacterial production. **Advances in Microbial Ecology** 12: 113-181.
Edgar, R. C., B. J. Haas, J. C. Clemente, C. Quince and R. Knight. 2011. UCHIME improves sensitivity and speed of chimera detection. **Bioinformatics** 27(16): 2194-2200.
Engelbrektson, A., V. Kunin, K. C. Wrighton, N. Zvenigorodsky, F. Chen, H. Ochman and P. Hugenholtz. 2010. Experimental factors affecting PCR-based estimates of microbial species richness and evenness. **ISME Journal** 4(5): 642-647.
Field, J. G., K. R. Clarke and R. M. Warwick. 1982. A practical strategy for analyzing multispecies distribution patterns. **Marine Ecology Progress Series** 8(1): 37-52.
Fu, F. X., Y. H. Zhang, Y. Y. Feng and D. A. Hutchins. 2006. Phosphate and ATP uptake and growth kinetics in axenic cultures of the cyanobacterium *Synechococcus* CCMP 1334. **European Journal of Phycology** 41(1): 15-28.
Fuhrman, J. A. 1999. Marine viruses and their biogeochemical and ecological effects. **Nature** 399(6736): 541-548.
Fuhrman, J. A. and M. Schwalbach. 2003. Viral influence on aquatic bacterial communities. **Biological Bulletin** 204(2): 192-195.

Fuhrman, J. A., T. D. Sleeter, C. A. Carlson and L. M. Proctor. 1989. Dominance of bacterial biomass in the Sargasso Sea and its ecological implications. **Marine Ecology Progress Series** 57(3): 207-217.

Fuller, N. J., W. H. Wilson, I. R. Joint and N. H. Mann. 1998. Occurrence of a sequence in marine cyanophages similar to that of T4 *g20* and its application to PCR-based detection and quantification techniques. **Applied and Environmental Microbiology** 64(6): 2051-2060.

Gihring, T. M., S. J. Green and C. W. Schadt. 2011. Massively parallel rRNA gene sequencing exacerbates the potential for biased community diversity comparisons due to variable library sizes. **Environmental Microbiology** doi: 10.1111/j.1462-2920.2011.02550.x.

Gobler, C. J., D. A. Hutchins, N. S. Fisher, E. M. Cosper and S. A. Sanudo-Wilhelmy. 1997. Release and bioavailability of C, N, P, Se, and Fe following viral lysis of a marine chrysophyte. **Limnology and Oceanography** 42(7): 1492-1504.

Groeneweg, J. and C. J. Soeder. 1978. An improved culture tube for axenic cultures of microalgae. **British Phycological Journal** 13(4): 337-340.

Haaber, J. and M. Middelboe. 2009. Viral lysis of *Phaeocystis pouchetii*: Implications for algal population dynamics and heterotrophic C, N and P cycling. **ISME Journal** 3(4): 430-441.

Haas, B. J., D. Gevers, A. M. Earl, M. Feldgarden, D. V. Ward, G. Giannoukos, D. Ciulla, D. Tabbaa, S. K. Highlander, E. Sodergren, B. Methe, T. Z. DeSantis, J. F. Petrosino, R. Knight, B. W. Birren and H. M. Consortium. 2011. Chimeric 16S rRNA sequence formation and detection in Sanger and 454-pyrosequenced PCR amplicons. **Genome Research** 21(3): 494-504.

Hall, J. A., K. Safi, M. R. James, J. Zeldis and M. Weatherhead. 2006. Microbial assemblage during the spring-summer transition on the northeast continental shelf of New Zealand. **New Zealand Journal of Marine and Freshwater Research** 40: 195-210.

Hamady, M., J. J. Walker, J. K. Harris, N. J. Gold and R. Knight. 2008. Error-correcting barcoded primers for pyrosequencing hundreds of samples in multiplex. **Nature Methods** 5(3): 235-237.

Hara, S., K. Terauchi and I. Koike. 1991. Abundance of viruses in marine waters - assessment by epifluorescence and transmission electron microscopy. **Applied and Environmental Microbiology** 57(9): 2731-2734.

Hennes, K., C. Suttle and A. Chan. 1995. Fluorescently labeled virus probes show that natural virus populations can control the structure of marine microbial communities. **Applied and Environmental Microbiology** 61(10): 3623-3627.

Hennes, K. P. and C. A. Suttle. 1995. Direct counts of viruses in natural-waters and laboratory cultures by epifluorescence microscopy. **Limnology and Oceanography** 40(6): 1050-1055.

Holmfeldt, K., J. Titelman and L. Riemann. 2010. Virus production and lysate recycling in different sub-basins of the Northern Baltic Sea. **Microbial Ecology** 60(3): 572-580.

Huber, J. A., H. G. Morrison, S. M. Huse, P. R. Neal, M. L. Sogin and D. B. Mark Welch. 2009. Effect of PCR amplicon size on assessments of clone library microbial diversity and community structure. **Environmental Microbiology** 11(5): 1292-1302.

Huber, T., G. Faulkner and P. Hugenholtz. 2004. Bellerophon: a program to detect chimeric sequences in multiple sequence alignments. **Bioinformatics** 20(14): 2317-2319.

Hughes, J. B., J. J. Hellmann, T. H. Ricketts and B. J. M. Bohannan. 2001. Counting the uncountable: Statistical approaches to estimating microbial diversity. **Applied and Environmental Microbiology** 67(10): 4399-4406.

Huse, S. M., L. Dethlefsen, J. A. Huber, D. M. Welch, D. A. Relman and M. L. Sogin. 2008. Exploring microbial diversity and taxonomy using SSU rRNA hypervariable tag sequencing. **PLoS Genetics** 4(11): e1000255.

Huse, S. M., D. M. Welch, H. G. Morrison and M. L. Sogin. 2010. Ironing out the wrinkles in the rare biosphere through improved OTU clustering. **Environmental Microbiology** 12(7): 1889-1898.

Kauserud, H., S. Kumar, A. Brysting, J. Nordén and T. Carlsen. 2011. High consistency between replicate 454 pyrosequencing analyses of ectomycorrhizal plant root samples. **Mycorrhiza**: 1-7.

Lebaron, P., N. Parthuisot and P. Catala. 1998. Comparison of blue nucleic acid dyes for flow cytometric enumeration of bacteria in aquatic systems. **Appl. Environ. Microbiol.** 64(5): 1725-1730.

Lemos, L. N., R. R. Fulthorpe, E. W. Triplett and L. F. W. Roesch. 2011. Rethinking microbial diversity analysis in the high throughput sequencing era. **Journal of Microbiological Methods** 86(1): 42-51.

Lennon, J. T., S. A. M. Khatana, M. F. Marston and J. B. H. Martiny. 2007. Is there a cost of virus resistance in marine cyanobacteria? **ISME Journal** 1(4): 300-312.

Lennon, J. T. and J. B. H. Martiny. 2008. Rapid evolution buffers ecosystem impacts of viruses in a microbial food web. **Ecology Letters** 11(11): 1178-1188.

Lenski, R. E. 1988. Dynamics of interactions between bacteria and virulent bacteriophage. **Advances in Microbial Ecology** 10: 1-44.

Lenski, R. E. and B. R. Levin. 1985. Constraints on the coevolution of bacteria and virulent phage - A model, some experiments, and predictions for natural communities. **American Naturalist** 125(4): 585-602.

Li, W. K. 1995. Composition of ultraphytoplankton in the central North Atlantic. **Marine Ecology Progress Series** 122: 1-8.

Li, W. K. W. 1998. Annual average abundance of heterotrophic bacteria and *Synechococcus* in surface ocean waters. **Limnology and Oceanography** 43(7): 1746-1753.

Liu, H. B., H. A. Nolla and L. Campbell. 1997. *Prochlorococcus* growth rate and contribution to primary production in the equatorial and subtropical North Pacific Ocean. **Aquatic Microbial Ecology** 12(1): 39-47.

Long, R. A. and F. Azam. 2001. Antagonistic interactions among marine pelagic bacteria. **Applied and Environmental Microbiology** 67(11): 4975-4983.

Longhurst, A. R. and W. Glen Harrison. 1989. The biological pump: Profiles of plankton production and consumption in the upper ocean. **Progress In Oceanography** 22(1): 47-123.

Mann, N. H. 2003. Phages of the marine cyanobacterial picophytoplankton. **FEMS Microbiology Reviews** 27(1): 17-34.

Mardis, E. R. 2008. The impact of next-generation sequencing technology on genetics. **Trends in Genetics** 24(3): 133-141.

Marston, M. F. and J. L. Sallee. 2003. Genetic diversity and temporal variation in the cyanophage community infecting marine Synechococcus species in Rhode Island's coastal waters. **Applied and Environmental Microbiology** 69(8): 4639-4647.

Martin, A. P. 2002. Phylogenetic approaches for describing and comparing the diversity of microbial communities. **Applied and Environmental Microbiology** 68(8): 3673-3682.

Matteson, A. R., S. N. Loar, R. A. Bourbonniere and S. W. Wilhelm. 2011. Molecular enumeration of an ecologically important cyanophage in a Laurentian Great Lake. **Applied and Environmental Microbiology** 77(19): 6772-6779.

Metzker, M. L. 2010. Sequencing technologies - the next generation. **Nat Rev Genet** 11(1): 31-46.

Meyerhans, A., J. P. Vartanian and S. Wainhobson. 1990. DNA recombination during PCR. **Nucleic Acids Research** 18(7): 1687-1691.

Middelboe, M. 2000. Bacterial growth rate and marine virus host dynamics. **Microbial Ecology** 40(2): 114-124.

Middelboe, M., A. Hagström, N. Blackburn, B. Sinn, U. Fischer, N. H. Borch, J. Pinhassi, K. Simu and M. G. Lorenz. 2001. Effects of bacteriophages on the population dynamics of four strains of pelagic marine bacteria. **Microbial Ecology** 42(3): 395-406.

Middelboe, M., K. Holmfeldt, L. Riemann, O. Nybroe and J. Haaber. 2009. Bacteriophages drive strain diversification in a marine *Flavobacterium*: implications for phage resistance and physiological properties. **Environmental Microbiology** 11(8): 1971-1982.

Middelboe, M. and N. O. G. Jorgensen. 2006. Viral lysis of bacteria: an important source of dissolved amino acids and cell wall compounds. **Journal of the Marine Biological Association of the United Kingdom** 86(3): 605-612.

Middelboe, M., N. O. G. Jorgensen and N. Kroer. 1996. Effects of viruses on nutrient turnover and growth efficiency of non-infected marine bacterioplankton. **Applied and Environmental Microbiology** 62: 1991-1997.

Moisa, I., E. Sotropa and V. Velehorschi. 1981. Investigations on the presence of cyanophages in fresh and sea waters of Romania. **Virologie** 32(2): 127-132.

Noble, R. T. and J. A. Fuhrman. 1998. Use of SYBR Green I for rapid epifluorescence counts of marine viruses and bacteria. **Aquatic Microbial Ecology** 14(2): 113-118.

Noble, R. T. and J. A. Furhrman. 1999. Breakdown and microbial uptake of marine viruses and other lysis products. **Aquatic Microbial Ecology** 20: 1-11.

Parameswaran, P., R. Jalili, L. Tao, S. Shokralla, B. Gharizadeh, M. Ronaghi and A. Z. Fire. 2007. A pyrosequencing-tailored nucleotide barcode design unveils opportunities for large-scale sample multiplexing. **Nucleic Acids Research** 35(19): e130: 131-139.

Partensky, F., J. Blanchot and D. Vaulot. 1999. Differential distribution and ecology of *Prochlorococcus* and *Synechococcus* in oceanic waters : a review. **Bull. Inst. Océanogr. Monaco Special** 19: 457-475.

Pomeroy, L. R. 1974. The ocean's food web, a changing paradigm. **BioScience** 24(9): 499-504.

Poorvin, L., J. M. Rinta-Kanto, D. A. Hutchins and S. W. Wilhelm. 2004. Viral release of iron and its bioavailability to marine plankton. **Limnology and Oceanography** 49(5): 1734-1741.

Proctor, L. M. and J. A. Fuhrman. 1990. Viral mortality of marine bacteria and cyanobacteria. **Nature** 343(6253): 60-62.

Proctor, L. M. and J. A. Fuhrman. 1992. Mortality of marine bacteria in response to enrichments of the virus size fraction from seawater. **Marine Ecology-Progress Series** 87(3): 283-293.

Pruesse, E., C. Quast, K. Knittel, B. M. Fuchs, W. Ludwig, J. Peplies and F. O. Glöckner. 2007. SILVA: a comprehensive online resource for quality checked and aligned ribosomal RNA sequence data compatible with ARB. **Nucleic Acids Research** 35(21): 7188-7196.

Quince, C., A. Lanzen, R. J. Davenport and P. J. Turnbaugh. 2011. Removing noise from pyrosequenced amplicons. **BMC Bioinformatics** 12.

Riemann, L. and M. Middelboe. 2002. Viral lysis of marine bacterioplankton: implications for organic matter cycling and bacterial clonal composition. **Ophelia** 56: 57-68.

Riemann, L., G. F. Steward and F. Azam. 2000. Dynamics of bacterial community composition and activity during a mesocosm diatom bloom. **Applied and Environmental Microbiology** 66(2): 578-587.

Rohwer, F. and R. V. Thurber. 2009. Viruses manipulate the marine environment. **Nature** 459(7244): 207-212.

Safferman, R. S. and M. E. Morris. 1963. Algal virus: isolation. **Science** 140(3567): 679-680.

Sanger, F., S. Nicklen and A. R. Coulson. 1977. DNA sequencing with chain-terminating inhibitors. **Proceedings of the National Academy of Sciences** 74(12): 5463-5467.

Schloss, P. D., S. L. Westcott, T. Ryabin, J. R. Hall, M. Hartmann, E. B. Hollister, R. A. Lesniewski, B. B. Oakley, D. H. Parks, C. J. Robinson, J. W. Sahl, B. Stres, G. G. Thallinger, D. J. Van Horn and C. F. Weber. 2009. Introducing mothur: Open-source, platform-independent, community-supported software for describing and comparing microbial communities. **Applied and Environmental Microbiology** 75(23): 7537-7541.

Shendure, J. and H. L. Ji. 2008. Next-generation DNA sequencing. **Nature Biotechnology** 26(10): 1135-1145.

Sherr, E. and B. Sherr. 1988. Role of microbes in pelagic food webs - a revised concept. **Limnology and Oceanography** 33(5): 1225-1227.

Sherr, E. B., D. A. Caron and B. F. Sherr.1993. Staining of heterotrophic protists for visualization via epifluorescence microscopy. **Handbook of Methods in Aquatic Microbial Ecology**. P. F. Kemp, B. F. Sherr, E. B. Sherr and J. J. Cole. Boca Raton, FL, Lewis Publishers: 213-221.

Smith, S. V. 1984. Phosphorus versus nitrogen limitation in the marine environment. **Limnology and Oceanography** 29(6): 1149-1160.

Sogin, M. L., H. G. Morrison, J. A. Huber, D. Mark Welch, S. M. Huse, P. R. Neal, J. M. Arrieta and G. J. Herndl. 2006. Microbial diversity in the deep sea and the underexplored "rare biosphere". **Proceedings of the National Academy of Sciences of the United States of America** 103(32): 12115-12120.

Stanier, R. Y. and G. Cohen-Bazire. 1977. Phototrophic prokaryotes: the cyanobacteria. **Annual Review of Microbiology** 31: 225-274.

Stoddard, L. I., J. B. H. Martiny and M. F. Marston. 2007. Selection and characterization of cyanophage resistance in marine *Synechococcus* strains. **Appl. Environ. Microbiol.** 73(17): 5516-5522.

Sullivan, M. B., J. B. Waterbury and S. W. Chisholm. 2003. Cyanophages infecting the oceanic cyanobacterium *Prochlorococcus*. **Nature** 426(6966): 584-584.

Suttle, C. A. 1994. The significance of viruses to mortality in aquatic microbial communities. **Microbial Ecology** 28(2): 237-243.

Suttle, C. A. 2005. Viruses in the sea. **Nature** 437(7057): 356-361.

Suttle, C. A. 2007. Marine viruses - major players in the global ecosystem. **Nature Reviews Microbiology** 5(10): 801-812.

Suttle, C. A. and A. M. Chan. 1993. Marine cyanophages infecting oceanic and coastal strains of *Synechococcus* - Abundance, morphology, cross-infectivity and growth characteristics. **Marine Ecology Progress Series** 92(1-2): 99-109.

Suttle, C. A. and A. M. Chan. 1994. Dynamics and distribution of cyanophages and their effect on marine *Synechococcus* spp. **Applied and Environmental Microbiology** 60(9): 3167-3174.

Suttle, C. A., A. M. Chan and M. T. Cottrell. 1990. Infection of phytoplankton by viruses and reduction of primary productivity. **Nature** 347(6292): 467-469.

Tamaki, H., C. L. Wright, X. Li, Q. Lin, C. Hwang, S. Wang, J. Thimmapuram, Y. Kamagata and W.-T. Liu. 2011. Analysis of 16S rRNA amplicon sequencing options on the Roche/454 next-generation Titanium sequencing platform. **PLoS One** 6(9): e25263.

Thingstad, T. F. and R. Lignell. 1997. Theoretical models for the control of bacterial growth rate, abundance, diversity and carbon demand. **Aquatic Microbial Ecology** 13(1): 19-27.

Torrella, F. and R. Y. Morita. 1979. Evidence by electron micrographs for a high incidence of bacteriophage particles in the waters of Yaquina Bay, oregon: ecological and taxonomical implications. **Applied and Environmental Microbiology** 37(4): 774-778.

Tringe, S. G. and P. Hugenholtz. 2008. A renaissance for the pioneering 16S rRNA gene. **Current Opinion in Microbiology** 11(5): 442-446.

Tripp, H. J. 2008. Counting marine microbes with Guava Easy-Cyte 96 well plate reading flow cytometer. **Nature Protocol Exchange** doi:10.1038/nprot.2008.29.

Tyrrell, T. 1999. The relative influences of nitrogen and phosphorus on oceanic primary production. **Nature** 400(6744): 525-531.

Wang, Q., G. M. Garrity, J. M. Tiedje and J. R. Cole. 2007. Naive Bayesian classifier for rapid assignment of rRNA sequences into the new bacterial taxonomy. **Applied and Environmental Microbiology** 73(16): 5261-5267.

Wang, Y. and P.-Y. Qian. 2009. Conservative fragments in bacterial 16S rRNA genes and primer design for 16S ribosomal DNA amplicons in metagenomic studies. **PLoS One** 4(10): e7401.

Waterbury, J. B. and F. W. Valois. 1993. Resistance to co-occurring phages enables marine *Synechococcus* communities to coexist with cyanophages abundant in seawater. **Applied and Environmental Microbiology** 59(10): 3393-3399.

Waterbury, J. B., S. W. Watson, R. R. L. Guillard and L. E. Brand. 1979. Widespread occurrence of a unicellular, marine, planktonic, cyanobacterium. **Nature** 277(5694): 293-294.

Waterbury, J. B. and J. M. Willey.1988. [6] Isolation and growth of marine planktonic cyanobacteria. **Methods in Enzymology**. A. N. G. Lester Packer, Academic Press. Volume 167: 100-105.

Weinbauer, M. G. 2004. Ecology of prokaryotic viruses. **FEMS Microbiology Reviews** 28(2): 127-181.

Weinbauer, M. G., O. Bonilla-Findji, A. M. Chan, J. R. Dolan, S. M. Short, K. Šimek, S. W. Wilhelm and C. A. Suttle. 2011. *Synechococcus* growth in the ocean may depend on the lysis of heterotrophic bacteria. **Journal of Plankton Research** 33(10): 1465-1476.

Weinbauer, M. G. and F. Rassoulzadegan. 2004. Are viruses driving microbial diversification and diversity? **Environmental Microbiology** 6(1): 1-11.

Wilhelm, S. W., M. J. Carberry, M. L. Eldridge, L. Poorvin, M. A. Saxton and M. A. Doblin. 2006. Marine and freshwater cyanophages in a Laurentian Great Lake: Evidence from

infectivity assays and molecular analyses of *g20* genes. **Applied and Environmental Microbiology** 72(7): 4957-4963.
Wilhelm, S. W. and C. A. Suttle. 1999. Viruses and nutrient cycles in the sea. **BioScience** 49(10): 781-788.
Wilson, W. H., N. G. Carr and N. H. Mann. 1996. The effect of phosphate status on the kinetics of cyanophage infection in the oceanic cyanobacterium *Synechococcus* sp. WH7803. **Journal of Phycology** 32(4): 506-516.
Wilson, W. H., I. R. Joint, N. G. Carr and N. H. Mann. 1993. Isolation and molecular characterization of five marine cyanophages propagated on *Synechococcus* sp. strain WH7803. **Applied and Environmental Microbiology** 59(11): 3736-3743.
Winter, C., T. Bouvier, M. G. Weinbauer and T. F. Thingstad. 2010. Trade-offs between competition and defense specialists among unicellular planktonic organisms: The "Killing the Winner" hypothesis revisited. **Microbiology and Molecular Biology Reviews** 74(1): 42-57.
Woese, C. R. 1987. Bacterial evolution. **Microbiological Reviews** 51(2): 221-271.
Wommack, K. E. and R. R. Colwell. 2000. Virioplankton: Viruses in aquatic ecosystems. **Microbiology and Molecular Biology Reviews** 64(1): 69-114.
Xu, X., I. Khudyakov and C. Wolk. 1997. Lipopolysaccharide dependence of cyanophage sensitivity and aerobic nitrogen fixation in *Anabaena* sp. strain PCC 7120. **J. Bacteriol.** 179(9): 2884-2891.
Youssef, N., C. S. Sheik, L. R. Krumholz, F. Z. Najar, B. A. Roe and M. S. Elshahed. 2009. Comparison of species richness estimates obtained using nearly complete fragments and simulated pyrosequencing-generated fragments in 16S rRNA gene-based environmental surveys. **Applied and Environmental Microbiology** 75(16): 5227-5236.
Yue, J. C. and M. K. Clayton. 2005. A similarity measure based on species proportions. **Communications in Statistics-Theory and Methods** 34(11): 2123-2131.
Zehr, J. P. and B. B. Ward. 2002. Nitrogen cycling in the ocean: New perspectives on processes and paradigms. **Applied and Environmental Microbiology** 68(3): 1015-1024.
Zhou, J., L. Wu, Y. Deng, X. Zhi, Y. H. Jiang, Q. Tu, J. Xie, J. D. Van Nostrand, Z. He and Y. Yang. 2011. Reproducibility and quantitation of amplicon sequencing-based detection. **ISME Journal** 5(8): 1303-1313.

APPENDIX

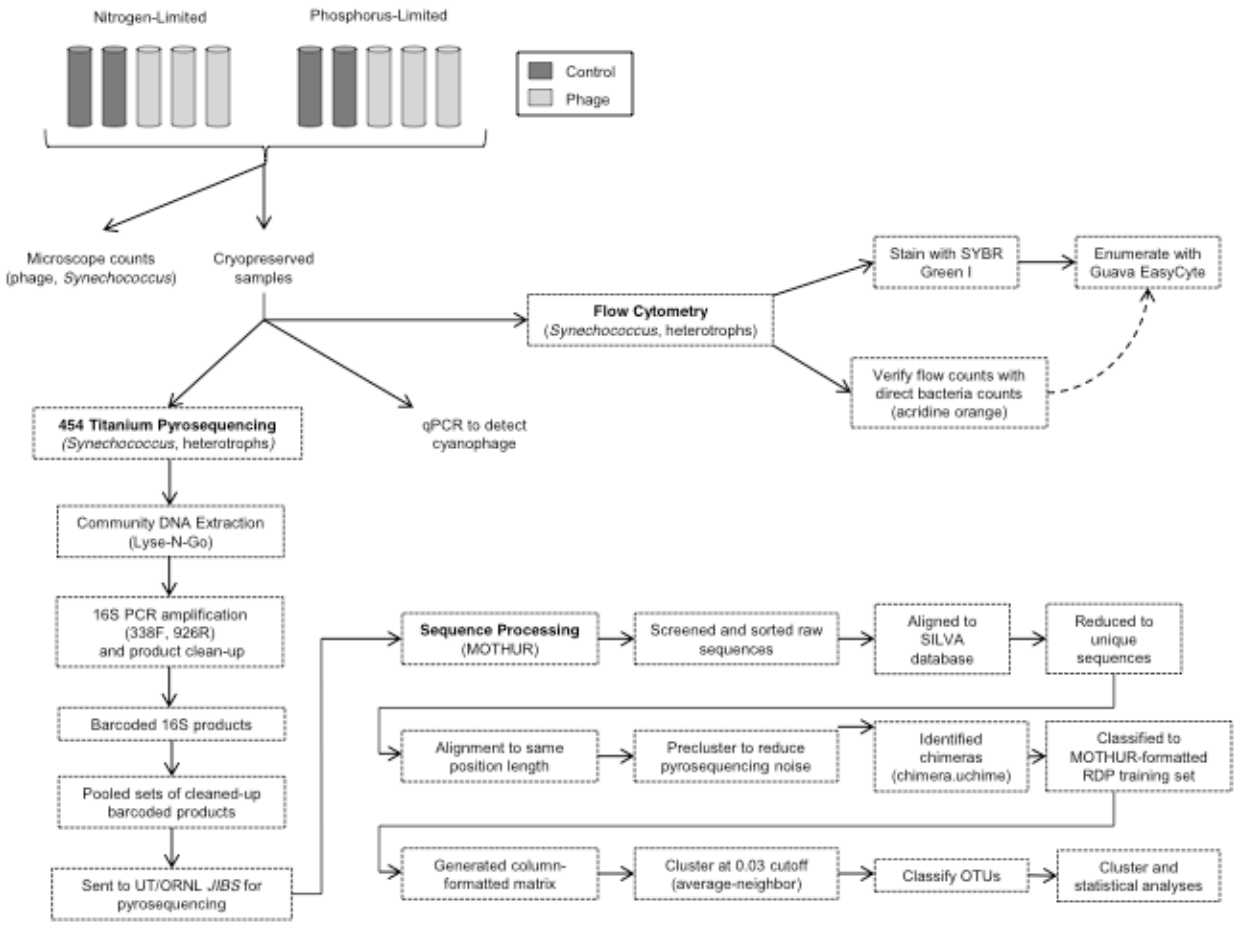

Figure 26: Flow chart of experimental setup and methods (flow cytometry, pyrosequencing and sequence processing).

(**A**)

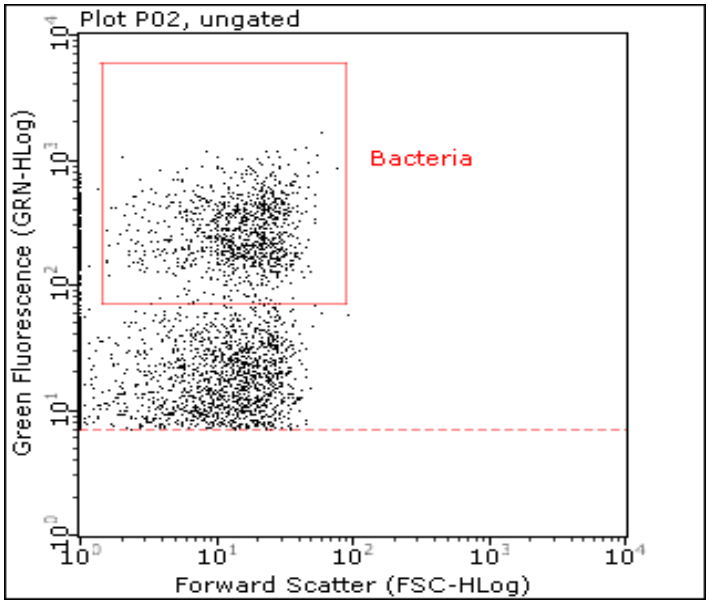

(**B**)

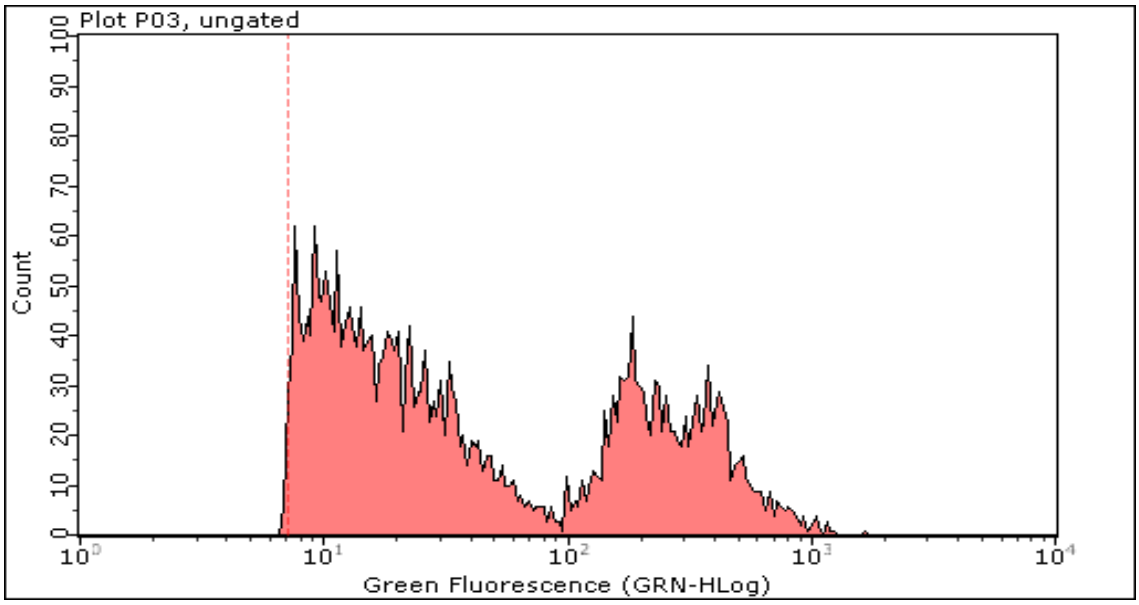

Figure 27. Sample dot plot (**A**) and histogram (**B**) of total bacterial counts. Total bacteria were counted for 100 seconds, set to count a maximum of 1000 events and set to the lowest flow rate on the Guava flow cytometer.

(**A**)

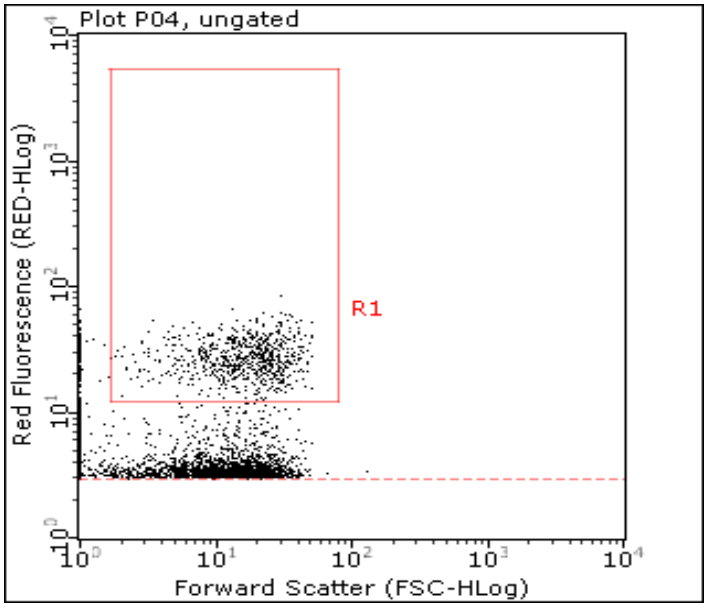

(**B**)

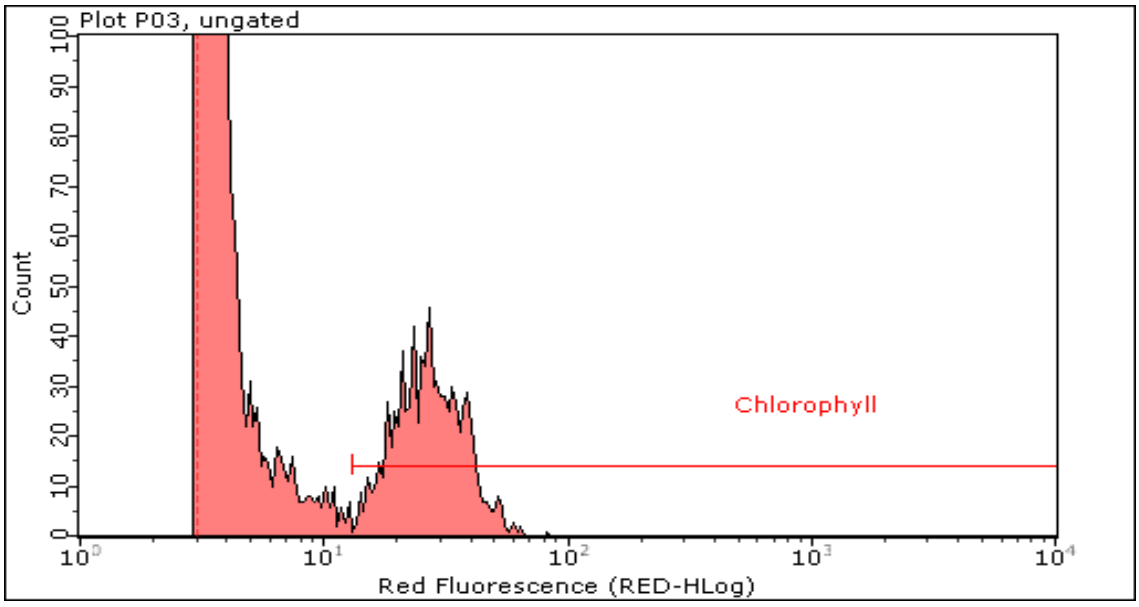

Figure 28. Sample dot plot (**A**) and histogram (**B**) of autotrophic cell counts. Autotrophic cells (*Synechococcus*) were counted for 180 seconds, set to count a maximum of 2500 events and set to the lowest flow rate of the Guava flow cytometer.

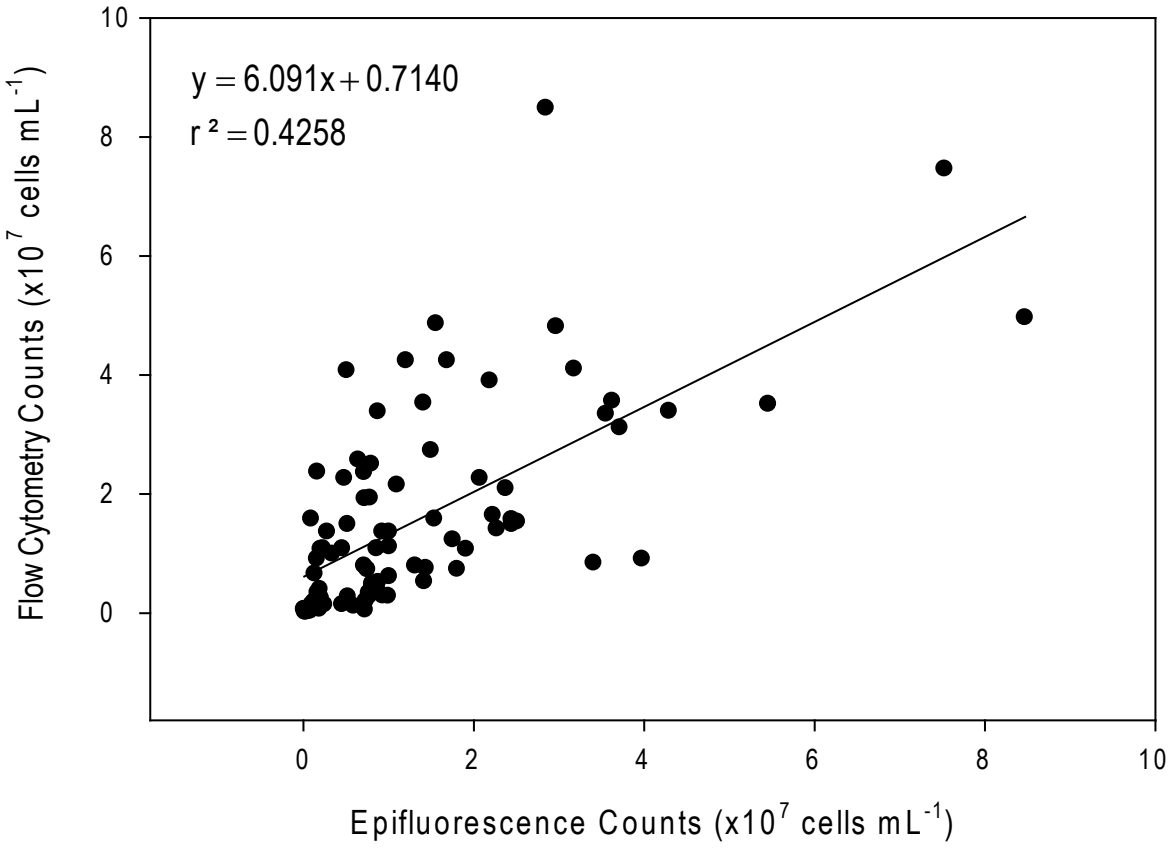

Figure 29. Scatter plot with linear regression of flow cytometry counts versus epifluorescence counts of *Synechococcus* (n=90).

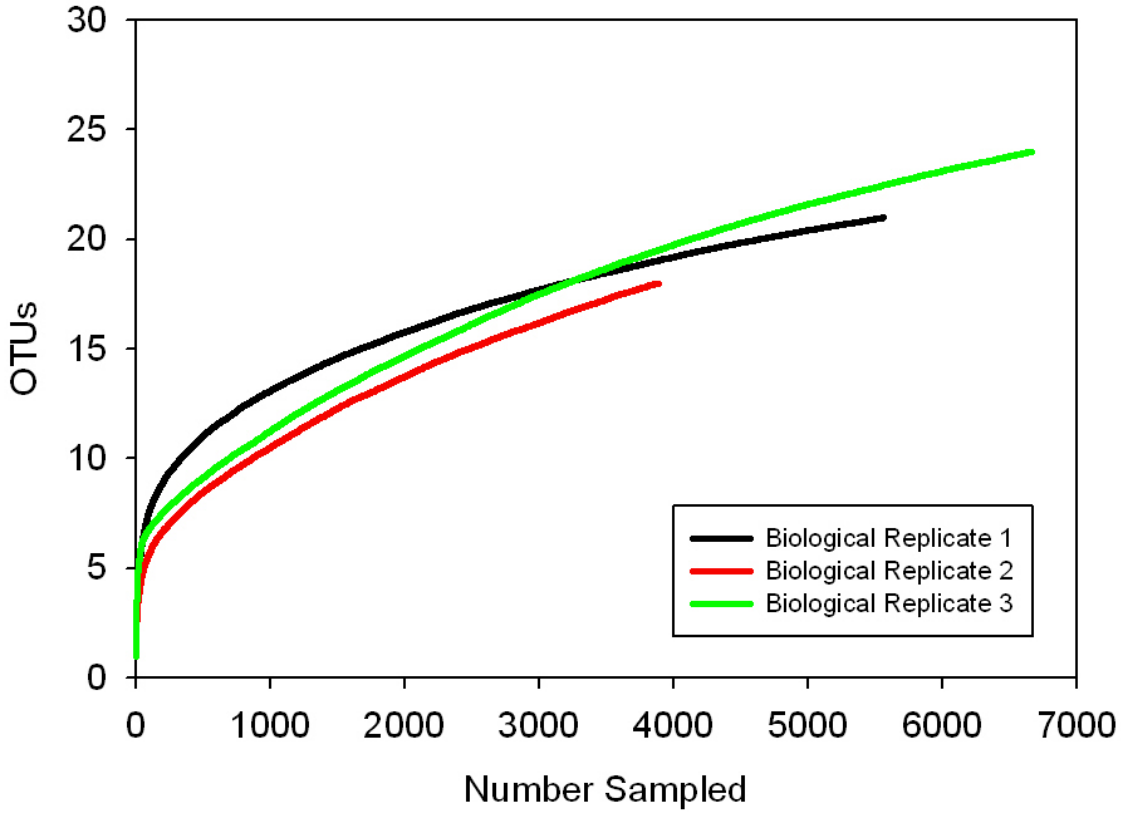

Figure 30: Example rarefaction curves generated using 1,000 randomizations in MOTHUR of 3 biological replicate libraries from day 73 of a phosphorus-limited, phage-amended chemostat.

Table 4: Universal primers, fusion primers and barcoded primers used to barcode chemostat libraries (Wang and Qian 2009).

Primer	Adapter Sequence	Key	Barcode Sequence
338F_A	CCATCTCATCCCTGCGTGTCTCCGAC	TCAG	AACCATGC
338F_B	CCATCTCATCCCTGCGTGTCTCCGAC	TCAG	ACACAGAG
338F_C	CCATCTCATCCCTGCGTGTCTCCGAC	TCAG	AACGCGTT
338F_D	CCATCTCATCCCTGCGTGTCTCCGAC	TCAG	ACTCAGTG
338F_E	CCATCTCATCCCTGCGTGTCTCCGAC	TCAG	AGACCACT
338F_F	CCATCTCATCCCTGCGTGTCTCCGAC	TCAG	CGTTCGTT
338F_G	CCATCTCATCCCTGCGTGTCTCCGAC	TCAG	CTGTCGTT
338F_H	CCATCTCATCCCTGCGTGTCTCCGAC	TCAG	CGTAATGC
338F_I	CCATCTCATCCCTGCGTGTCTCCGAC	TCAG	CAGTCTCT
338F_J	CCATCTCATCCCTGCGTGTCTCCGAC	TCAG	CCAATACG
338F_K	CCATCTCATCCCTGCGTGTCTCCGAC	TCAG	ACCACATG
338F_L	CCATCTCATCCCTGCGTGTCTCCGAC	TCAG	ACCAGTAC
338F_M	CCATCTCATCCCTGCGTGTCTCCGAC	TCAG	ACCTAGCA
338F_N	CCATCTCATCCCTGCGTGTCTCCGAC	TCAG	ACCTTCGT
338F_O	CCATCTCATCCCTGCGTGTCTCCGAC	TCAG	ACGAAGCA
338F_P	CCATCTCATCCCTGCGTGTCTCCGAC	TCAG	CCTTCGAT
338F_Q	CCATCTCATCCCTGCGTGTCTCCGAC	TCAG	CACAGAGA
338F_R	CCATCTCATCCCTGCGTGTCTCCGAC	TCAG	CACAACAC
338F_S	CCATCTCATCCCTGCGTGTCTCCGAC	TCAG	CCTAGCTT
338F_T	CCATCTCATCCCTGCGTGTCTCCGAC	TCAG	CCAAGGTT
338F_U	CCATCTCATCCCTGCGTGTCTCCGAC	TCAG	AACGTACC
338F_V	CCATCTCATCCCTGCGTGTCTCCGAC	TCAG	AAGCAAGC
926R	CCTATCCCCTGTGTGCCTTGGCAGTC	TCAG	

Forward Fusion Primer:
CCATCTCATCCCTGCGTGTCTCCGAC-[Key]-Barcode-ACTCCTACGGGAGGCAGCAG

Reverse Fusion Primer:
CCTATCCCCTGTGTGCCTTGGCAGTC-[Key]-CCGTCAATTCMTTTRAGT

338F Primer Sequence: ACTCCTACGGGAGGCAGCAG
926R Primer Sequence: CCGTCAATTCMTTTRAGT

VITA

Claire Elyse Campbell was raised in a small, rural town in the Appalachian region of Virginia. She graduated salutatorian from James River High School (Buchanan, Virginia) in 2005. After her experience in high school with Mrs. Barbara Kolb, an inspiring science teacher, she decided to consider a career in the biological sciences. She graduated with honors from Elon University in 2009 with a Bachelor of Science with dual degrees in Biology and Environmental Studies with a concentration in Science. During her undergraduate career, she was lucky enough to have research experiences working in academia, government and industry that led her to pursue a graduate program in microbiology. In August 2009, she began the Masters program in Microbiology at the University of Tennessee working under Dr. Steven Wilhelm. She completed the requirements for the Masters of Science degree in December 2011.